U.PORTO

FEUP FACULDADE DE ENGENHARIA
UNIVERSIDADE DO PORTO

M 2022

nTOPOLOGY OPTIMIZATION APPLIED TO ADDITIVE MANUFACTURED HYDROFOIL WING COMPONENTS

MARGARIDA MATA

DISSERTAÇÃO DE MESTRADO APRESENTADA À FACULDADE DE ENGENHARIA DA UNIVERSIDADE DO PORTO EM ENGENHARIA DE MATERIAIS

ORIENTADOR
PROFESSOR MANUEL VIEIRA

CO-ORIENTADOR
PROFESSORA ELSA SEQUEIROS

Porto, julho 2022

U.PORTO
FEUP FACULDADE DE ENGENHARIA
UNIVERSIDADE DO PORTO

CANDIDATO	*Margarida Pereira Moutinho Cavaco Mata*	*Código*
TÍTULO	*nTopology optimization applied to additive manufactured hydrofoil wing components*	
DATA	*__ de _____ de _____*	
LOCAL	*Faculdade de Engenharia da Universidade do Porto – Sala _____ - __:__h*	
JÚRI	*Presidente*	*DEMM/FEUP*
	Arguente	*DEMM/FEUP*
	Orientador	*DEMM/FEUP*

Resumo

O presente trabalho tenta responder ao desafio proposto pela empresa 4DCTech, Unipessoal, Lda. onde foi realizado o estágio curricular. Foi proposto o desenvolvimento de componentes para hydrofoils para um barco de testes não tripulado.

Os foils são um componente com uma forma hidrodinâmica que produzem a força de sustentação, elevando o barco e aumentando a sua velocidade. Usando o software Fusion 360, foi desenvolvido um mecanismo que altera o ângulo de ataque das asas de hydrofoil. Depois, usando o nTopology e o Eiger os componentes foram otimizados e preparados para a manufatura aditiva (AM) com o objetivo de reduzir a massa. A tecnologia AM escolhida foi extrusão de material (MEX) com as impressoras da Markforged Metal X e Mark S.

Os passos de otimização funcionam de uma forma iterativa, em que cada alteração necessita de validação, que consequentemente podem levar a novas modificações que serão novamente verificadas.

nTopology é um software inovador, que proporciona ao utilizador um maior controlo nos parametros da otimização. A workflow criada é personalizada e pode ser reutilizada, adaptando-se aos três (3) materiais escolhidos: Inconel 625, Onyx reforçado com fibras de carbono e Onyx. As estratégias de desenho generativo estudadas para os dois modelos de asa foram Field-driven design, estruturas lattice e otimização topológica.

A criação de uma casca variável foi uma forma eficiente de reduzir a massa, diminuindo até 37% numa das asas de Inconel. A otimização topológica de uma pequena alavanca de Inconel alcançou uma redução de 66%. Comparando os custos de material e o peso final, concluiu-se que a solução adequada é a manufatura das asas de Onyx reforçado com fibras de carbono, com uma massa estimada de 340 g e um custo total de material de 450 USD.

Palavras-Chave

Manufatura aditiva; Extrusão de Material; Hydrofoils; Onyx; Onyx reforçado com fibras de carbono; Inconel; Desenho generativo

Abstract

The present work tries to answer the challenge provided by the 4DCTech, Unipessoal, Lda. where the curricular internship took place. It proposed the development of hydrofoil components for an unmanned boat for test control.

Foils are components with a hydrodynamic shape that produces the lifting force and elevate the boat above the water increasing speed. Using Fusion 360 it was developed a device that could change the angle of attack of the hydrofoil wings. Then, using nTopology and Eiger the components were optimized and prepared for additive manufacturing (AM) with the objective of weight reduction. The AM technology chosen for this production was Material Extrusion (MEX) with the Markforged printers Metal X and Mark X.

The optimization steps function in an iterative process in which each alteration made to a design requires validation, which can lead to a new set of modifications that will need to be verified.

nTopology is an innovative software that gives the user greater control over the optimization parameters. The workflow created is customizable and was reused and adapted for three (3) materials Inconel 625, Onyx reinforced with Carbon Fibers, and Onyx. Field-driven design, lattice structures, and topology optimization were the generative design techniques applied to the two model solutions for the foil wings.

Creating a shell of variable thickness proved to be an efficient way to reduce mass, decreasing up to 37% in an Inconel wing. The topology optimization of an Inconel lever achieved a 66% decrease in mass. Comparing the material cost and weight it was concluded that the suitable solution would be carbon fiber reinforced Onyx wings, with a total estimated mass of 340 g and 450 USD material cost.

Key Words

Additive Manufacturing; Material Extrusion; Hydrofoils, nTopology; Onyx; Carbon fiver reinforced Onyx; Inconel; Generative design

Agradecimentos

Começo por agradecer ao Professor Manuel Vieira pela disponibilidade, esclarecimentos e preciosas sugestões. Agradeço à Professora Elsa Sequeiros pelo encorajamento e pelas generosas apreciações. Agradeço o apoio e paciência do Engenheiro José Costa. Sem o contributo dos três, esta dissertação estaria com certeza mais pobre.

Obrigada ao Engenheiro Ricardo Bencatel pela oportunidade oferecida e acompanhamento e suporte técnico para responder ao desafio proposto.

Agradeço os contributos do Professor Marcelo Moura e dos Engenheiros Bruno Peixoto e Pedro Costa da Norcam.

Uma palavra aos meus colegas e amigos, André Morais, Mariana Pinto e Pedro Ferro. Obrigada pelo companheirismo e partilha nesta caminhada.

Um agradecimento especial aos meus pais, Suzana e Elísio que, desde muito cedo, procuraram fomentar o meu gosto pelo conhecimento e estimular a minha criatividade. À minha irmã pela solidariedade e momentos de alienação. À família que aguentou estoicamente as explicações dos mecanismos e teorias sobre hydrofoils. Aos meus avós pelo exemplo de persistência e entrega.

A todos, Obrigada!

Table of Contents

List of Figures

List of tables

List of abbreviations

ABS - Acrylonitrile Butadiene Styrene

AFP - Automated Fiber Placement (AFP)

AM - Additive Manufacturing

BJ - Binder Jetting

CAD - Computer-Aided Design

CAE - Computer-Aided Engineering

CAM - Computer-Aided Manufacturing

CFRP - Continuous Fiber Reinforced Plastics

DED - Direct Energy Deposition

DfAM - Design for Additive Manufacturing

DLP - Digital Light Processing

DMLS - Direct Metal Laser Sintering

DOD - Drop on Demand

EBAM - Electron Beam Additive Manufacturing

EBM - electron beam melting

FDM - Fused Deposition Modeling

FE - Einite Element

FEA - Finite element analysis

FEM - Finite Element Modeling

FFF - called Fused Filament Fabrication

HSHT - High Strength High Temperature

LENS - Laser Engineered Net Shaping

LOM - Laminated Object Manufacturing

MEX - Metal Extrusion

MFP - MarkForged Print

MJ - Material Jetting

MSLA - Masked Stereolithography

NACA - National Advisory Committee for Aeronautics

NASA – National Aeronautics and Space Administration

PA - Polyamide

PCB - Printed Circuit Board

PDEs - Partial Differential Equations

PLA - Polylactic acid

PP - Polypropylene

ROM - Rule of Mixtures

RP - Rapid Prototyping

SLA - Stereolithography

SLM - Selective Laser Melting

SLS - Selective laser sintering

STL - Standard Triangle/Tessellation Language

UC - Ultrasonic Consolidation

1. Introduction

The present work was developed as part of the conclusion to the master's degree in Materials Engineering at the Faculty of Engineering of the University of Porto. The current study tries to answer the challenge provided by the company 4DCTech, Unipessoal, Lda. where the curricular internship took place. It proposed the development of hydrofoil components for an unmanned boat for test control. This work focused on developing a device that could change the angle of attack of the hydrofoil wings, as well as the preparation and optimization for additive manufacturing with the objective of weight reduction.

The dissertation is divided into four (4) main sections: the literature review, the development and optimizations, the results and discussion, and the conclusions. The literature review explores what hydrofoils are and the materials used. It also explores some of the processes and materials available in additive manufacturing, along with the exploration of design for additive manufacturing concepts. The development and optimization section initially covers the design of the wing and its rotation mechanism in Fusion 360. Then it reports the various operations and optimization attempts for different materials using nTopology. The results and discussion compare the results and discuss the adequate solution. Finally, in the last section, the conclusions of this work are drawn.

2. Literature Review

2.1. Foils

A foil is a component designed to produce lifting force acting across the direction of the incoming flow. The foil's lifting action arises from the difference in the average pressure of the fluid over the upper and lower surfaces of the lifting foil [1]. The objective in the design of the foils is to obtain the necessary lift with the lowest drag possible [2]. The typical uses for these foils are aircraft wings, hydrofoils, rudders, stabilizers fins, propeller blades, and sails [1].

Horatio F. Philips created the first patented airfoil in 1884 and conducted the first wind-tunnel experiments on airfoils. Later, in 1902 the Wright brothers carried out their airfoil tests in a wind tunnel and developed relatively efficient airfoil shapes that contributed to the success of the first flight on December 17th, 1903 [3]. Those designs at that time were very customized and personalized, and in the 1930s, NACA - National Advisory Committee for Aeronautics – (that would later become NASA – National Aeronautics and Space Administration) developed and tested a series of airfoil shapes that were constructed rationally and systematically, shown in Figure 1, that is still used to this day [3, 4].

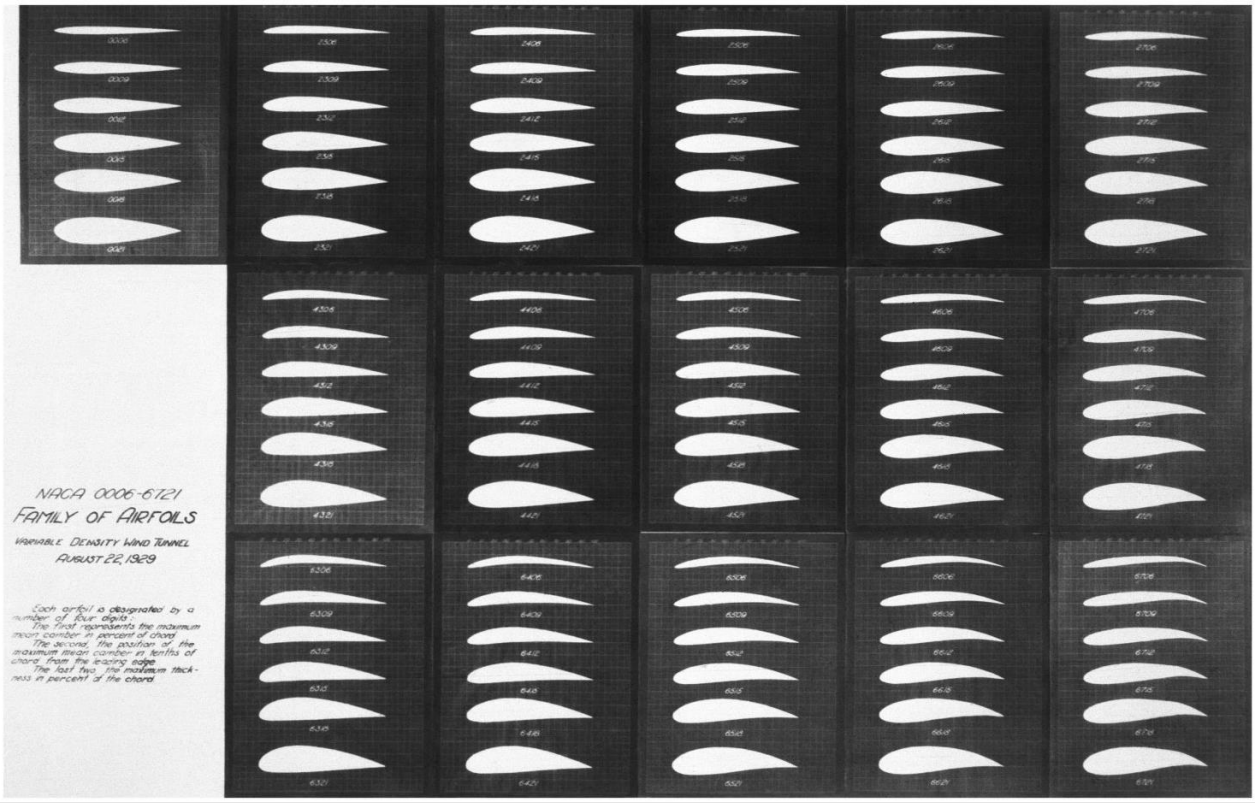

Figure 1- NACA 4 Digit series Airfoils [4]

The advancements in the aeronautic industry led to many improvements in foil development throughout the years [3]. In 2012, hydrofoils were introduced in America's Cup racing boats, revolutionizing the sailing world, and becoming a vital component for

their performance, where teams are increasing their efforts in optimizing the designs. They aim to minimize the drag force in a large range of boat speeds while ensuring that at lower speeds there is enough lift force for the boat to fly [5, 6].

As it was previously seen in some examples in Figure 1, foils can have many distinctive designs that vary in chord size, thickness, and camber. As seen in Figure 2, the chord line is a straight line that connects the leading edge – the most forward point - and the trailing edge – the most rearward point of the airfoil. The shape at the leading edge is usually rounded. The mean camber line is the line that marks the midway points between the upper and lower surface. The thickness is the distance between the upper and lower surfaces, while the camber is the maximum distance between the mean camber line and the chord line. An airfoil with a coincident mean camber line and chord has a camber of 0 and is called a symmetrical airfoil [3].

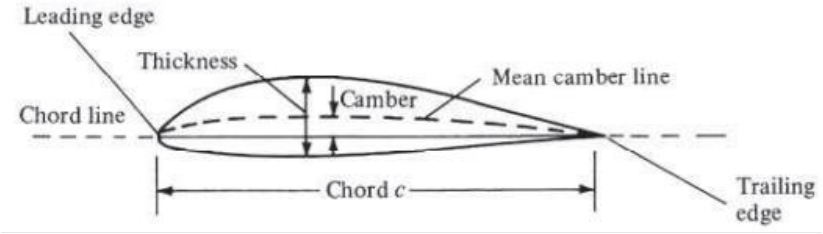

Figure 2- Foil nomenclature [3]

2.1.1. Hydrodynamic and Forces applied on the foils

A fluid is considered a continuous medium that will deform continuously, changing its shape and boundaries to its container, being incapable of remaining in a fixed shape of its own, unlike solid materials. There are two types of fluids, liquids and gases since the movement between molecules in gases and liquids have a similar physical characteristic [1, 2]. Liquids are more compressible and naturally occupy a fixed volume in the lowest available space within a container whilst in gases the intermolecular forces are weaker, becoming more easily compressed and it is able to expand in order to fill the space available within a container [1, 2]. Usually, the distinctions between these two fluids, for flows at low speed are negligible, since the changes in pressure are not large enough to change density [1]. Therefore, some physical behaviors in liquids can be determined based on the behavior of gases, and vice versa.

In a solid the molecules are closely packed together by high intermolecular forces forming a rigid structure and when within a fluid, it is in a state of stress involving direct stress and shear stress distributed over the body surface [1]. The direct stress acts normal to the surface and is called fluid pressure (p) and the shear stress (τ) acts tangential to the surface and creates friction [1, 2]. The resultant force on the body is the integration of the net effect of the surface pressure distribution and surface shear stress distribution, over the complete body. Figure 3 shows the representation of these forces on a foil surface. This resultant/net force can be split into two components, the lift that is perpendicular to the fluid stream (Uo) and drag that is parallel to the fluid stream [1, 2].

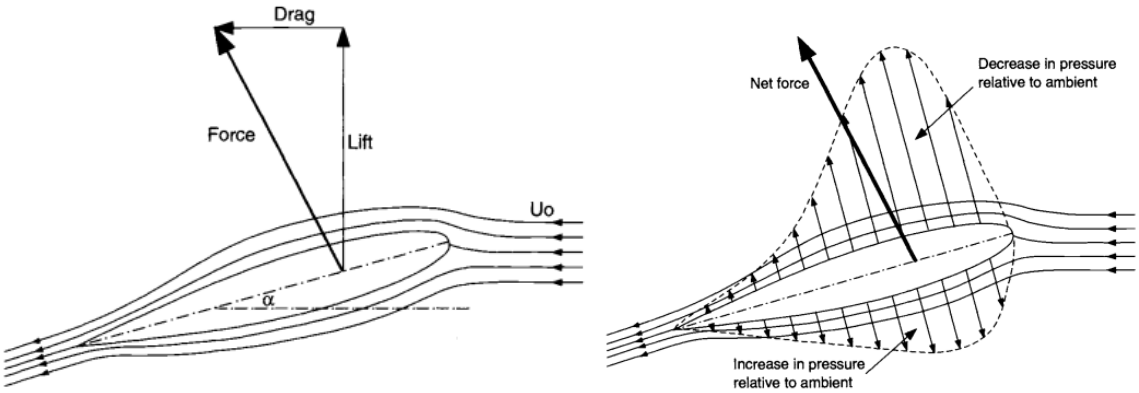

Figure 3 - Forces (left) and pressures (right) on a lifting foil [1]

There is another way to explain lift force. To understand that it is necessary to know that a streamline is an imaginary curve in the fluid in an instant and the velocity of every particle on the streamline is in a direction tangential to the line [1], as it is shown in Figure 3 and Figure 4. In Figure 4 it is represented the way the streamlines are affected by the presence of the foil. We can observe that it gains curvature alongside the foil and therefore has centripetal acceleration, pointing to the curvature's center, and in this case pointing down. When we look at the portion above the foil, the pressure on the fluid that is further away from the foil is higher than the pressure alongside the foil's top surface. Since the pressure that is further away from the foil is considered the pressure of the environment, the pressure on the top surface of the foil is lower than the environment pressure. The opposite happens below the foil, where the pressure alongside the foil's bottom surface is higher than the pressure in the fluid further below the foil, considered to be the environment pressure. The lift force is created due to both of these effects that create a pressure difference between the top and bottom surfaces, where the pressure immediately below the foil is higher than the pressure immediately above the foil [7]. This explanation is a simplification since molecules in a fluid are in constant motion, and it ignores the variation of pressure in the fluid [2, 7].

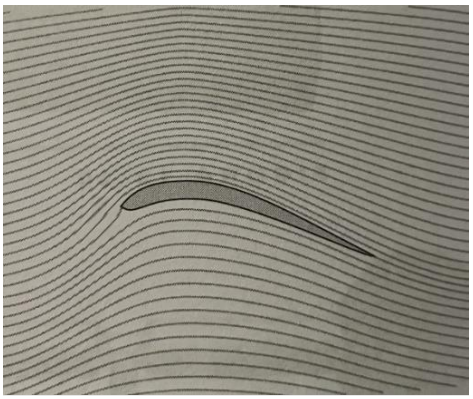

Figure 4 - Thin airfoil and its effect on the streamlines [7]

It is also important to note that in a fluid in motion, one part may be traveling at a different velocity from another part, and both speed and direction can vary. [2]. For

example, in the streamline that moves alongside the foil's surface, the portion of the fluid in front of the leading edge has environmental pressure and as this fluid portion moves towards the foil's top surface, it gains speed due to the lower pressure, as explained by the Venturi effect [7].

The fluid's interactions with the foil create some phenomena that may condition the foil performance when they occur, depending on the conditions of the fluid and the shape of the foil. Cavitation happens when the local fluid pressure drops to the pressure at which the liquid vaporizes. This may occur when suction (negative pressure) becomes high on a lifting device and may negatively affect its performance forming voids or cavities in the liquid. This phenomenon can happen on marine rudders, control surfaces, support struts, and propellers. Ventilation (or aeration) is like cavitation, but the voids are filled with air drawn from the free surface. In the voids, the pressure is usually atmospheric, but it may eventually close, and the pressure drops as the volume of the void increases. This may occur on surface piercing rudders [1].

2.1.2. Materials used in hydrofoils

Hydrofoils are usually made with continuous fiber reinforced plastics (CFRP) [8]. Fiber-reinforced plastics are a well-established way to improve the material properties of plastics by embedding reinforcing fibers and have become the most common choice for lightweight design. They are anisotropic materials that can reach superiority over other materials like metals and engineering plastics when adjusting the material properties according to the future conditions of the product [9]. However, some compromises must be made during the design process because it creates a layered structure that cuts and lays down flat semifinished goods, like prepreg, and therefore are hard to automate [8].

Hydrofoils usually use the traditional hand lay-up method, or more recently automated fiber placement (AFP) [8]. The hand lay-up technique is the oldest method for woven composite manufacturing and needs to following steps. First, a surface treatment is made by releasing an antiadhesive agent in the mold surface to avoid the polymer sticking to the surface. Then a thin plastic sheet is applied at the top and bottom of the mold plate to get a smooth surface. The woven reinforcement is cut with the desired shapes, then is placed on the surface mold and a resin mixture is uniformly brushed and spread on the mold surface, as well as infused in the woven reinforcement. After this, mats are placed on top of these layers, and with rollers, pressure is applied to remove trapped bubbles and excess polymer. Then the mixture needs to cure and in the end, the mold is opened and the woven composite is removed from it [10]. This method allows the production of complex and long shapes and does not require expensive material. However, the production time is longer, and the high amount of manual work may vary the quality, according to the operator's skills. It is hard to automate the production due to the complexity of some shapes and compromises that need to be made. However, AFP can provide higher productivity, repeatability, low material waste, and shorter production

times and a robot arm permits constant contact pressure creating a constant thickness. However, there are limitations in the mold shapes [8, 9].

2.2. Additive Manufacturing

Additive Manufacturing (AM), also known as 3D printing, is a term that includes the family of manufacturing technologies that joins sequential units of standard input material to fabricate a discrete physical product. Depending on the chosen method, it adds material layer-by-layer, and they are united together by applying thermal, chemical, or mechanical energy. It is a relatively recent technique, described as a disruptive technology since it provides new and significant commercial opportunities mostly in design innovation and enables the production of a low volume of high complexity components. There are many differences and benefits when compared to other traditional manufacturing techniques of material removal, deformation, and solidification, such as subtractive manufacturing - sequentially removes material from a bulk input to create a new component - and formative manufacturing - physically changes the geometry of a material to shape a new part [11, 12].

Its differences make this process a game-changer and its advantages facilitate the evolution of the manufacturing business and industry because it builds a part layer-by-layer selectively depositing material, minimizing waste of raw material, and therefore promoting a sustainable manufacturing environment as well as providing freedom of design and new possibilities in complex geometry creation [12, 13]. An example of this is shown in Figure 5 with a topology optimized automotive upright bracket, designed in nTopology [14].

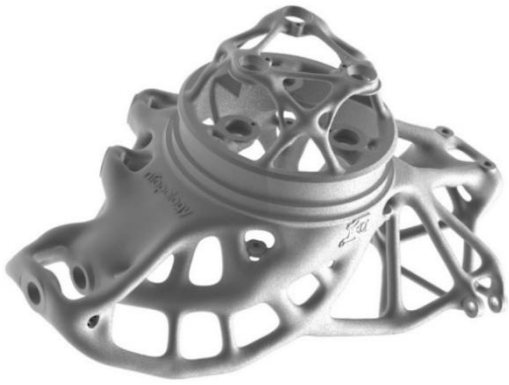

Figure 5 - Lightweight and organic-looking topology optimized automotive upright bracket designed by Lions Racing Team e.V. [14]

Additive manufacturing and 3D printing have been around since the 1980s and it started as rapid prototyping (RP) technique, creating prototypes for fitting tests and visual evaluation. RP is a fast and more cost-effective process for fabricating prototypes for product development within the industry, but it has limitations in fulfilling the needs for mass production. The first patented 3D printing technique was for stereolithography (SLA) in 1983 by Charles (Chuck) Hull [13]. SLA is a liquid-based process that uses an ultraviolet laser to solidify/cure the photosensitive polymer resin. Upon the solidification of each

layer, the build platform lowers enabling the creation of a new [12]. In 1992, after many advancements in the additive manufacturing field, Scott Crump patented the first fused deposition modeling (FDM), a Material Extrusion (MEX) technique in which a polymer filament is continuously fed to a heated nozzle where the material is liquified and selectively deposited [13, 15]. Dr. Carl Deckard developed the first Selective laser sintering (SLS) technology for polymers in the late 80s and paved the way for metal 3D printing. Then Fraunhofer Institute patented the first laser melting of metals in 1995. Since then, there has been a lot of development in metal 3D printing, and nowadays the most used methods for 3D printing in metals are Direct Metal Laser Sintering (DMLS) and Selective Laser Melting (SLM), followed by Binder Jetting (BJ) and MEX [16].

Currently, there are many different techniques in AM and industries are now more focused on design optimization relating it to complex design [13]. The wide variety of AM technologies and processes, lead to the creation of ISO/ASTM 52900, in 2015 to standardize the terminology and classify the different types of 3d printers. There are seven (7) additive manufacturing technologies, that can be divided further into processes [17, 18]. Material Extrusion is the technology behind the FDM process (also called Fused Filament Fabrication - FFF) and a solid filament is pushed, heated, melted, and selectively deposited. It is one of the most common (and affordable) processes and has a wide range of materials that can be printed, such as thermoplastics, carbon fibers, metal pastes, biogels, and even concrete and chocolate. Vat Polymerization was the first AM technology and is behind SLA, Digital Light Processing (DLP), and masked stereolithography (MSLA), to name a few processes. Each process used a different light source to selectively cure layers of a photopolymer resin. Another technology is Powder Bed Fusion which creates a power bed by laying thin layers of powder and uses thermal energy to selectively induce fusion (complete or partially) between powder particles. It is used for metals, thermoplastic, and ceramic powders, and can create functional parts with complex geometries and excellent mechanical properties. Some of the processes in this technology are SLS, SLM, electron beam melting (EBM), and DMLS [17, 18]. Similar to SLS, Binder Jetting is another technology that selectively binds areas of a powder bed with a liquid bonding agent. This process does not require heat and when the object is completed it needs to cure to gain its strength. It can be used for polymers or metal powders, sand, and ceramic-metallic composites [17, 18]. One more technology is Material Jetting which droplets of a photopolymer or wax are selectively deposited, forming layers cured by exposure to light. In the processes that use this technology, such as Material Jetting (MJ), Polyjet, and Drop on Demand (DOD), it is possible to print different materials in one object and allow the creation of supports with secondary material. Direct Energy Deposition (DED) can be used as a 3D printing technology as well as used to repair objects in the processes of Laser Cladding, Laser Engineered Net Shaping (LENS), and Electron Beam Additive Manufacturing (EBAM), to name a few. The material is fused and deposited simultaneously by a thermal energy source, such as a laser, electron beam, or plasma. The feedstock deposited is usually a metallic powder or wire. Finally, Sheet lamination is the technology behind Laminated Object Manufacturing (LOM), and Ultrasonic Consolidation (UC) is a form of 3D printing in which sheets of very thin material are staked

together and laminated. It can be used in polymer, metal, and paper sheets and can be fused using heat or sound [17, 18].

In general, AM has a lower material wastage, which is very important since, in some, industries, such as aerospace, it is common to machine away as much as 80% of the raw material stock [12]. AM can be applied to the manufacture of high-performance parts in the industry because it allows the use of different materials, creates intricate geometries, and design customization with little excess tooling cost, where products can be made lightweight, with optimized usage of material and reduction in multiple manufacturing steps and processes [12, 13]. One of the main reasons that justify the application of AM in the industry context is the reduction of cost and few limitations in product design complexity (in comparison with traditional manufacturing). Complex internal features can be developed to optimize the product performance parameters that otherwise would be impossible [13]. It also possibilities the manufacturing of small batches, in which tolling would make it more expensive, such as customizable medical devices for patients, aeronautical and aerospace components, where performance is supreme and replacement parts, to mention a few. These characteristics have caught the attention of researchers and the aerospace, automobile, medical, and tool and die industries [12].

2.2.1.MEX - How it works

AM involves a series of processes, from design development to final product manufacturing, and the steps may vary according to the manufacturing method used. It all starts with a digital model of the part designed using Computer-Aided Design (CAD) software. The model's design can be created from scratch, or 3D scanning and reverse engineering can be used to develop the digital model [19]. Afterward, this digital model is converted into a Standard Triangle/Tessellation Language (STL) file, which uses triangles to store information on model surface geometry and is then fed to the slicer program. Here the model is divided into layers and is set the 3D printing conditions according to the machine that will be used, a crucial step in determining the quality of the printed parts. The slicer then generates a G-code that defines the movement of the extruder and platform during printing [19].

The printing process depends on the type of AM method involved. As previously mentioned, MEX is a process based on material extrusion technology and where a filament is pulled and fed into a melting head that heats the polymer above the glass transition temperature, melting it and then extruding it through the nozzle, as it is represented in Figure 6. The nozzle moves and deposits the molten filament layer by layer based on the G-code instructions, which controls the nozzle's movement, the amount of material extruded, and extruding time. The material solidifies firstly on the build plate and afterward onto other already deposited layers [19-21]. When laying the sequential layers, there are different strategies for nozzle and building platform movement. In some cases, the build platform moves upwards or downwards in the Z-direction and the nozzle moves in the XY-direction [19], in other cases the nozzle moves in the ZX-direction and the

platform moves in the Y-direction. In either way, layer height is the distance of the movement in the Z-direction and usually varies from 100 to 300 μm [19].

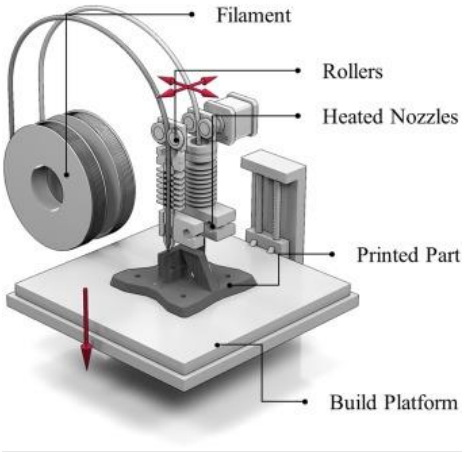

Figure 6- Schematic representation of MEX with two materials from [22]

In MEX the most common material filaments are thermoplastics such as Polylactic acid (PLA), Acrylonitrile Butadiene Styrene (ABS), Polypropylene (PP), and Polyamide (PA), and their diameter can vary from 1.75 to 2.85 mm depending on the nozzle used in the machine. In recent years MEX-based polymers research has increased because there is significant flexibility that can be used in many different applications including biomedical applications, automobile parts, aerospace and aircraft in industries, sport and music equipment, and household applications [19]. There are MEX systems that can print composite material with the incorporation of fibers, either continuous or chopped fibers and there are many new special materials available like metal, wood, and clay-filled polymer, bio-materials, chocolate, polyurethane foam, silicone, and others [21].

The quality and mechanical performance of an MEX polymer printed part depends on the proper tunning and control of several factors and variables. The quality verification begins in the STL file, which must have the correct surface geometries without errors to avoid significant geometric and dimensional differences between the part and CAD model [19, 23]. When slicing, many important parameters must be considered, including the nozzle diameter, deposition speed, layer thickness, infill style, raster orientation and pattern, and flow rate. Another factor determining the mechanical performance is the build orientation chosen for the printed part, which may induce anisotropic properties in the final product, and it also might produce geometries that require building supports. The temperature conditions are an important variable to control namely the extrusion temperature at the nozzle and platform. The temperature conditions are an essential variable to control, namely the temperature of extrusion at the nozzle, as well as in the platform and environment. These temperatures are set according to the chosen material, and it is also necessary to control the variations in water content, density, and filament quality. Another, key factor in controlling the quality is the machine calibration, which guarantees the correct implementations of all the variables set. After print, according to the material and manufacturing process, post-processing may be necessary to improve the product quality even further [19]. Still, some limitations must be controlled and

overcome, such as problems with porosities and detachment between layers. Likewise, the aesthetic aspect can be a disadvantage, since the layer thickness restricts the minimum representable geometry and creates the staircase effect, making layers distinctly visible and generating anisotropy in the process [9, 23]. Also, the mechanical properties of 3D printed parts usually deviate significantly from the material bulk properties due to these anisotropic structures formed during printing [20].

2.2.2.MEX in Metals

There are three (3) types of Additive manufacturing in metals based on Material Extrusion. They can be Filament-based, Syringe based, and Screw-based, however the most used and commercialized is the filament-base [24]. Since this method is so widely used, FDM in metals commonly referred to as just Material Extrusion (MEX).

Part of the filament based MEX process is similar to the one processed in polymers since it builds a part layer-by-layer by extruding material through a nozzle, however, the feedstock used is a filament based on a mixture of metal powder and polymer binders [16]. Usually, the metallic powder content ranges from 50-65% in volume, and in some cases can be up to 80% [24]. The materials available to print in Markforged printer Metal X are 17-4 PH Stainless Steel, Copper, H13 Tool Steel, Inconel 625, and A2 and D2 Tool Steel [25]. During printing, if support material is necessary, it is deposited a ceramic material, with a different nozzle, in between the support and the part to facilitate its removal [16].

Initially, MEX forms a metal/polymer composite due to the nature of the feedstock, and because of that, the process is divided into three steps: printing, debinding, and sintering. The deposition of material (printing step) forms a "green part" which has the oversized geometry of the part. However, it does not have the wanted strength and properties since the metallic powders are only held in place by the polymeric binder. To remove the binder from the "green part", it must be washed in a solution for several hours (debinding) and then placed in a furnace to burn the remnants of the polymer and consolidate the metallic powder (sintering). The final part is fully metallic and can shrink up to 20% after sintering [16, 21]. Eiger is the slicing software connected to Markforged printers that control the parameters of the printing, debinding, and sintering processes. When the STL file is placed on the software, it considers the shrinkage of the part according to the material and it automatically compensates for that geometrical contraction.

Inconel 625 is a nickel-chromium based superalloy and is one of the materials available by Markforged. It is highly resistant to corrosion and high temperatures. According to Makforged, after sintering Inconel 625, the reported relative density is 96.5%, and the mechanical properties do not deviate substantially from a Wrought AMS 5599 Inconel, having an ultimate tensile strength of 765 MPa and a 0.2% Yield strength of 334 MPa. The Figure 7 shows the similarities between the microstructure of hot rolled Inconel 625 alloy [26] and an Inconel 625 printed in Metal X, washed in Wash-1, and sintered in Sinter-1 [27].

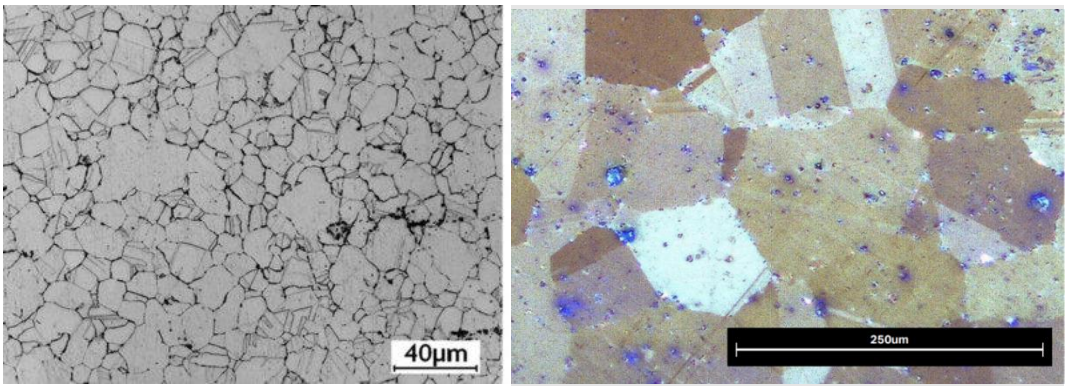

Figure 7 – Final microstructure of Inconel 625 after sintering from Markforged [27]

2.2.3. Carbon fiber composite fabrication by MEX

Fabrication of fiber composites involves adding two different materials to form a single component and is considered an original form of additive manufacturing [28]. As stated before, the established traditional methods of fiber reinforced composite manufacturing involve a manual layup, resin transfer molding, fiber replacement, and automated filament winding. It is a process limited to simpler geometries, requiring curing, complex tolling, and expensive equipment, since it needs pressure to be applied over an entire surface area. It is also characterized as a method that needs intensive labor and may create hazardous waste material. More recently AM has been considered an alternative to streamline and automate the fiber fabrication process [9, 20, 28]. Incorporating fibers in a polymeric matrix can significantly improve the strength of a polymer and provides a key role when used in AM polymers. Various AM techniques can produce parts with fiber composites, but the most preferable method is MEX [19]. One of the major companies developing commercial 3D printers capable of processing continuous fiber reinforced composite materials is Markforged [20].

MEX is a more straightforward and economical method to produce these composites and it may provide some advantages since the reinforcement can be accurately placed and each layer of the laminated structure can be optimized [19, 20]. Additionally allows the adjustments in the fiber placement and orientation to better suit the component's requirements while giving a new level of freedom in design since it doesn't use the traditional flat layer construct, allowing adjustment of fiber orientations in all dimensions [9]. However, it is a relatively underdeveloped research topic, and some aspects bring some limitations such as fiber/matrix interactions and void formation [19, 20]. Many variables must be considered in developing these composites, such as fiber/matrix weight percentage and interaction, and fiber type, length, and orientation. Adding carbon fibers, carbon nanotubes, nanoparticles, and other synthetic fibers to the polymer filaments improves the mechanical properties of the composites produced by AM. It is considered a very cost-effective way to produce fiber composites although this technique still has some issues need to be solved [19].

It is also noteworthy to state that there is a lack of mechanical properties related to the parameters, like the fiber content present in the filament and performance under static loading. Furthermore, due to the complexity of the AM parts, analyses made based on finite element modeling (FEM) should consider an orthotropic model for these composite materials, which includes the different properties of the fiber and matrix [23], and the influence of the fiber placement direction, since it isn't an isotropic material. However, isotropic models can be used as a simplification [23].

In MEX there are three (3) possibilities to introduce the fiber reinforcement in the thermoplastic matrix, considering the time and location of the fiber embedding process, which can happen before the printing process, in the printing head, or on the component. Embedding before the printing process is a more straightforward approach since the composite filament is prefabricated and fed to the machine. As a result, this method does not require changes to the machine, being already commercially available using a filament with a constant fiber volume ratio. Another alternative is embedding in the print head where the reinforcing fiber is supplied as dry roving to the head, and mixed with a thermoplastic matrix, offering the possibility of adjusting the fiber volume ratio during the printing process. This can cause some problems because dry roving is more challenging to handle than a pre-impregnated filament and can induce air inclusions during the infiltration process. The third method is embedding on the component, which has a closer approach to conventional fiber placement, since the fiber embedding takes place on the component using two separated systems, like the printer shown in Figure 6, where one nozzle deposits matrix and a second nozzle places the fiber [9].

The latter approach is a more complex process with more variables to consider like the adequate adhesion between fiber and matrix and therefore more susceptible to defects [9]. Markforged has MEX composite printers that can produce CFRP with this third approach. Figure 8 shows a scheme of the deposition mode in the printer machine Markforged X7 that has this dual extruder system, in which the first nozzle behaves as a standard filament extruder, depositing polymer material mainly in the outer walls and parts of the matrix (a and b from Figure 8), while the nozzle deposits a continuous reinforcing filament (c and d from Figure 8) [29, 30].

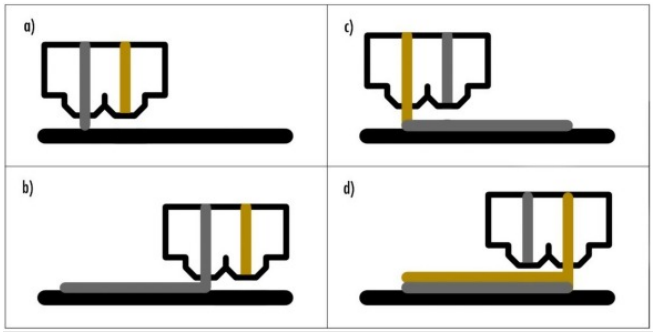

Figure 8 - Deposition mode scheme of Markforged X7 printer [29]

The materials used for these composites in the matrix are Onyx, Onyx FR (Flame Retardant), Onyx ESD (static-dissipative), and Nylon [30]. Onyx is based on tough nylon

filled with micro carbon fibers, making it 3.5 times stiffer than conventional nylon and reducing shrinkage and warping. Therefore, this Onyx filament is a composite since it comprises microscale carbon fibers embedded in a polymer matrix that melts when heated and then extruded [31, 32]. The addition of short fibers to the printing filament done in Onyx, increases the stiffness of the part, but the strength increase is limited since fiber pull may occur before fiber breakage [20].

The fibers used for the reinforcement are carbon fibers, fiberglass, Kevlar, and High Strength High Temperature (HSHT) Fiberglass [30]. These continuous fiber filaments are made of a bundle with a 30-40% volume fraction of carbon, glass, or Kevlar fibers, within a nylon matrix that acts as a binder and allows for the adhesion of inter and intra layers. In the continuous fiber filament there is approximately [33]. Avanzini, A. et al. [33] reported that the carbon filament provided by Markforged has a diameter between 0.340 and 0.374 mm and consists of several carbon fibers embedded in a nylon matrix with a fiber volume fraction that ranges between 34.5 and 36.4%.

Figure 9 shows the comparison of their mechanical properties, flexural stress (MPa) function of flexural strain, for the mentioned materials. Still, there are some limitations due to the selection of different materials available is small, limiting the application areas and design flexibility [20], and information about mechanical characterization is still very scarce. Although the macroscopic properties for each filament are documented by Markforged and shown in Figure 9, their exact composition and constituent properties are not disclosed [30, 33]. Besides, the printing process parameters are controlled by Eiger software [33].

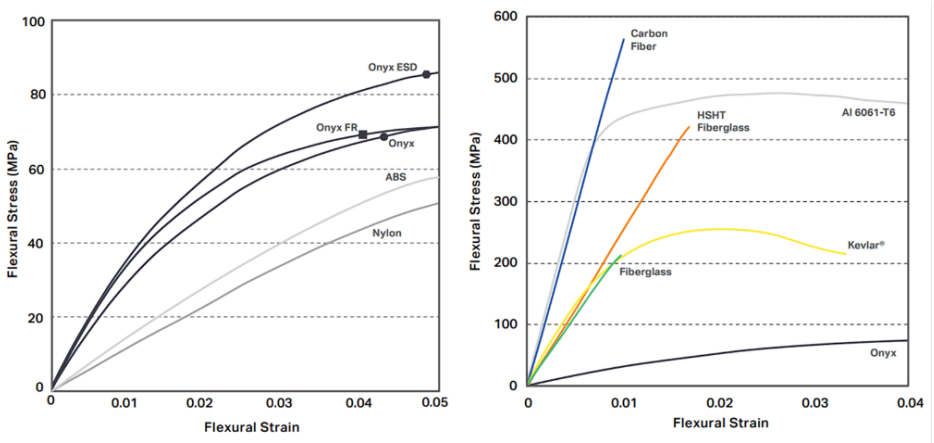

Figure 9- Flexural Stress function of Flexural strain, for composite-based materials (left) and fiber reinforcement (right) [30]

Markforged's latest property datasheet (from January 2022) indicates that Onyx has a tensile modulus of 2.4 GPa, a Tensile Stress at a Yield of 40 MPa, and a density of 1.2 g/cm^3. On the other hand, Carbon Fiber was tested with unidirectional fibers and has a Tensile Modulus of 60 GPa, a tensile stress at a yield of 800 MPa, and a density of 1.4 g/cm^3. They also note that part and material performance may vary according to some parameters, such as part design, fiber layout, and specific load conditions, to name a few [30].

2.2.3.1. Determination of mechanical properties in composites

Composite materials generally are anisotropic, which means they have different properties depending on their direction. The Cartesian coordinate system defines the directions, and they can be described by looking firstly at the lamina – the single layer of material -, since laminate composites are a combination of plies/lamina stacked together. As seen in Figure 10 the "lamina" coordinate system uses the notation x_1, x_2, and x_3, where x_1 corresponds to the direction of the fibers in a unidirectional ply and x_3 is the direction of the thickness. Each lamina in the laminate composite has a coordinate system based on the primary fiber direction and can be considered an orthotropic material. For convenience during structural analysis, the global laminate coordinate system is denoted by x, y, and z, where x is parallel to the longitudinal axis of the fibers (if there is one) and z is the thickness [34].

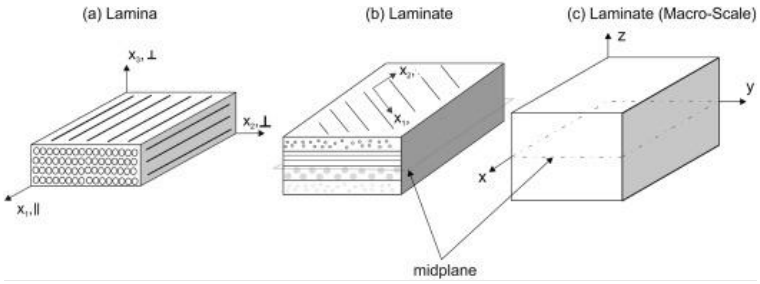

Figure 10- Coordinate system for a) lamina with local coordinates, b) laminate with many laminas stacked together and c) laminate with global coordinate system [34]

Robert Hooke created Hooke's law that developed the constitutive equations that defined the linear characteristics of a material. Using Hooke's law, it is possible to define orthotropic materials by the nine (9) constants in the compliance matrix. In that matrix it is present Youngs Modulus (E_i), Poisson's ratio (ν_{ij}), and shear modulus (G_{ij}) in the different directions *ij*. When the long fibers are along the 1-axis direction the G_{12} and G_{13} indicate the axial shear moduli and G_{23} is the out-of-plane shear modulus.

The rule of mixtures (ROM) is a simpler method used to predict the elastic properties of composite reinforced with aligned continuous fibers, based on the ratio between fiber (V_f) and matrix (V_m) content [35, 36]. Knowing the densities of the fiber (ρ_f) and matrix (ρ_m), and the elastic modulus of the fiber (E_f) and matrix (E_m), ROM uses a set of equations that allows the determination of the density of composite (ρ_c) according to

$$\rho_c = \rho_f V_f + \rho_m V_m \quad (1)$$

as well as the elastic modulus in the longitudinal direction (E_{11}) calculated by

$$E_{11} = E_f V_f + E_m V_m \quad (2)$$

and the elastic modulus in the transverse direction (E_{22}) by [35, 36]

$$\frac{1}{E_{22}} = \frac{V_f}{E_f} + \frac{V_m}{E_m} \quad (3)$$

It is also able to determine the in-plane shear modulus (G_{12}) based on equal shear stress assumption with the equation 4, knowing the shear moduli of the fiber (G_f) and matrix (G_m) [36]

$$\frac{1}{G_{12}} = \frac{V_f}{G_f} + \frac{V_m}{G_m} \quad (4)$$

Markforged composite design guide explains that 3D printed composites are transverse isotropic, in which the material has a set of properties along an axis and a distinct set of properties on the planes normal to that axis. Therefore, it is necessary to consider print orientation during the design process, since in 3D printed reinforced with continuous fibers parts the strength on the XY plane is higher than along the Z-axis [32].

2.2.3.2. Experimental determination of the CFRP properties

This next section covers some experimental studies conducted to obtain values for elastic properties of polymeric composites reinforced with continuous fiber using MEX processes with Markforged machines, specifically Onyx reinforced with carbon fibers.

Fernandes et al. [31] studied the impact of fiber placement on the mechanical and viscoelastic properties of an Onyx reinforced with carbon fiber by comparing the "isotropic" and concentric fiber patterns, as seen in Figure 11 [31].

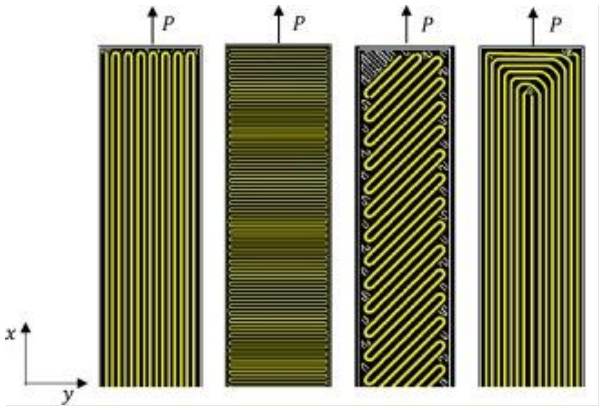

Figure 11- Section of tensile test specimens with "isotropic" pattern at orientation angles of 0º, 90º, 45º and concentric. White lines represent polymer and yellow for the fibers [31]

The "isotropic" fibers are the ones that are deposited unidirectionally in a zig-zag pattern and provide bending resistance in the XY plane. In contrast, the concentric pattern lays down material parallel to the perimeter of the model, providing resistance in the z-direction and strengthening the walls [31, 32]. When comparing the tensile results of continuous fiber reinforced with the Onyx samples it was found that the reinforced samples were ~23 times stiffer (~40 GPa), while concentric fibers were 14 times (546 MPa) and 0º "isotropic" fibers were 12 times (472 MPa) stronger, then Onyx (38 MPa), which showed a significantly higher deformation [31].

Fernandes *et al.* [31] also compared the different orientations of fiber placement in the isotropic patterns to obtain the mechanical properties in different directions. Figure 11 demonstrates the samples with three (3) different angles in the deposition of the fibers,

0º, 90º, and 45º and after tensile testing, the stress-strain curves were plotted to obtain the experimental values shown in Table 1- Mechanical properties of isotropic carbon fiber composite [31]. The subscripts 1 and 2 indicate the fiber and matrix direction in the elastic modulus (E) and the ultimate strength (σ), where 1 corresponds to the x-direction obtained from 0º, 2 to the y-direction obtained from 90º.

Table 1- Mechanical properties of isotropic carbon fiber composite [31]

E_1 (GPa)	E_2 (GPa)	E_x (GPa)	v_{12}	G_{12} (GPa)	σ_{1T} (MPa)	σ_{2T} (MPa)
39.4	3.1	5.6	0.3	2.5	472.0	24.5

Additionally, they reported that the samples with 0º and de concentric exhibited a linear behavior in the stress-strain curves until the catastrophic failure, unlike the remaining samples that reveal an elastic-plastic transition. Poisson's ratio is represented by v_{12} and is obtained by dividing lateral and longitudinal strain. The 45º angle sample was used to get the shear modulus G_{12} (in the plane XY) using equation 5, being E_x the transformed axial modulus from this 45º angle [31]:

$$\frac{1}{E_x} = \frac{1}{E_1}\cos^4\theta + \left(\frac{1}{G_{12}} - \frac{2\nu_{12}}{E_1}\right)\cos^2\theta\sin^2\theta + \frac{1}{E_2}\sin^4\theta \quad (5)$$

Fiber-reinforced composites are stronger and designed to carry loads in the fiber direction and transverse loads can cause early failure. Furthermore, the overall transverse strength can be lower than the strength of the matrix because of the imperfections and adhesion between the matrix and fibers [31].

Avanzini, A. *et al.* [33] used finite element (FE) techniques with embedded elements (EE) to simulate composite parts made by continuous fiber reinforced additive manufacturing and also calculated homogeneous orthotropic lamina values. Usually, this method can be applied to traditional composites where fibers are uniformly aligned. However, the 3D printed composited fibers can be laid in different patterns between different layers, proving to be more challenging to get accurate results. They noted that the out-of-plane shear moldi G_{13} and G_{23} could be considered the same as G12 and changing these values between 0.23 and 1.51 impacts the result lower than 1% [33].

Avanzini, A. *et al.* [33] also compared experimental values with results from finite element techniques. Three (3) rectangular samples were tensile tested, in which two (2) of them had unidirectionally reinforced layers (0º orientation) differing the number of roof and bottom layers, and another sample with four (4) different layer orientations (0º, 45º, 90º and 135º). The latter is stacked in a sequential pattern, creating a *quasi-isotropic* and symmetric composite as represented in Figure 12. Their results showed that the *quasi-isotropic* sample fails at lower levels and has a higher elongation at break. It was explained that this happens due to fewer layers with 0º fiber orientation than uniaxial specimens, having a closer behavior to the matrix. The *quasi-isotropic* sample had four (4) Onyx layers for the roof and four (4) for the floor, and eight (8) layers of reinforcement material, and

obtained the experimental values of 11.8 GPa for the Elastic modulus, and 194 MPa for the ultimate tensile stress. All the samples that were tensile tested had a linear behavior until failure, in their load-elongation curves.

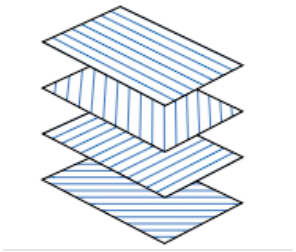

Figure 12 – representation of the layers with 4 different orientations [32]

Comparing Table 1 with the values of the *quasi-isotropic* sample it is possible to see a considerable variation between values, that may depend on the number of bottom and roof layers and fiber volume fraction. Díaz-Rodríguez, J.G. *et al.* [23] collected and analyzed data from literature about the mechanical properties of the materials printed in MEX using Markforged and concluded that there is a significant dispersion in the properties collected. They verified that fiber orientation and content significantly impact these composites' properties. They also pointed out that most studies estimate V_f from the average volume data reported by Eiger which can lead to misleading results. Similarly, Avanzini, A. *et al.* [33] noted that values in literature could fluctuate significantly, in which the elastic modulus can diverge from 7.6 to 51.7 GPa and the ultimate tensile strength vary from 96.6 to 436.7 MPa.

2.3. Design for Additive Manufacturing

All these new possibilities in design creation, and new ways of approaching and solving problems provided by AM, can be easier and more efficiently achievable using Design for Additive Manufacturing (DfAM) tools [11]. DfAM is a process of creating, optimizing, and/or adapting the form of a part, assembly, or product, based on numerical simulation and automated structural optimization algorithms. With these tools it can be made numerical optimizations that create optimized complex geometries, where material is placed in selected places, usually creating a product that only AM can produce. It is considered an out-of-the-box process since it can be personalized according to the specific needs regardless of functional complexity, material complexity, and part integration or assembly. [11, 13, 14].

In DfAM, tools and workflows use generative design to develop high-performance 3D printed products and give the possibility to create highly complex and high-performance parts that would be almost impossible to optimize manually in traditional CAD software as well as impossible or prohibitively expensive to produce by conventional technologies [37]. The mentioned opportunities AM can provide in part production depend on robust DfAM tools that grant engineers and product designers the ability to predict the technical response, define the commercial opportunities and automate the process of product design in AM systems [11].

2.3.1. DfAM tools

There are many CAD software that incorporate generative design, and that can be used as a DfAM tool, such as Fusion360, Netfabb, Siemens, Ansys, and Paramattares, to name a few. Still, nTopology is currently the only generative design solution that grants direct and predictable control over every aspect of the process and its outputs. It allows the user to create and reuse workflows, providing freedom to develop his methodology to solve a specific problem [38]. It is also important to mention that in DfAM the use of simulations can give more certainty in commercial production, because it is possible to predict the effect that a design decision will have on an AM outcome, minimizing failing risks and satisfying the technical requirements. These tools also allow the exploration of the manufacturing limits using sophisticated experimental and numerical analysis of AM process parameters [11].

Generative design is a broad concept that refers to the methodology that includes several design tools such as topology optimization, performance driven lattice structure, and field driven design as demonstrated in Figure 13. This concept combines geometry generation, design analysis, and evaluation based on simulation [37]. Lattice structures consist of unit cells with a pattern that repeats within a space. They are usually used to reduce weight, improve manufacturability, or achieve a specific response by controlling the lattice parameters. Topology optimization refers to a simulation-drive structural optimization technique where designers define the technical requirements and constraints and through iterative simulation steps, the software removes material from the designated design space. The third approach is field driven design which uses fields to establish a direct relationship between the physical principles and part geometry, using simulation results and test data as inputs in design features such as lattices and wall thickness [37].

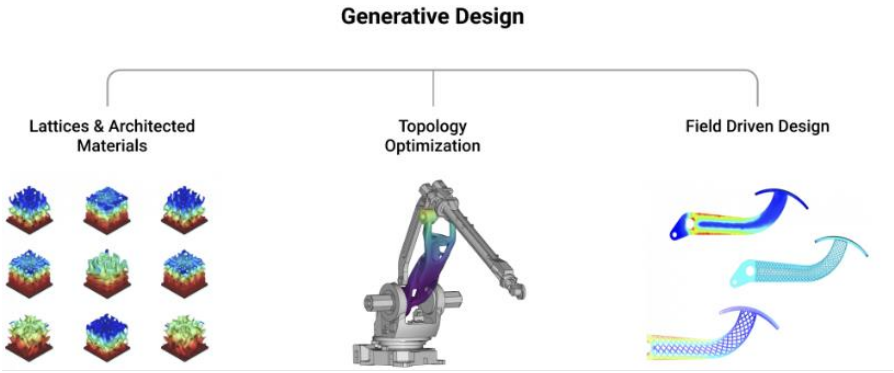

Figure 13- Different design tools used in Generative design [37]

Generative design starts with understanding the problem, finding a goal, and setting the design requirements. The requirements that will define the design of the final part can be either technical like a weight goal, stiffness, and heat transfer coefficient, or non-technical like cost, manufacturability, and regulatory compliance. Afterward, it needs to be chosen the appropriate generative design approach that best fits the application and

set goal. Throughout this process, several simulations are made, for design analysis and verification [37].

The digital capabilities of generative design tools allow the creation of innovative solutions and bring benefits to the product development such as the creation of high-performing products, accelerating all stages of product development and due to the use of an algorithmic approach it can produce unbiased engineer solutions. However, some limitations can compromise the quality of the obtained results namely the existence of non-transparent workflows since some software solutions use a "black box" approach where engineers don't have visibility or control over the process, due to the complexity of algorithms [37]. This effect is minimized with nTopology software, since it enables greater control over the produced geometry and the optimization workflow, allowing control over the algorithm and understanding how it fits in the process [38]. Additionally, the output quality depends on the quality of the input which in its turn depends on the accurate definition of the two main input components: design space and loading conditions, defined by the engineer. Furthermore, these simulations and optimizations are also restrained by the limited range of optimization requirements, because many physical phenomena aren't supported by most generative design software [37].

As stated previously, generative design presents unique ways to create solutions specifically tailored for each application's needs. It can be used with the objectives of light weighting, thermal management, creating architected materials, customer-specific products, and industrial design improvement. One of the main applications is weight reduction seeing that it can remove material or replace solid structures with lattices and being able to not only increase performance but also reduce manufacturing cost. This is important for aerospace and automotive industries since it reduces fuel consumption and improves energy efficiency, which are vital factors for a sustainable and green economy. It is also relevant for medical applications since lighter prosthetics can increase patient comfort [37]. Figure 14 show examples of these methods, specifically a brake pedal in Figure 14-a), designed in nTopology, where topology optimization was used to reduce 40% of the mass and evaluated the use of lattice geometries to identify the optimal solution [38].

The creation of architected materials, which are cellular structures optimized for specific functions and properties, can improve structural, thermal, acoustic, and electromagnetic characteristics without changing the original outer boundaries of the component. It is an iterative process requiring close control over lattice geometry and may contribute to mass reduction. It can be applied in thermal management, for example, in heat exchangers for automotive and aerospace industries, where the heat transfer's effectiveness is mainly determined by the surface area in contact with the colling medium, and lattice structures provide these large surface areas per volume [37]. Figure 14- b) shows an example of these possibilities where the cross section of an air-cooled cylinder of the internal combustion UAV engine, designed in nTopology, optimizes the performance having into account temperature, air velocity, stresses, and pressure [38]. Another popular use of architected materials is 3D printed foams applied in prosthetic devices and

medical implants with lattice structures that promote bone growth, as well as light weighting and shock absorption in sports equipment, such as the 3D printed foam inside helmets or a portion of the bike saddle represented in Figure 14- c), designed in nTopology [14].

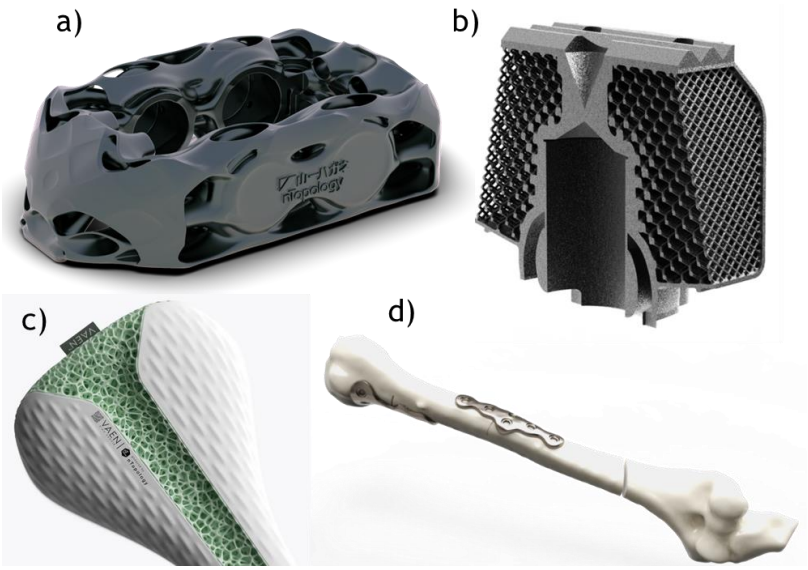

Figure 14- Examples of optimized components designed in nTopology. a) Automotive brake caliper designed by Yamaichi Special Steel [38]; b) Cross-section of a drone engine cylinder designed by Cobra Aero [38]; c) Bike saddle with a 3D printed foam for cushioning designed by VAEN [14]; d) Patient-specific bone plates designed by an established medical device company [38]

Generative design also provides the possibility to transform data, such as a mesh cloud from a 3D scan, pressure map, or simulation results that enable the personalization of medical devices for a patient, sports equipment, high-end automotive, and luxury items [37]. One case that illustrates this strategy is in Figure 14-d), where it is possible to see a custom medical implant, designed in nTopology, where it was imported patient data and inputs were specifically defined by the user to generate bone plates [38].

2.3.1.1. Finite Element Analysis (FEA)

Finite element analysis (FEA) is a numerical method that can predict how a part will behave under certain conditions and is the base for modern simulation software. The results are usually depicted via a color scale distributed over the object helping engineers find the weak spots and areas of tension and allowing the detection of vulnerabilities in prototypes [39, 40].

It uses calculations, models, and simulations to predict and understand an object's behavior under various physical conditions. Quantifies structural or fluid behavior, thermal transport, wave propagation, and other conditions described by Partial Differential Equations (PDEs). In engineering mechanics, PDEs are complicated equations that are solved to estimate the structural behavior under a given load and quantify relevant quantities such as stresses, strains, and displacements. FEM is the numerical technique that divides an object structure into elements to perform FEA simulations. Dividing the model into millions of small elements and stitching them back together

creates a mesh. The calculations are made for every single element and combining the individual results of the mesh produces the final outcome of the structure [39, 40].

2.3.2. Advantages and limitations of AM technologies

As previously mentioned, one of the most significant advantages of AM comes from the sequential addition of material which provides its design freedom that allows the fabrication of high-complexity components with optimized geometries and cellular structures as well as the possibility to control the interior of a component by including lattice structures, functionally gradient structures and internal cooling channels [11, 12]. This technology can fabricate parts without sacrificing the strength-to-weight ratio and can create complex parts with lightweight characteristics [28]. The way material is laid in AM also allows integration of multiple functional single parts (after careful studying and developing the system), that would need to be assembled, into a system with fewer components that accomplishes the same function with fewer steps in assembly and reduces the number of parts [13].

AM materials are processed in unique manners enabling the innovation in material science such as polymer chemistries, manufacture of complex biological constructs, and metallurgical properties not feasible with traditional manufacture [11]. Additionally, there has been developed multiple printing head techniques that can combine materials and properties, allowing the creation of composite materials [19]. Simultaneously, AM has a very efficient way of material usage, given that it selectively places material only in the regions, reducing raw material waste and making the product more cost-effective [11, 13]. Moreover, the digital nature of AM turns it into a very flexible manufacturing process providing an automated approach to designing, documenting, and manufacturing complex engineered systems. Also, considering that the digital files can be easily shared globally to manufacturing centers and be fabricated as required, it reduces lead-time and design costs associated with transport [11, 19].

AM has a lot of advantages; however, like any other technology, it has limitations, such as a longer processing time per part which leads to a not completely efficient industrial manufacturing process [12, 13]. Regarding the material limitations, it is known that raw material for AM is more expensive, there is limited material availability and the properties of the final product usually suffers when matching with properties from parts manufactured by traditional methods, namely density, porosity, and crystal structure [12, 19]. Another limitation is the manufacturing system size which may restrict the size of the parts that are supposed to be produced. These constrain can decrease efficiency and increase the cost. The need to add support material in complex parts with overhangs to overcome geometrical instability is undesirable since it adds material that will need to be removed, preferably without undergoing any mechanical postprocessing. In some AM technologies, it is possible to use the unhardened material (for example a powder bed) to act as support material [13]. However, in the last few years, many advancements have been made to overcome these AM technology shortcomings [12].

3. Development and Optimization

This section will cover the development of this project aimed at fulfilling the main objectives of the proposed challenge: develop the device that could change the angle of attack of the hydrofoil wings, as well as prepare and optimize for additive manufacturing with the objective of weight reduction. It starts by exposing the framework and understanding the problem, as well as describing the methods and software used. Then describes the design process of the hydrofoil system and the series of optimizations on the designed components. In the end, a comparison is made between the various optimizations performed for the three (3) different materials to find the most appropriate solution.

3.1. Flow Hygh boat and Hydrofoil system

The boat will have four (4) hydrofoils systems attached to the hull, and the design is composed of five (5) main components, as shown in Figure 15. One of the main components focused on in this work is the wing foils responsible for the creation of the lift, elevating the boat, and causing it to "fly". The strut is a vertical foil that supports and transmits the forces between the torpedo and the hull, and it needs to incorporate spaces for the shafts that control propulsion and the wing's angle of attack. The torpedo is a structural component that supports the wings and the propulsion unit, along with the volume to incorporate the mechanism that controls the angle of attack. The propulsion unit will only be present on the rear hydrofoils and is a preexisting component that will transform the vertical movement of the propulsion shaft into a horizontal movement of the helix. The hull is what provides the floatability of the boat when it is not flying, and it will need to have a mechanism that provides the rotation of the strut maintaining the water tightness.

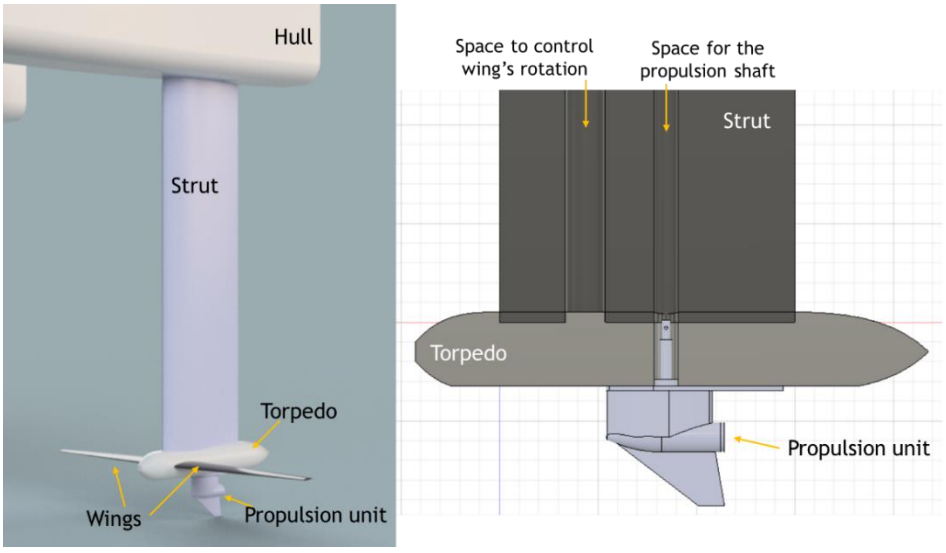

Figure 15- Given design of the boat and hydrofoil system and its cross section, taken from Fusion 360

3.1.1. Methods

The development of the present work is divided into three (3) main stages, Figure 16 demonstrates the flow chart of the work. The first stage is characterized by the adaptation and design of some components from the hydrofoil system, namely the foil wings and the

mechanism in the torpedo that would provide their movement. Then, it proceeded with the optimization processes in stages 2 and 3, which focused on the optimization steps for the wings for different materials: Inconel 625, Onyx reinforced with Carbon Fibers, and Onyx. The nTopology is a particular software where it is possible to produce a workflow that later can be adapted for other materials. The second stage prepared the generative design alterations for Inconel 625 and simultaneously created the base of the workflow for the other two materials. Stage three (3) corresponds to the workflow adjustments for the other two materials. In the end, it is analyzed and compared the optimization results of each part to choose the material according to weight reduction, final weight, and price.

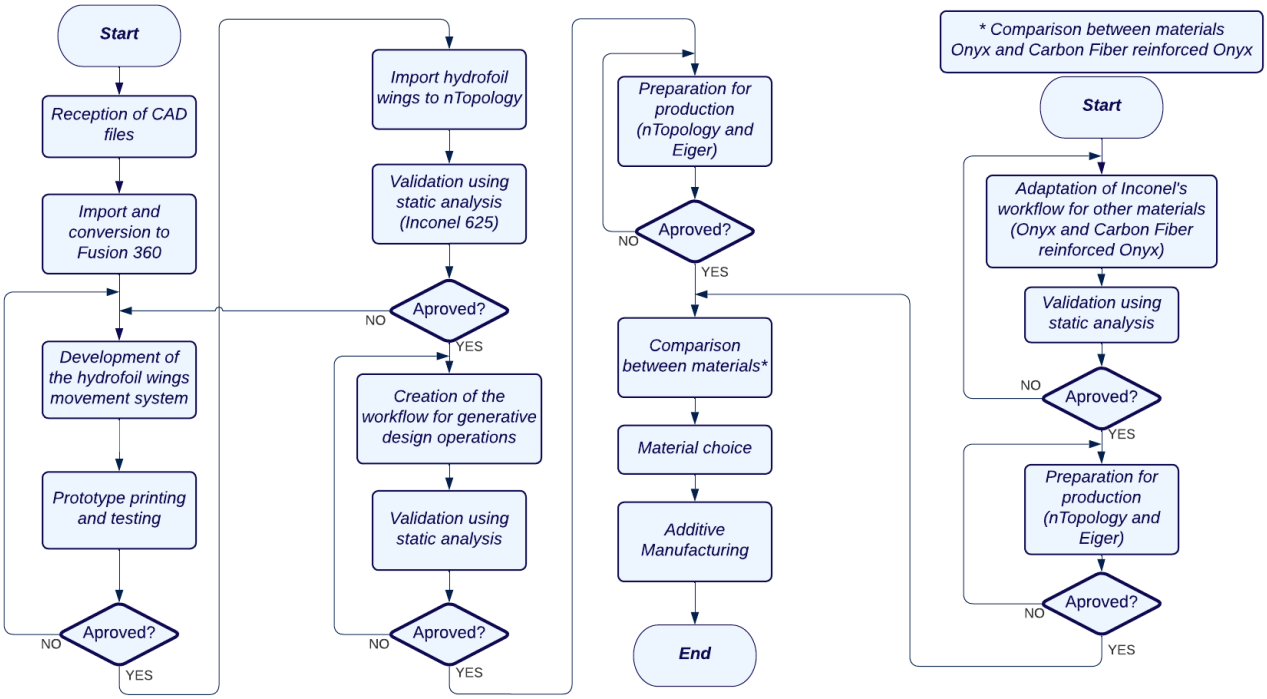

Figure 16 - Flow chart of the development and optimization

3.1.2. Software used

This section describes the different software used during this work, to achieve the objectives proposed for the movement system design, weight optimization, and preparation for additive manufacturing.

3.1.2.1. Fusion 360

Fusion 360 is a cloud-based 3D modeling software from Autodesk, it integrates CAD, computer aided manufacturing (CAM), computer aided engineering (CAE), and printed circuit board (PCB) tools for product design and manufacturing. It is a flexible software that can also be used for generative design, as well as, FEA verification, test, and simulation [41]. However, for this work Fusion 360 was only used for the adaptation and design of the different components, namely the torpedo, the foil wings, and the movement mechanism.

Currently, Fusion is a paid software, but there are free options available for students and educators or institutions, for some start-ups, and for personal use with basic functionalities [41].

3.1.2.2. nTopology

The main objective is to remove the most amount of mass possible and keep the structural integrity of the wings. The software used for these steps was nTopology, which uses generative design tools to create optimized products. The method of optimization is an iterative process where simulations accompany any change to the model to verify the results and identify if and where it is necessary to alter the design.

nTopology is an innovative software that allows the creation of custom workflow to target the specific problems and solutions, including design alteration and validation. The "Notebook" is where this workflow is displayed using "blocks" that represent functions. "Blocks" are the fundamental elements that create and modify geometries, combining input and output data. A "block" needs inputs to generate output data, and each one can be turned into a variable and used as input in another block. This block system provides a visual programming environment while creating geometry, using a color code to differentiate the different outputs. The system grants the possibility to "drag and drop" blocks to create and organize the workflow, including the ability to comment, get information about a block, and change visibilities. In Figure 17 it is possible to see part of a workflow created in the Notebook.

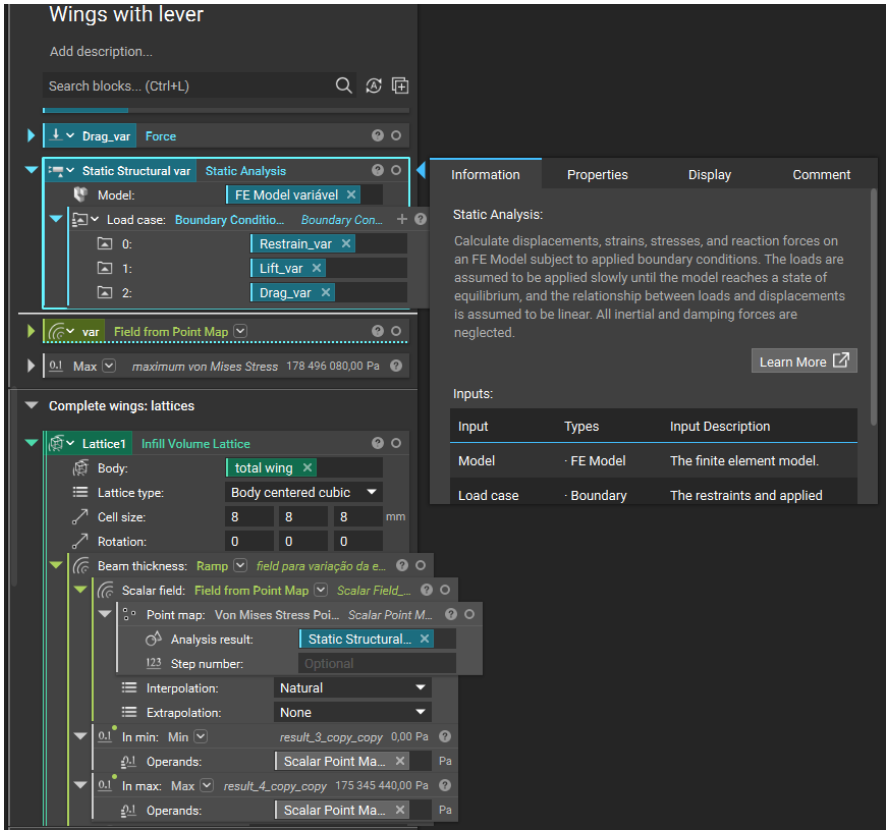

Figure 17- Sample of a workflow and information display for the static analysis, from nTopology

nTopology uses implicit bodies when performing most geometries creations and transformations since it is a lightweight way to represent three-dimensional objects using a single mathematical equation to describe a solid body. In most CAD tools, geometries are defined by vertices, edges, and faces, but in nTopology, the bodies are defined by equations. This characteristic causes calculations and processes to be easier and faster to compute, maintaining the pure form of the body because it is not a discrete representation. The discretization (transforming a CAD model into a mesh) occurs at the end of the design process, and therefore the final manufacturing data is more precise [42]. However, when performing the static analysis (finite element methods) and topology optimization it is necessary to divide the body into elements.

The mesh created for static analysis does not directly interfere with the modeling process, since it is an analysis. On the other hand, the geometry created by topology optimization is influenced by the mesh and, in the end, must be transformed back into an implicit body, to complete the design process. To maintain consistency throughout the process and to be able to compare results, the mesh definitions for all the models in static analysis and topology optimization were kept the same and defined by the block represented in Figure 18. To create the finite element mesh represented in blue it is necessary to have a volumetric mesh generated from a surface mesh. The definitions were chosen based on nTopology recommendations while balancing the feature size with time spent in mesh and result calculation.

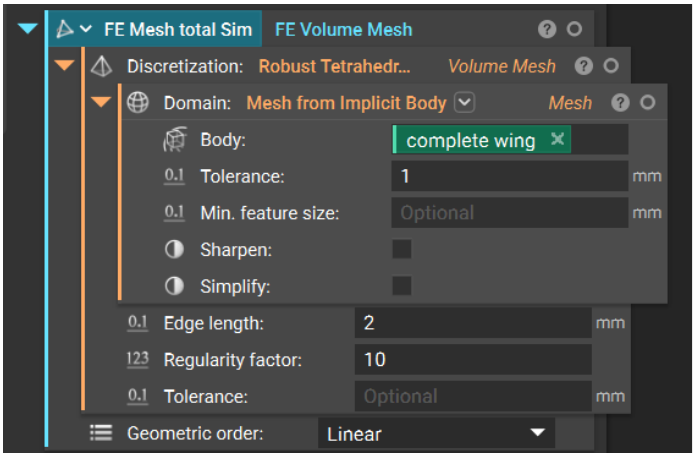

Figure 18 - Example of the block with the mesh definitions for the static analysis of the complete wing, from nTopology

3.1.2.3. Eiger

Markforged developed Eiger, a 3D printing software that functions not only as a slicer but as a part and builds management solution and is an interface between Markforged devices. Access to Eiger software happens through a Google Chrome browser window: eiger.io and the MarkForged Print (MFP) files are sent to the printer via the internet [43].

Eiger interacts with STL files, internal slice data, MFP files, and generic application data. STL files are a simplified mesh of the surface geometry and are the standard file type for AM technologies. The representation of the intermediate slice data is visualized

in the internal view of the sliced STL file, and MPF files have the output data for the Markforged printers to print the part. The generic application data is the code sent from the server to the user, and from the user to the server to verify that user data is not corrupted between updates [43].

The software allows the adjustment of various parameters, such as printer and material selection (or combination of materials in case of reinforcement material use), part orientation on the bed, infill type and density, number of walls, floor, and roof layers, to name a few. This software was used for the parts slicing and build preparation since it is directly connected to the Markforged printers, which can only print from MFP files.

3.2. Development of the hydrofoil wings movement system

The given boat's design was incomplete, and this work aims to adapt, design, and optimize the foil wings. The chosen foil geometries by the company were NACA0015 for the strut foil and H105 for the wings. The chosen hydrofoil form for the wings is a preexisting geometry designed to avoid laminar separation and ventilation at lower speeds (20 to 30 knots) and moderate angles of attack, while at small angles of attack lowers velocities to avoid cavitation. H105 foil sacrifices some upper-range cavitation envelope to reach higher lifts while maintaining low drag and a high incipient cavitation speed [44].

The components sizes were also established by 4DCTech defining the strut foil with a symmetrical constant chord of 150 mm, with a height of 500 mm, and the torpedo with a 260 mm length and a 40 mm diameter tapered at the ends to be hydrodynamic. The wing chords sizes vary along the 440 mm wingspan with three (3) segments on each side of the torpedo, with the root chord being 61 mm, the mean chord 44 mm, and the tip chord 21 mm, as shown in Figure 19 the PLA printed prototype. The maximum angle of attack for the rotation of the wings is 15º. Figure 20 shows a render of the boat's design incorporating the final four (4) hydrofoils, including the strut, torpedo, foil wings, and propulsion unit.

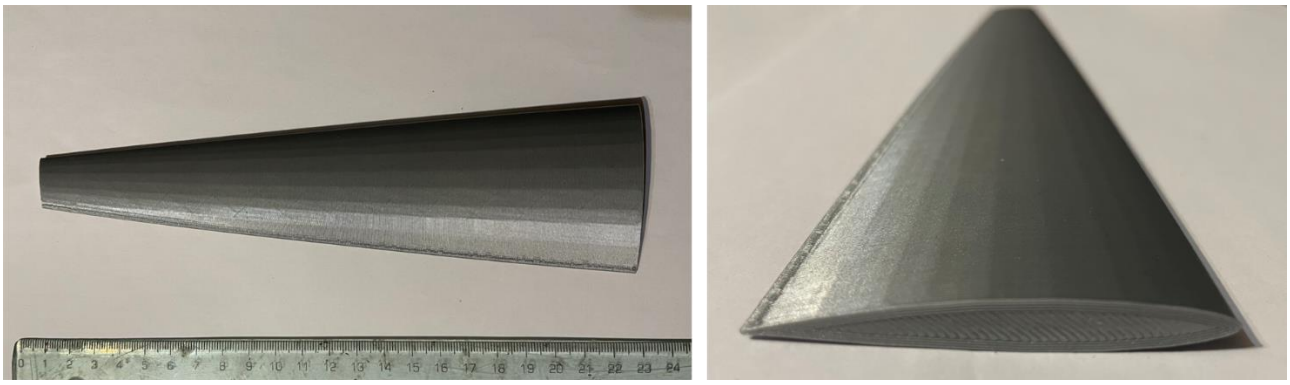

Figure 19 - Prototype of the left wing 3d printed in PLA

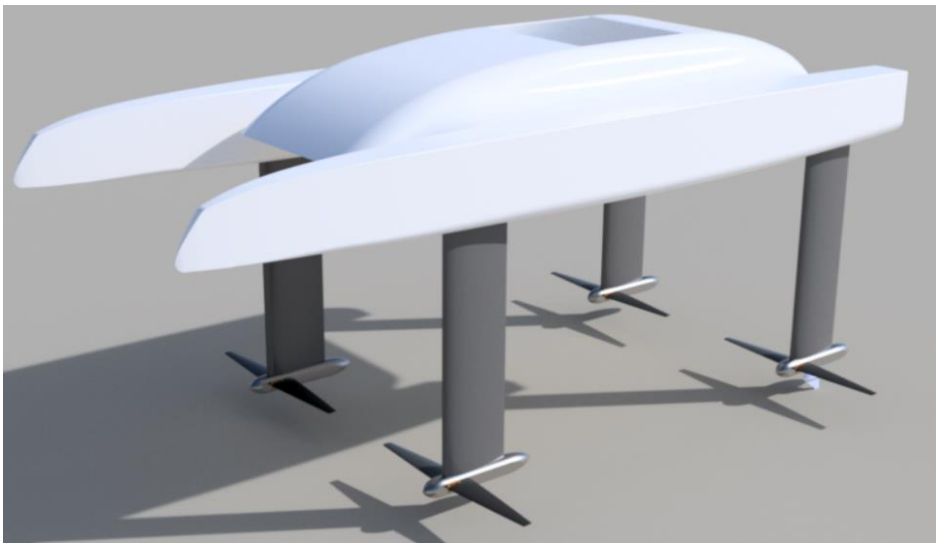

Figure 20 - Boat design with the four (4) hydrofoils in place, taken from Fusion 360

3.2.1. Design of the Mechanism for rotation of the wings

After modeling the components, one of the objectives was the creation of a rotation mechanism in the torpedo that could change the angle of attack of the wings. Figure 21 shows the wings and the torpedo with the rotation system, made in Fusion 360. This mechanism was developed considering that in additive manufacturing, it is possible to incorporate multiple functional parts in the same piece (that usually would be produced individually and then assembled).

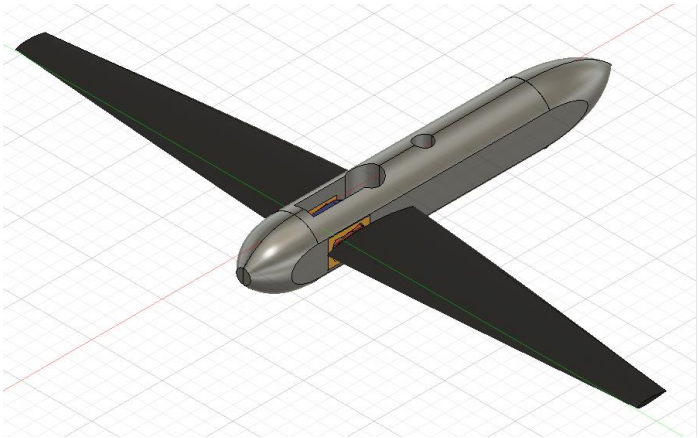

Figure 21- Torpedo coupled with the wings taken from Fusion 360

Represented in Figure 22 is the efficient bearing system created to provide the movement, that only rotates the necessary 30º (15º+15º). For demonstration purposes, it was used different colors to differentiate each component. The middle blue piece provides the connection between the two wings and works as a lever. This part enables the wing's rotation when pulled or pushed, as demonstrated on the prototype prints in Figure 23. The bearing pieces are divided into two parts (one colored in red and the other in yellow) and will secure the position of the wings as well as allow its rotation. Parts in yellow are part of the torpedo where inside secures and allows the constricted movement of the red piece. In summary, a cable in the boat connected to the blue lever is pushed or pulled,

transmitting the movement to the wings secured between the red bearing that has its movement constricted by the yellow static piece. This bearing system is part of the torpedo and can be manufactured as one single part and still provide rotation.

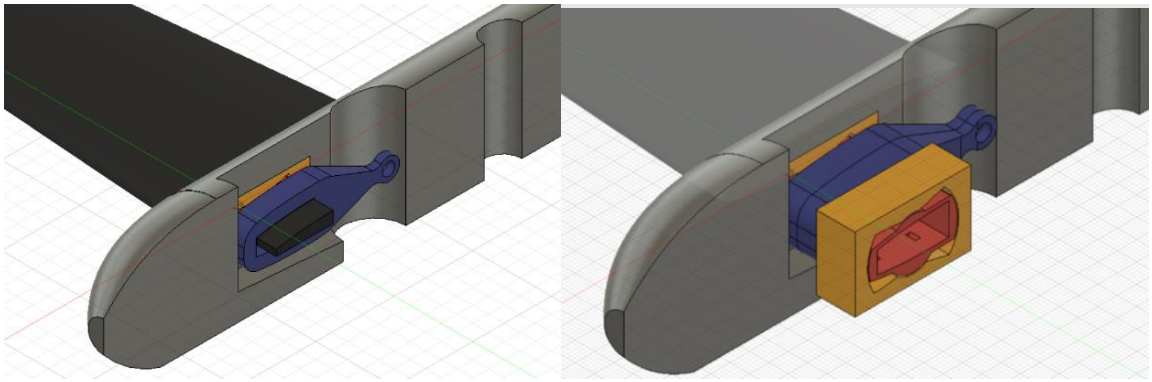

Figure 22- Cross section of the torpedo showing the bearing system in the torpedo, which allows the rotations of the wings, taken from Fusion 360

This prototype system was then printed in PLA in a commercial 3D printer (Creality CR10-V2), as shown in Figure 23, to test the rotation movement, clearances, and tolerances. For demonstration purposes and to save material, it displays sections of the torpedo and wings. For these prototype prints, the clearances used for the close fit joints were 0.5 mm, where parts can be assembled or disassembled by hand, such as the ones with contact between the wings, between the wings and lever, and between the wings and bearing red piece. For free fits in which parts are allowed to slide and rotate, like the components of the bearing (red and yellow pieces from Figure 22), it was used a clearance of 0.6 mm. However, these values may vary according to the materials and machines used in the process. According to the Design Guide for 3D Printing with Composites [32] from Markforged, the clearances for close fits are 0.05 – 0.10 mm, and for free fits are 0.10 – 0.20 mm.

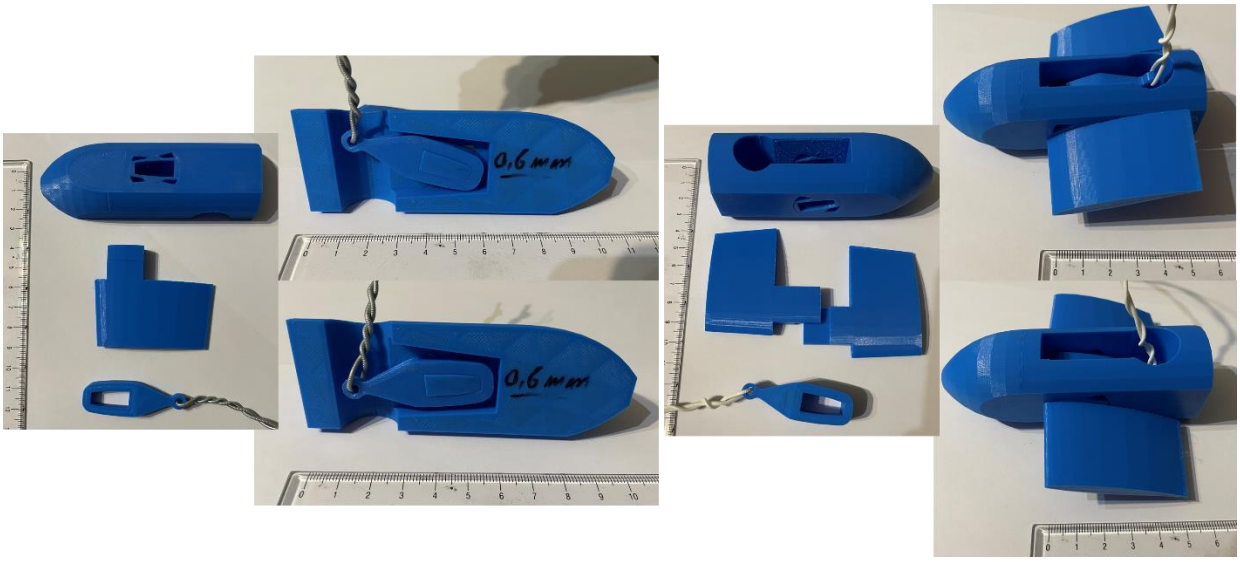

Figure 23- Prototype movement mechanism pieces printed in PLA, exemplifying the rotation movement of the wing. On the Left is the mechanism cross section and on the right is the complete mechanism

In case of the complete mechanism of the movements visible in Figure 23, the wings had to be divided in half and then assembled, creating fit joints that proved efficient in locking the PLA pieces in their place by friction forces. The optimal approach regarding the number of parts and complexity in assembling and having in mind AM as the manufacturing process would be to incorporate the wing in the printing process of the torpedo. This concept could be achieved by printing everything in place; however, it would waste a lot of material in support. The other approach would be to print the wing with the lever as a unique part, as shown in Figure 24, and incorporate it while the torpedo is being printed. Before the bearing system is finished, the machine would stop, and the wing would be placed on the bearing mechanism. Then the printing process would resume, not requiring any assembly. However, there are limitations to this method, namely the size of the build volume of the printing machines available (X7 and Metal X from Markforged), as well as the sintering furnace for the metallic parts (Sinter-1).

The printer X7 is one of the Markforged 3D printers available at Norcam, with CFRP process that can print a full range of composite base materials and reinforce it with continuous fibers. It has a build volume of 300x270x200 mm [45]. Metal X is another of the Markforged 3D printers available at DEMM, that can print a wide variety of advanced metals and has a build volume of 300x220x180 mm [25]. The size is also limited by Sinter-1 having a furnace chamber with 235x68.3x 80.9-69.2 mm (the top is curved). Therefore, since this piece, from Figure 24 was a wingspan of 440 mm, it is not currently possible to build. However, the optimizations will still be made and demonstrated, on the assumption that in the future it is available a printer with a larger build volume, such as FX20 from Markforged with CFR process as well, and has a build volume of 525x400x400 mm [46]. Because of this limitation, the wings were divided in two, previously shown in Figure 23 and here in Figure 25. It is also essential to state that printing individual wings is conditioned since they measure 220 mm in length, and their placement on the build plate is limited, not being possible to build them vertically (in the z-direction).

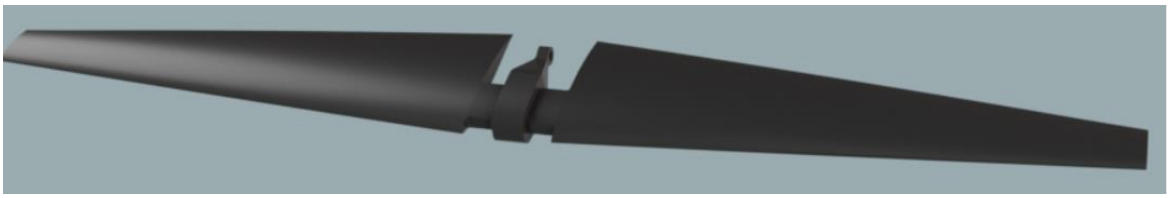

Figure 24- Render of the complete wing, with the incorporation of the lever, and it would be placed on the bearing mechanism mid printing, taken from Fusion 360

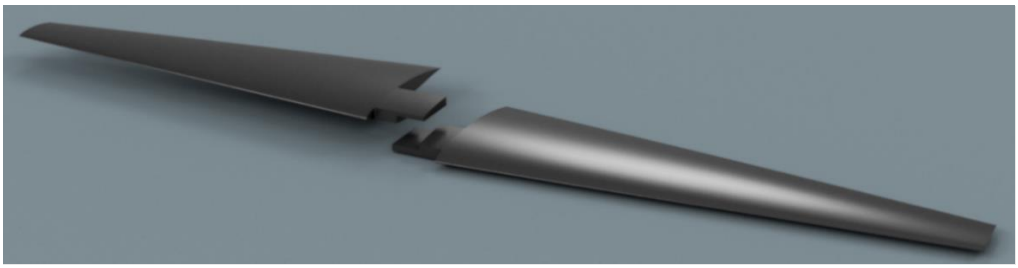

Figure 25- Render of the individual wings, taken from Fusion 360

3.3. Validation of the developed hydrofoil wings

The generative design process starts by studying and performing simulations on the original component to understand how it reacts to the forces and constraints and where can the design be modified. To ensure that results are closer to reality it is necessary to provide the correct inputs to nTopology block. The initial inputs for this project are the material properties, the CAD model and its boundary definitions, and the forces and constraints to which it is subjected. For this work, the two CAD models studied are present in Figure 24 - complete wing - and Figure 25- individual wings - and their boundary conditions and forces will be defined in the next section. The choice of material takes into account the available AM materials and processes, as well as the materials of the existing hydrofoils. Inspired by the traditional method of producing hydrofoil it was studied Onyx and Onyx reinforced with carbon fibers, produced by MEX. The other material was Inconel 625, a metal that can be processed in AM by MEX and printed in Markforged Metal X. Although, it is an expensive material, it is very resistant to corrosion underwater. Each material has a different behavior to the same conditions and optimizations need to be adapted to their properties.

3.3.1. Definition of forces and constraints

As previously established in generative design software such as nTopology, many physical phenomena are not supported. In the case of this work, the simulations run in nTopology are static analyses and therefore are only an approximation to give the output necessary to optimize.

This section presents the definition of the inputs - forces, and constraints - for the foils to obtain outputs - the various simulations for each material and topology optimizations. It was made static analysis of the components and used the von Mises criteria to determine if a component yields or not. This criterion indicates that material will yield if the von Mises stress is equal to or higher than the yield limit of the same material under simple tension [47, 48]. The results are usually represented with a color code in which red is where there is a higher amount of von Mises stress, and blue/purple is where there is less stress concentration.

To run the static analysis, it's necessary to define the boundary conditions and the forces and constraints acting on the component. The main forces acting on the wings are Lift and Drag, as represented in Figure 26 - complete wing - and Figure 27 - individual wings. There are three (3) ways to define the boundary conditions in nTopology: FE Boundary by Body – selects the entities in the FE Mesh that lie within the tolerance of an implicit body -, FE Boundary by Flood Fill – selects the FE Mesh entities using flood fill operation, in which the block shoots a ray with a certain angle and direction at the mesh and selects the entities of the intersection - and FE Face Boundary – selects the mesh entities using a CAD face list. For the three (3) elements that define load case (lift, drag, and displacement constraint) the boundary definition used the FE Boundary by Body block. The selection of the elements depends on the body, and therefore it is necessary to create bodies that, when intersected with the mesh, select the correct boundary elements. The

Lift force is applied on the bottom of the wing, and through a series of boolean subtractions, an Implicit Body was created that only has the bottom half of the wings, isolating the Lift regions. For drag, it was necessary only to subtract the center of the connection, and for the displacement constraint, it was subtracted the wings, leaving only the centerpiece.

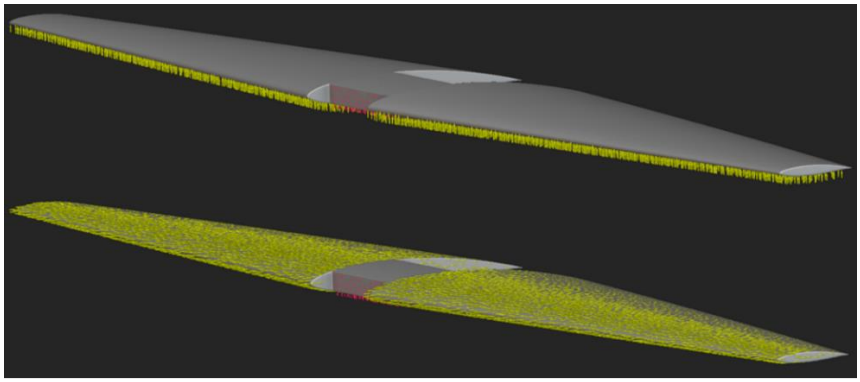

Figure 26 - Application of: Lift force on top, the Drag force on the bottom, and in red the displacement constraint in the complete wing, taken from nTopology

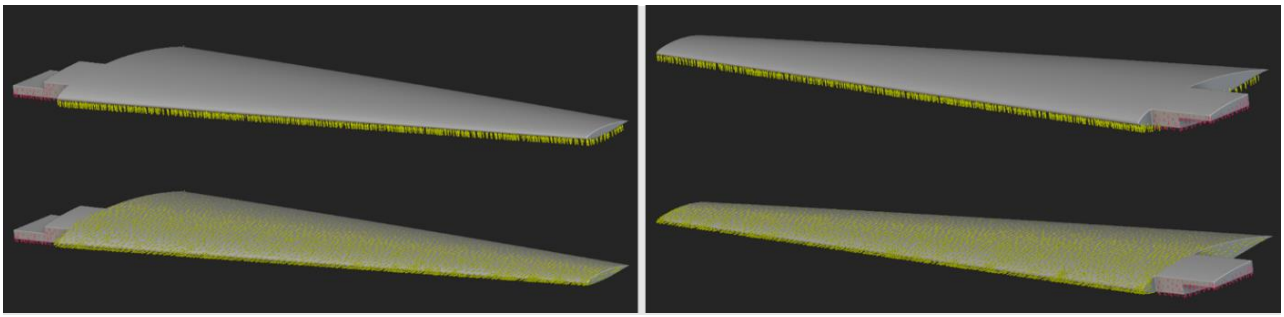

Figure 27 - Application of: Lift force on top, the Drag force on the bottom, and in red the displacement constraint for the two individual wings, taken from nTopology

Lift is the force with a direction upwards on the z-direction, applied below the foil. All the foils together must sustain the weight of the boat, and the oversized value given was 25 Kg. This reveals that the Lifting Force when at starting position (angle of attack is 0º) is 250N, meaning that all the wings together endure a maximum of 250 N. However, considering the angle of attack, there is an increase in the Lifting force to 500 N, and in the static analysis, it will use this maximum limit. In summary, each complete wing and individual wings must sustain an upwards lifting force of 125 N and 62.5N, respectively. The Drag force direction coincides with the direction of the water flow in front of the foil and causes friction. Drag is 10% off Lift, and once again, using the limit conditions, it will be 12.5 N for the complete wings and 6.25 N for the individual wing. Small yellow arrows in each node represent the lift and drag forces, and the small red dots represent the displacement constraint. This constraint is in the center of the wings where it connects with the bearing system and the lever.

For the lever, the considered forces were 50 N upwards and the displacement constraint in the connecting region, as represented in Figure 28. This piece can be placed between

the individual wings or incorporated into the complete wing. Either way, the static analysis and topology optimization will be made separately and then united to simplify the design processes.

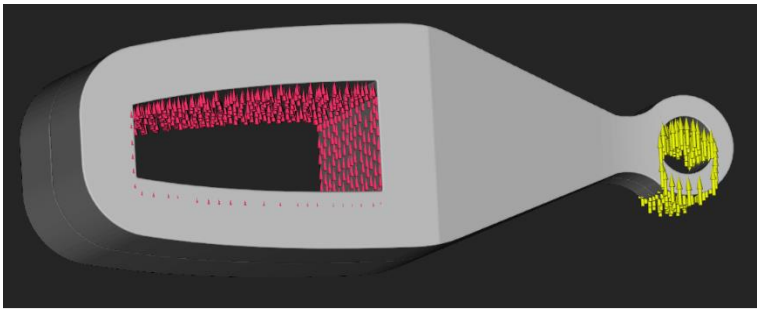

Figure 28 – Application of the forces and displacement constraint in the lever, taken from nTopology

Since the validation depends on each material properties, the results of the static analyses for each material are in their corresponding development sections of the generative design operations.

3.4. Development and optimization for Inconel 625

The development of optimizations is an iterative process in which each alteration made to a design requires verification (in this case static analysis), which can lead to a new set of modifications that will need confirmation. In this case, the objective of said optimizations is the decrease in mass of the wing component, maintaining the structural integrity of the part while in function. Before making any alterations to the model, it is necessary to analyze its original form and understand where it can be modified.

In this section, it is revealed the static analysis for Inconel 625, as well as the construction of the workflow with all the generative design approaches and operations. Once the workflow has been constructed for this material, it is possible to reuse it, making the necessary changes.

3.4.1. Initial static analysis

As previously stated, for each static analysis, it is necessary to define the material properties. For Inconel 625, it was used the integrated "block" from nTopology software with the material properties displayed in Table 2.

Table 2- Mechanical properties of Inconel 625 provided by nTopology

Density (g/cc)	Elastic Modulus (GPa)	Poisson ratio	Conductivity (W/m/K)	Specific Heat (J/g/C)
8.44	208	0.28	9.7	0.41

Figure 29 displays the results from the static Analysis for the complete solid wings with the application of the boundary conditions in Figure 26, where the areas in red represent the maximum von Mises Stress. These differences in color only represent the range of the

values obtained, and according to Markforged, the yield strength for this material is 334 MPa, and the maximum values obtained were 42.1 MPa, which is far from the limit and the material does not yield. The most affected area on the bottom and the regions near the connection between the wings and the torpedo. Regarding the displacement, the regions that suffer the maximum upward displacement of 0.40 mm are the tip of the wings, since they are regions further away from the displacement constraint.

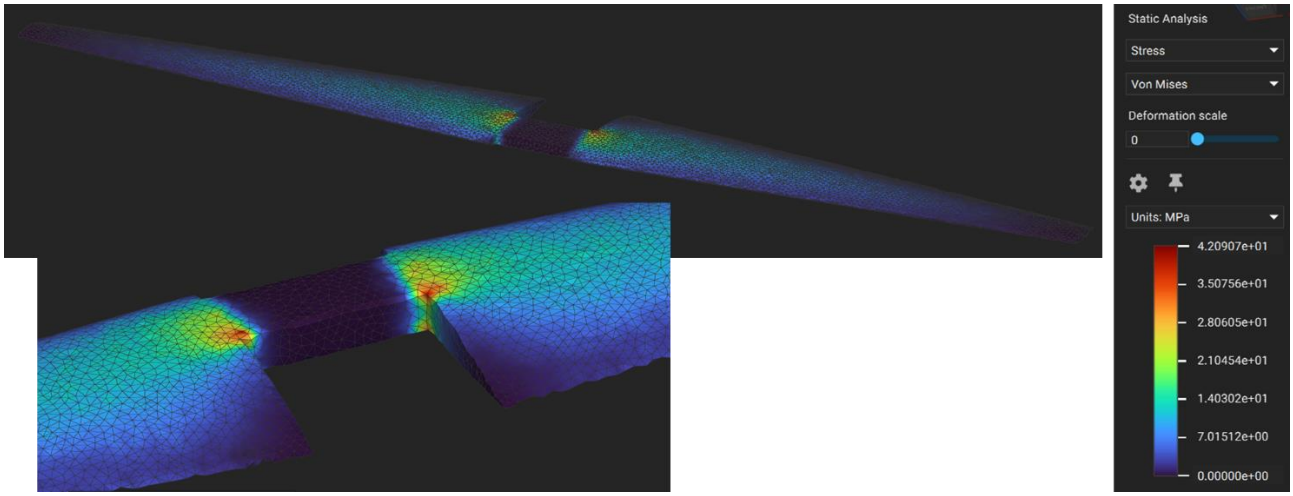

Figure 29 - Front and back view of the Static Analysis for the complete wings in Inconel 625, from nTopology

The results from the initial static analyses of the individual wings, with the boundary conditions from Figure 27, can be seen in Figure 30 for the right-wing and Figure 31 for the left wing. The regions with a higher stress concentration are similar to the complete wings, and on the right wing the maximum von Mises stress was 42.96 MPa and on the left wing was 47.53 MPa. Nonetheless, those values guarantee that the component does not yield since it is lower than the material yield strength.

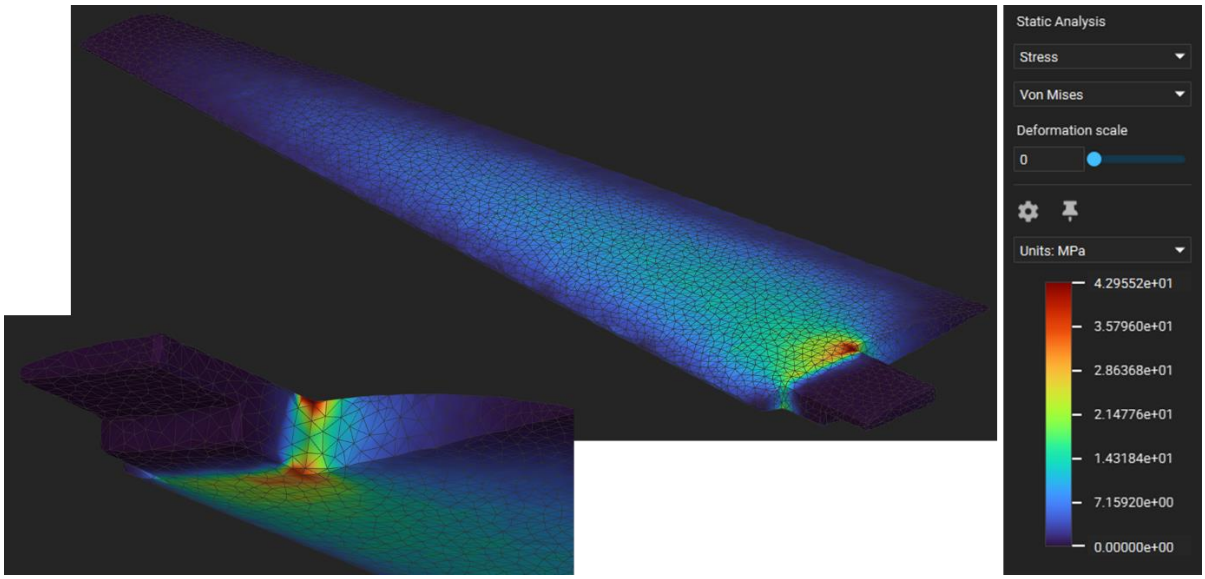

Figure 30 - View of the Static Analysis for the right wing in Inconel 625, from nTopology

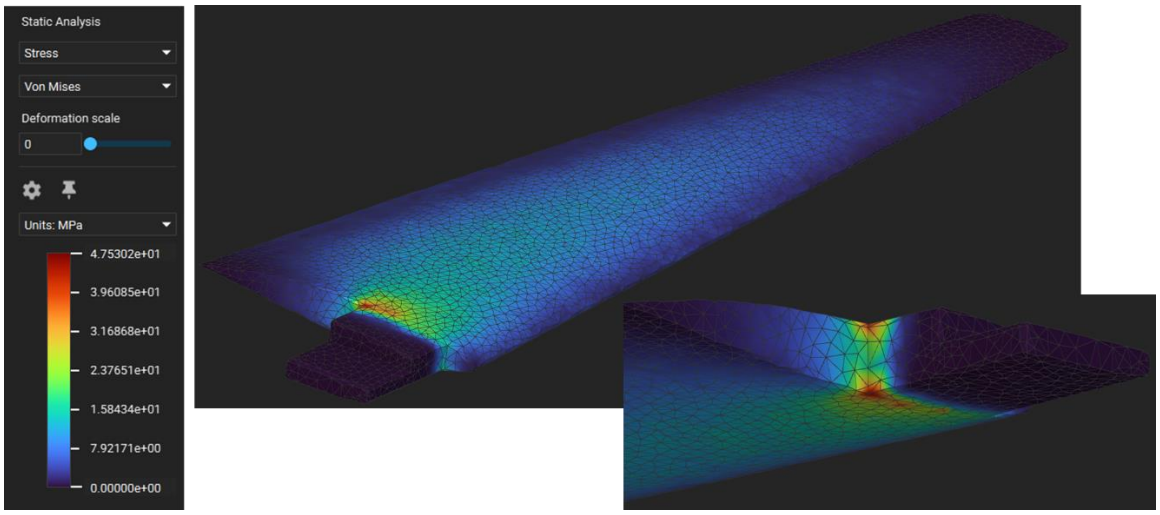

Figure 31 - View of the Static Analysis for the left wing in Inconel 625, from nTopology

It was made a simulation to the lever, using the boundary conditions represented in Figure 28, and the results are shown below in Figure 32. The maximum stress obtained was about 19.8 MPa, and once again according to the von Mises criteria, it does not yield.

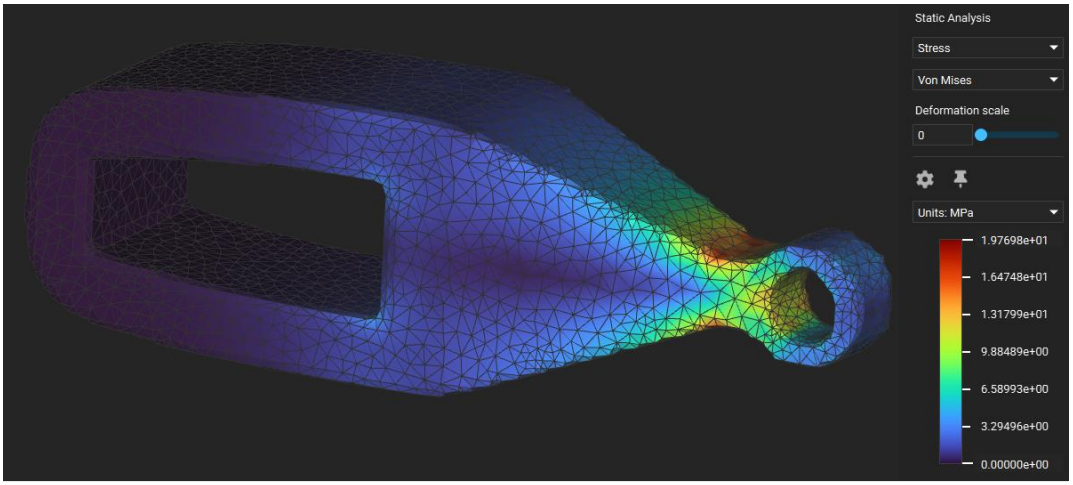

Figure 32 - Static Analysis for the lever in Inconel 625, from nTopology

nTopology estimated the initial for the solid completed wing with the lever is 622.38 g (lever mass is 37.69 g) and individual wings with 291.61 g (right) and 292.48g (left).

With nTopology many generative design approaches can be made, and the presented results from the static analysis show that none of the parts yields and that there is wide range for alteration and improvements. This section will explore field-driven design and lattice structures for the wings design, as well as topology optimization for the lever piece.

3.4.2. Generative design for the complete wing

The first model subjected to generative design operations is the complete wing and will inspire mass optimizations for the other models. The wing's outer boundaries cannot be

changed, since it is a hydrodynamic geometry, and its shape provides the Lift force. Therefore, all the alterations in the design need to be done to the interior, intending to decrease mass. Different optimization techniques were studied to achieve the objective proposed, such as topology optimization, field-driven design, and lattice structures.

3.4.2.1. Shell creation and validation

The first technique used was field driven design, in which the results from the static analysis were transformed into a field where each point has the stress values measured. Figure 33 demonstrates the different planes of those fields generated from the static analysis. Each point area comes from the three-dimensional mesh used in the static analysis and has the color associated with the amount of von Mises stress.

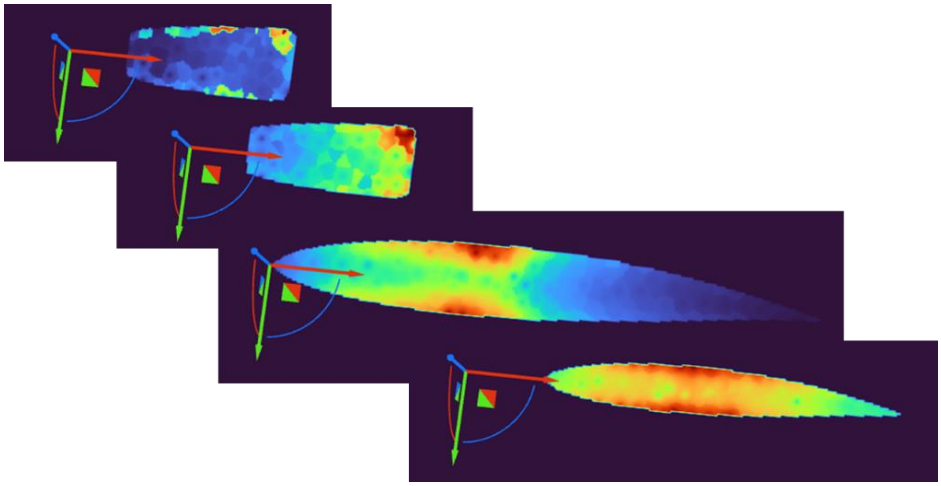

Figure 33 - Four scalar fields in the xz plane with the von Mises stress from static analysis, from nTopology

With the intent to drastically remove material from the part, using the scalar field and the block variable shell, a shelled complete wing was produced with variable thickness, represented in Figure 34. With this, regions with higher stress values would be attributed with more material, becoming thicker, and in zones with less stress would be applied less material, having thinner walls.

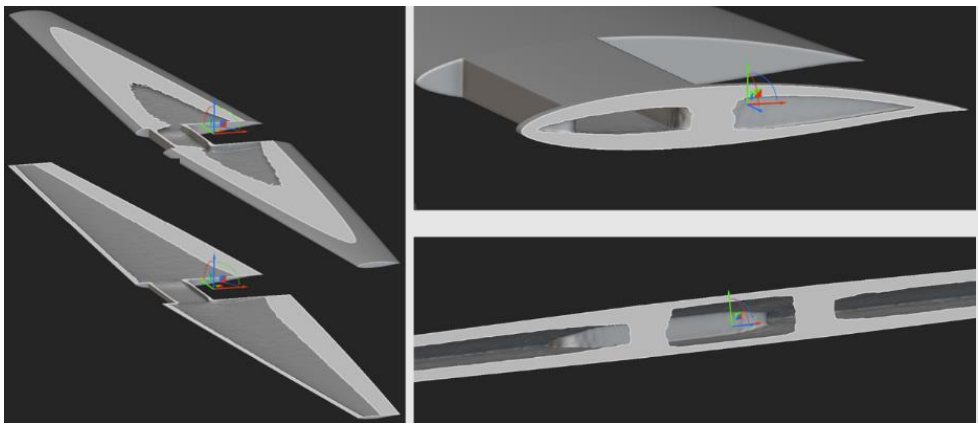

Figure 34 - Cross sections in different perspectives of the variable shell thickness, from nTopology

The maximum thickness was defined as 7 mm when the stress is at its peak, at 42.1 MPa, and the minimum thickness of 2 mm where the stress is minimum (0 MPa). The creation of a variable shell proved to be highly effective since it lowered the mass from 585.45 g to 542.10 g and a decrease in maximum von Mises stress to 43.36 MPa. Tunning further the values used for thickness, defining a minimum thickness of 1 mm and a maximum of 5 mm.

While performing the static analysis in the variable shell sample, it was noticed that the boundary's definition was incorrect, and forces and constraints were applied not only to the exterior faces but also to the interior surfaces. The bodies defining the boundary conditions had to be changed because the intersection between the FE Mesh of the variable shell sample and the solid bodies were selecting the interior surface. New bodies for the boundary selection were created to correct this inaccuracy, to choose only the exterior surface nodes by making a shell operation to the bodies that defined the previous boundary conditions. This proved to solve the mistake that only increased 2.09 MPa in the von Mises stress.

The static analysis obtained maximum stress of 48.7 MPa, a mass of 372.11 g, and a displacement of 0.47 mm. The result of this variable thickness is displayed in Figure 34. The representation of the static analysis from the complete wing with a variable shell is very similar to the one made for Inconel in Figure 29, and it can be consulted in Annex 1.

According to Eiger software, four (4) wall layers and eight (8) roof and floor layers correspond to the 1mm after sintering, being an attainable thickness in MEX for this material and proving to be a satisfactory solution. However, since the foil is hollow the roof would be overhanging with little to no support. Adding structures to the interior, not only would support those regions, but also lower the stress imposed, although increasing mass.

3.4.2.2. Lattice study

Lattice structures are the solution for this problem, and they usually are intricate geometries with repeating units throughout the volume chosen that substitute a bulk. nTopology has a wide variety of lattices available and an infinite way to combine strategies. The importance of the lattice structures in this context is to provide supports to the roof printing since the internal supports that Eiger would introduce would be impossible to remove.

According to the design guide for metals [49], from Markforged, the minimum angle to the horizontal for Inconel that a feature can print without needing support is 45º, and below that Eiger generates supports in that area. Some lattices were explored, as shown in Figure 35, and using the field from the von Mises stress created previously, the lattice thickness changed between 1 and 3mm. Table 3 indicates the types of lattices and discriminated masses represented in the parts from Figure 35.

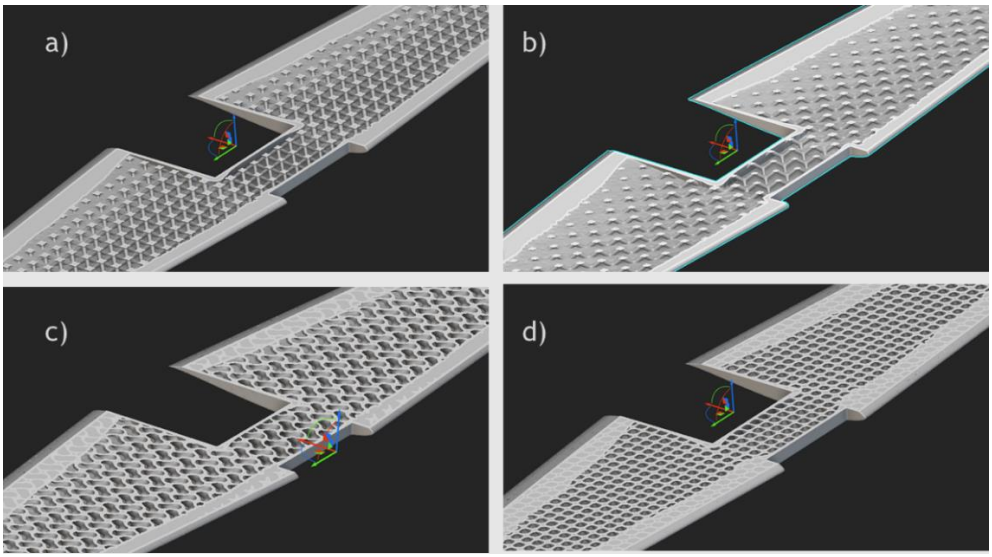

Figure 35 – Cross section of different lattices in the interior to create support, from nTopology

Table 3 – Lattice types and discriminated masses for each part in Figure 35

Part	Lattice Type	cell size (mm)	mass w/shell (g)
a)	body centered cubic	5	423.23
b)	Dimond	8	492.48
c)	Gyroid (TPMS)	7	441.62
d)	Dimond (TPMS)	7	455.96

However, when placing the wing in Eiger to test these modifications, it was found that the software would generate more support than expected. The support material was being placed not only on the outside, as expected, but also everywhere in the interior. In Figure 36 it is possible to see this problem in the internal view, where the supports in purple fully cover the interior. This is not desirable since it adds material to the interior of the part that is impossible to remove while keeping the piece completely close and watertight.

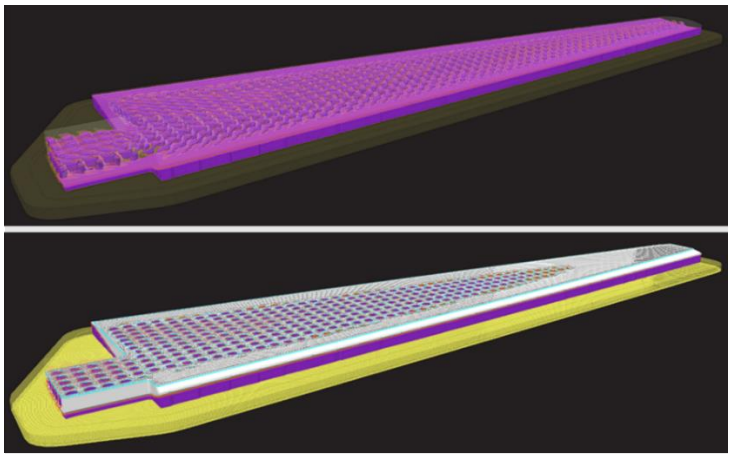

Figure 36 – Internal view of Lattice d), generated by Eiger. Isolated supports on top and cross section on the bottom, taken from Eiger

One possibility to accommodate the overhangs is the decrease of size cell of each lattice but knowing that when the size decreases, the material and mass increase, the use of lattices with this build orientation will likely not be a viable option. And, even though the Diamond (TPMS) (d) from Figure 35) has the most amount of part mass and interior volume coverage, it still generates a substantial number of supports.

To avoid this issue and understand where supports are generated, it can be used the Manufacturing Support Volume Block in nTopology, which predicts the volume of supports based on the overhang angle indicated. Figure 37 shows the result of this method that tests the volume of support generated for a Gyroid lattice 4mm cell size and varies the thickness between 0.8 and 1.6 mm according to the stress field. This component would weigh 462 g, in which the support material generated increases the mass by 79.24 g, giving a total mass of 541.24 g, and adding the lever gets to 578.93 g. Once again, with an overhang angle of 45º, the whole interior region is covered with support material. This might be happening since, in nTopology it is not possible to define overhang length, causing support placement in areas that would not be necessary.

To confirm these results the wing was placed in Eiger, and as expected, it generated support almost everywhere, proving that, like in nTopology, the overhang length in Eiger is 0 (or close to 0). Yet, as demonstrated in Figure 37, Eiger has the option to create a gyroid infill in solid regions and does not create support for it. This is a software limitation since it does not consider overhang length when it comes to another infill, but the ones created by Eiger. Using the infill option from Eiger would replace the interior with the lattice generated by the slicer, though it is necessary to place a solid body and discard the advantages of the shell thickness variation.

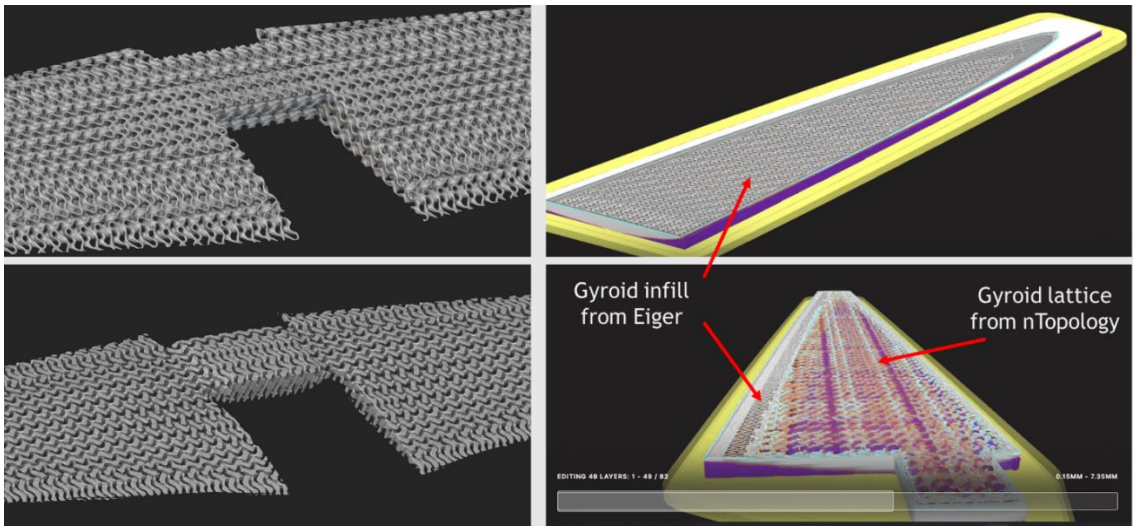

Figure 37 – On the left the gyroid lattice and its support (isolated on the bottom), calculated by nTopology. On the right Eiger's internal view of the gyroid infill from Eiger in a solid wing (top) and in a wing with Gyroid lattice from nTopology (bottom)

Eiger allows the replacement of the generated support material with the ceramic interface material, which would be easier to destroy and then could be removed through a hole. The ceramic material would work as the support material, however, this method

can bring some problems during washing and sintering due to contraction, and it could lose the support and deform the top of the foil wing. It becomes challenging to identify the appropriate lattice structures to use since overhang length is not disclosed by Markforged. Therefore, the use of lattices proved inefficient, and a different approach was carried out using the Minimum Support Orientation block. This block allows the discovery of the orientations that attempts to minimize the volume of supports. However, this technique will be used after optimizing and adding the lever to the complete wing because this step affects the orientation that creates the least amount of support volume and will be covered in the next section.

3.4.2.3. Topology optimization and validation of the lever

As previously described, this approach has in mind the incorporation of the complete wing while the printing process is happening; therefore, the lever can be part of the wing design. Nonetheless, its optimization was done separately and then united with the component because its outer boundaries can be changed, unlike foils. The topology optimization method was used to optimize the mass use in the lever, in which the software selectively removes material after defining the boundary conditions and the objectives. The objective was to maintain the structural compliance response and the optimization constraint was the reduction of the volume fraction to 20%. The boundary conditions needed for the structural compliance response block are the same as the ones used for the static analysis. The volume fraction value is merely indicative, and after calculations, the amount of removed material is controlled by a density threshold, presented in Figure 38, where it is possible to see the colors differentiating the density values assigned to each density element. In red are the elements considered more important to keep the structural compliance response according to the objective defined. In purple are the least important and the first to be removed as the value of the threshold increases.

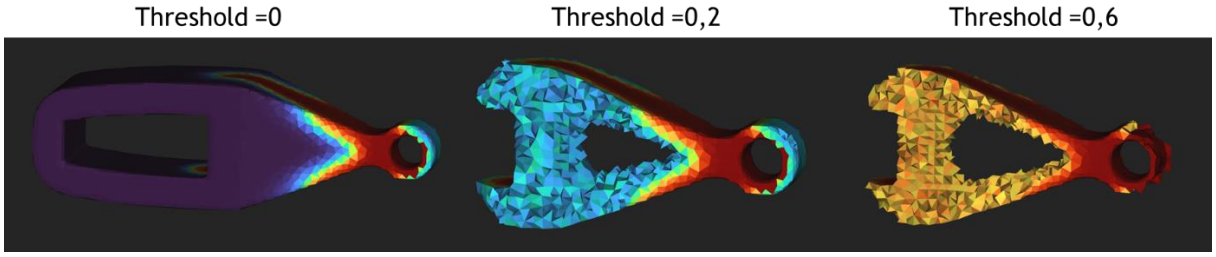

Figure 38 - Impact of the change in the density threshold, taken from nTopology

The result from the *Topology Optimization* block needs further work, and the steps to obtain the final part are demonstrated in Figure 39. After choosing a threshold of 0.3, the model was transformed into an implicit body where it proceeded with smooth and boolean operations. The boolean operations added the central piece and the part where the force on the lever is applied. It is worth noting that once the workflow is completed, it is possible to iteratively tune, and change specific parameters, such as the threshold, blend radius, and boolean operations, to further improve the optimization.

After the static analysis verification, the results demonstrated that the von Mises stress increased to 28.96 MPa, still not enough to yield. Also, there was a significant decrease in mass and a displacement almost negligible of 0.007 mm. Together, the mass of the lever and central piece is 52.38 g, and the optimized lever is 23.50 g. Then a boolean union was performed between the optimized lever and the complete wing, as demonstrated in Figure 40.

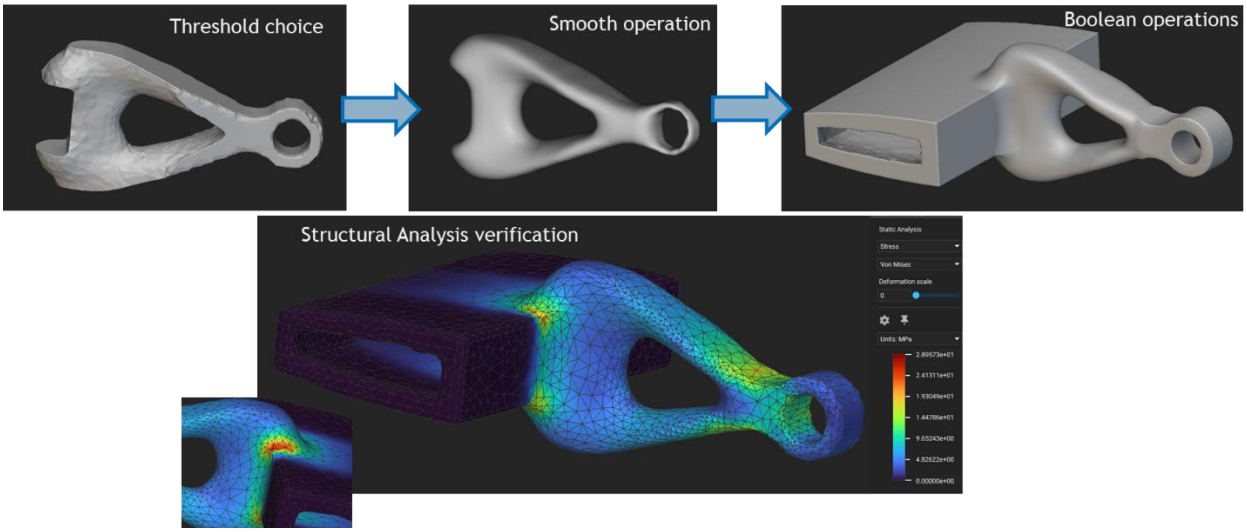

Figure 39 - Development of the topology optimized lever taken from nTopology

3.4.2.4. Part Orientation and building supports

As previously mentioned, since using lattices proved not to be the solution, it is possible to use the Minimum Support Orientation block to find the orientations where it produces fewer supports. Then, using the Manufacturing Support Volume block, it is generated and united a small interior volume that will function as support. This method found four (4) orientations considering minimum support in the interior and exterior and are represented in Figure 40.

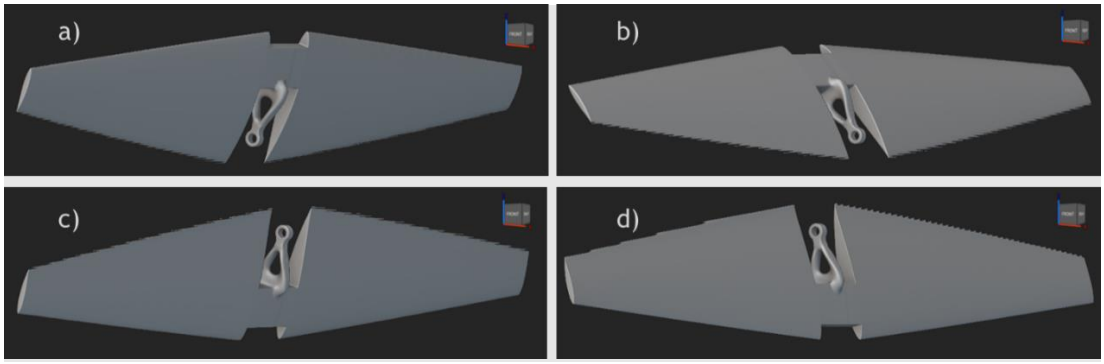

Figure 40 - Minimum support orientations for complete wing with topology optimized lever, taken from nTopology

The orientations represented in a) and b) were excluded because the printing process would start with a thinner region of the foils. The interior (purple) and exterior (blue)

support for c) and d) are represented in Figure 41. When generating the “interior support” nTopology considered some volumes in the exterior of the lever, since they wouldn’t be touching the build plate. The differences in the support material (infill) mass between c) and d) are almost negligible, since they are 12.82 g and 12.79 g, respectively, as well as the placement of the exterior material. Since they are so similar, the decision came down to printing the concave face facing down (orientation c) to maintain the foil’s trailing edge detail.

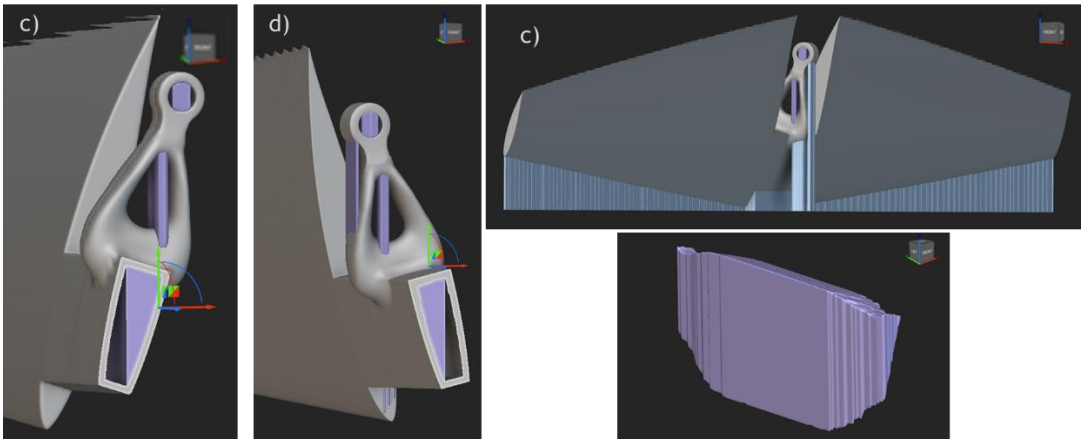

Figure 41 – Cross section from c) and d) orientation with supports in purple and isolated infill, taken from nTopology

Finally, the interior supports were united with the complete wing with a variable shell, and the final mass is 392.84 g, decreasing 229.54 g from the original. When slicing in Eiger this added volume can then be filled by a gyroid or triangular pattern to reduce even further the mass.

Due to the complete wing size, it is not possible to print in Metal X, and to approximate results, the part was cut in half for slicing it in Eiger. Then, using four (4) wall layers and the recommended triangular infill, the supports were generated, and the values for masses, print and dry times, and cost were calculated. As is demonstrated in Figure 42, Eiger placed more supports (in purple) than expected, both in the interior and exterior. However, the mass calculated for half of the complete wing after sintering was 190.43g with solid infill and 188.48 with triangular infill, which is inferior to the expected 196.42g (since it was only possible to slice half of the complete wing).

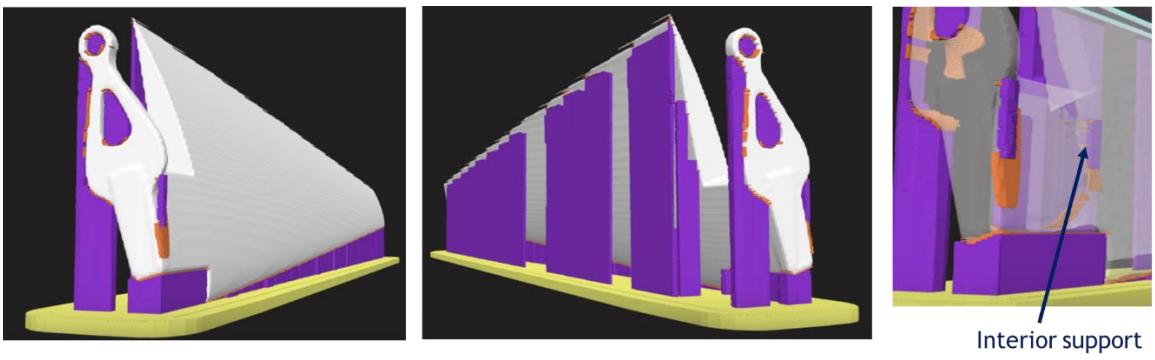

Figure 42 – Internal view of the supports generated by Eiger

3.4.3. Generative design for individual wings

The alteration strategy of the design for the individual wings will be similar to the process previously demonstrated for the complete wings. However, it needs to be adjusted since there are two wings with a connection and variations in the static analysis.

3.4.3.1. Development of the connecting system between foil wings

The workflow from the complete wing can be used as the base for this optimization, and just like the previous approach, the shell thickness was produced with the same parameters as the complete wing. Before running the rest of the workflow, it was necessary to fill the inside of the constraint volume to allow the development of the connection mechanism that better connects the wings to the lever and guarantees that the wings will not disassemble while performing their function. As seen in Figure 43, material from the interior was removed to create the shell, added material to the connection volume, and perforated the region where a cylinder pin would be placed to connect both wings and the lever.

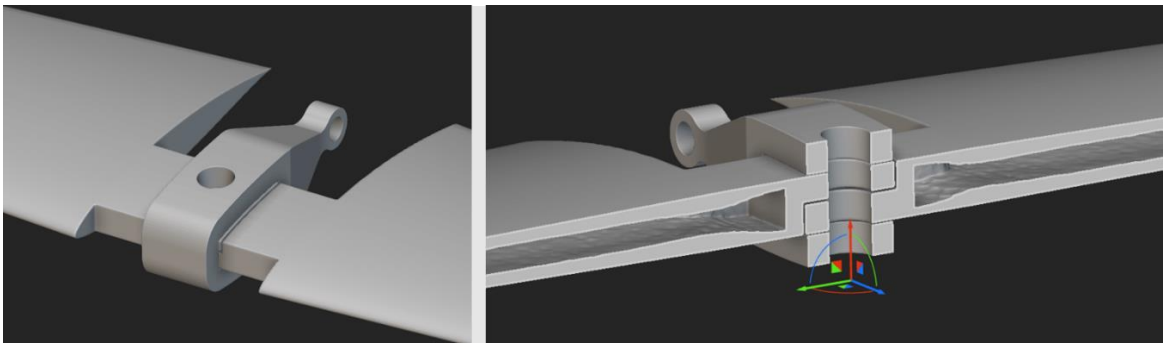

Figure 43 - Top view and cross section of the cylinder hole created to connect both wings, from nTopology

The static analysis demonstrated that they don't yield since the maximum von Mises stress was 45.55 MPa for the *right wing* and 71.40 MPa for the *left wing*, and there was a decrease in mass to 190.24 g and 188.69 g. Although it is predicted not to fail, the left wing has a significantly higher amount of stress, which can happen due to the geometry of the part, since the edges are not chamfered or have a fillet. It can also happen due to imperfections in the volumetric mesh (although the mesh definitions are the same for all static analyses). The static analyses performed before and after these alterations have a similar visual representation to the Inconel static analysis, and they can be consulted in Annex 2 and Annex 3 for the before and after optimization operations.

3.4.3.2. Part orientation and building supports

Identical to the complete wing optimization process, lattice structures are not the appropriate approach, and once again, it was used the Minimum Support Orientation Block. The maximum overhang angle is 45º, but in this approach will be inferior (40º) as precaution, making sure that Eiger builds enough support during printing, washing, and sintering. In Figure 44 are the different orientations obtained for the right and left wings. Because of the filled connection region, it becomes a bit heavier on that area, excluding

one (1) and five (5) for the right wing, and one (1) and two (2) from the left wing. The wings closer to the Z limit for the Metal X printer were excluded since Eiger will expand the parts to compensate for the shrinkage. Besides, they have a higher inclination that can be troublesome for printing, washing, and sintering. Leaving orientations two (2) and three (3) from the right wing, and three (3) from the left wing. The two remaining right wings have an identical orientation, and the chosen part has a slightly lower inclination.

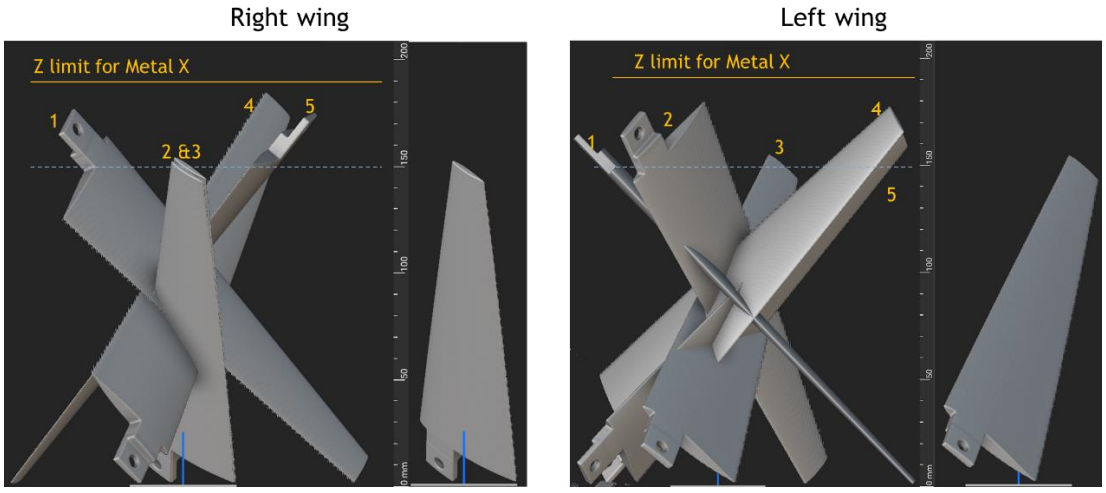

Figure 44 - Minimum support orientations the right and left wings, taken from nTopology

Afterward, using the *Manufacturing Support Volume* Block the volume of infill calculated that would act as support was inexistent. According to nTopology, no supports were needed because no supports were generated. To confirm, the wings were converted into an STL file and then placed and sliced in Eiger. However, when placed on the slicer, they were found to be above the upper limit and exceeded 180 mm in height. Due to the expansion done to compensate for the contraction, the right wing had a height of 180.3 mm and the left wing 183.9 mm, corresponding to 151.3 mm and 153.4 mm after sintering. Therefore, the maximum height must be inferior to 150 mm, and all the orientations found in Figure 44 are not feasible.

There is currently no option to limit a part to a build volume box or restrict the maximum height on a transformation. The Minimum Height Orientation Block could be used, but it would discard the minimum support orientation, which influences the amount of material placed in the interior. In attempting to solve this issue the left wing was manually rotated 3º in Eiger. This angle was enough to be printed in the Metal X, but sintering would have to be external. The slicing result shown in Figure 45 demonstrated the creation of very few supports, which is desirable for less material waste and printing time. However, the part has a very high inclination in a large area without supports, and according to the Metal X design guide, during sintering, the heat induces a clay-like state making the part malleable, being essential stability in tall and thin features.

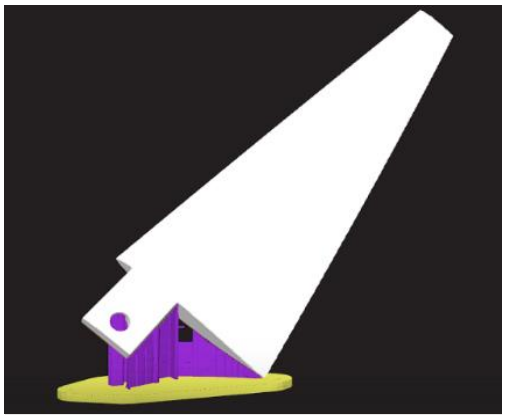

Figure 45 – Left wing with a 3º rotation to be able to be printed, taken from Eiger

It was performed several rotations in nTopology to find an orientation that could stabilize the part while printing and is adequate for sintering too. Afterward, it was studied to see where inside supports would be necessary. The obtained orientations were similar to the one in the complete wing and are present in Figure 46, along with the interior support generated by Eiger. Although it was added material to eliminate the interior supports in nTopology, a small portion of supports was generated by Eiger.

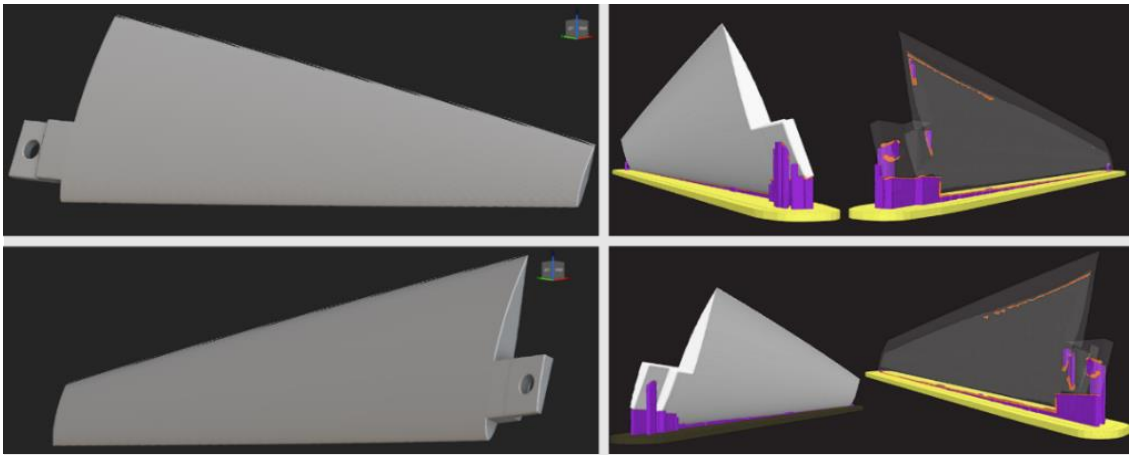

Figure 46 – On the left the orientations from nTopology and on the right the support generation on Eiger. Left wing on top, Right Wing on the bottom.

After adding material, nTopology estimated that the wings would weigh 190.62 g (right) and 192.19 g (left), corresponding to a weight reduction of between 34 and 35%. The wings were sliced with triangular infill with four (4) walls, roof, and floor layers. Eiger predicted that the left wing would weigh 182.29 g after sintering and a material cost of 87.76 USD, and the right wing would be 184 g and cost 85.49 USD.

3.4.3.3. Topology optimization and validation of the lever

As done before, the lever was optimized using the Topology Optimization Block, but the piece is not integrated and needs to connect to the wings. Therefore, when defining the parameters, passive regions constraints were added to the volumes that are supposed to be kept. The other objectives and boundary constraints were the same as the previous

lever, adding the boundary constraint of the hole and altering the volume fraction constraint to adapt to the threshold.

Initially, the passive regions were defined as demonstrated in Figure 47, determining that it would keep those areas of the pin placement, the center of the wings, and the lever force. The process with the density threshold is similar to the former lever, and the threshold chosen was 0.3, using a volume fraction constraint of 0.4. The final result is displayed in Figure 47, after several boolean operations of union and intersection to ensure the connection areas stay intact. Static analysis was made, which showed a maximum von Mises stress of 10.3 MPa, with 18.5 g.

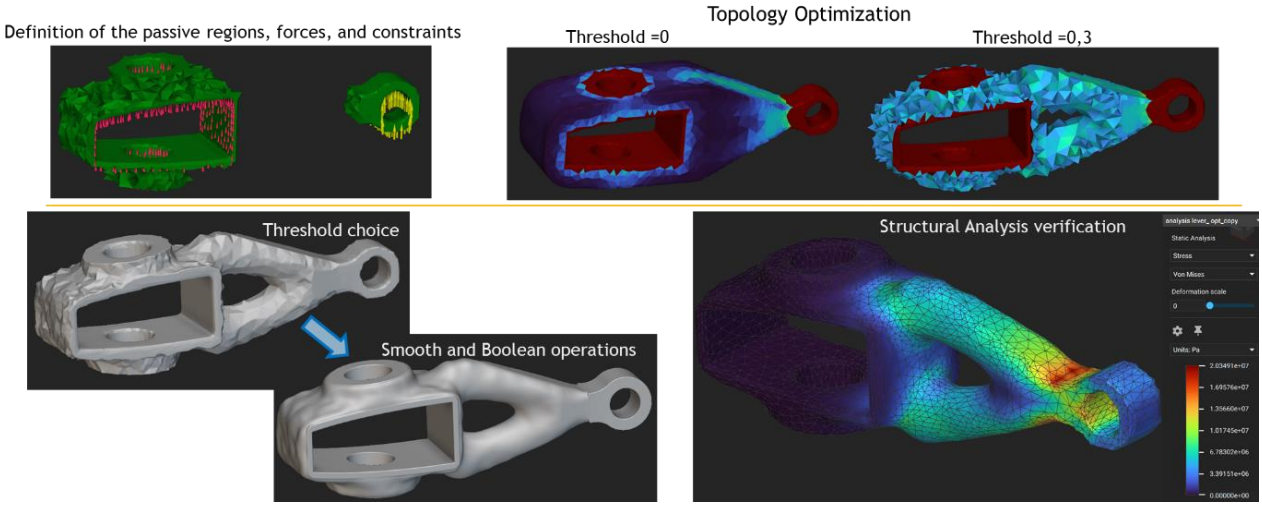

Figure 47 – Development and static analysis of a topology optimized lever, taken from nTopology

Removing one of the passive region constraints, as demonstrated in Figure 48, optimized the lever even further. The connection region of the wings was eliminated since the inserted pin does the same job, and it would already be secured in the torpedo by the bearing system. The development of the final lever is represented in Figure 48 using a threshold of 0.3 with a volume fraction constraint of 0.3. The static analysis shows that it does not yield, exhibiting a maximum von Mises Stress of 19.5 MPa, with 12-99 g, decreasing 5.51 g in comparison with the previous optimization. Furthermore, compared with the original lever there is a decrease in 24.70 g, corresponding to a 65.5% reduction in weight. It is relevant to note that coincidentally the threshold value is the same in all the lever topology optimizations while the volume fraction constraint value changes. This happened because the in levers from Figure 47 and Figure 48 need a higher volume fraction constraint that must become higher as more regions are being kept, facilitating the threshold value choice. In some cases, keeping the same value for volume fraction, all the material would be removed from the lever before the threshold reached 0.5. The threshold value choice was made intuitively and iteratively considering the smooth operations (that remove material).

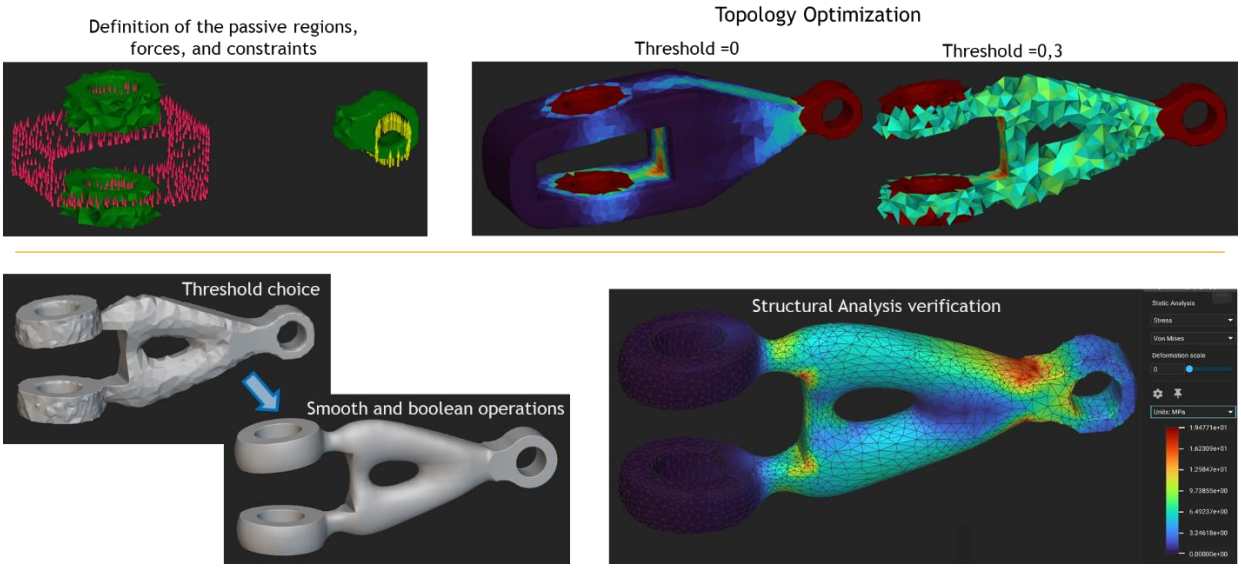

Figure 48 -Second approach to the development of a topology optimized lever, taken from nTopology

Figure 49 displays the result with the lever and pin in place, between the wings. The pin has an estimated mass of 4.80 g. Represented in Figure 50 are the lever and pin prototypes printed in PLA after finalizing the optimization processes to test the movement mechanism.

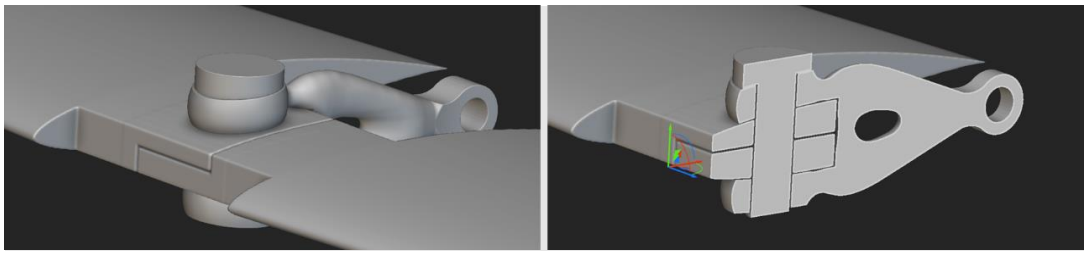

Figure 49 - Final lever placed between the wings and its cross section, taken from nTopology

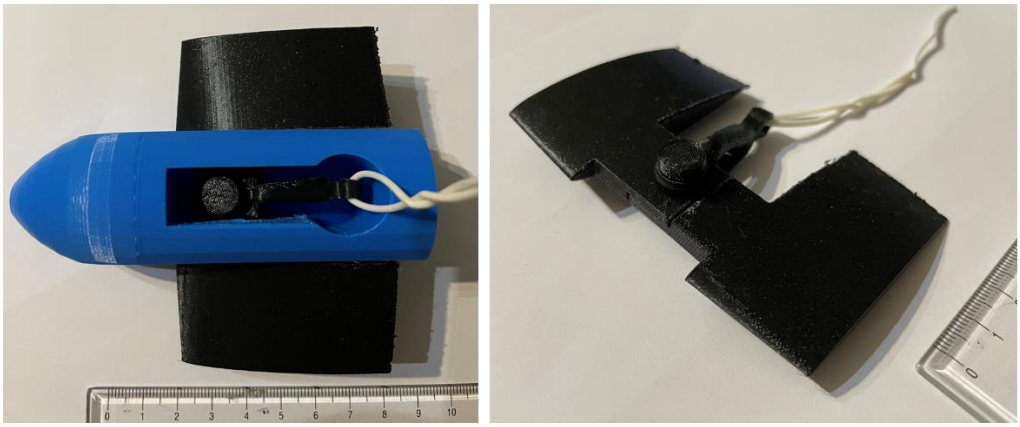

Figure 50 - Wing's movement mechanism after lever optimization. With and without torpedo

The lever and pin were sliced in Eiger, as represented in Figure 51. The orientations chosen considered the direction of the forces, and that usually, parts are weaker in the Z-direction, than in the XY-direction. Therefore, with this orientation, the detachment effect between layers is minimized. The lever and pin were sliced with triangular infill

with four (4) walls, roof, and floor layers. Eiger predicted that the lever would weigh 9.75 g after sintering and a material cost of 10.92 USD, and the pin would be 3.55 g and cost 4.31 USD.

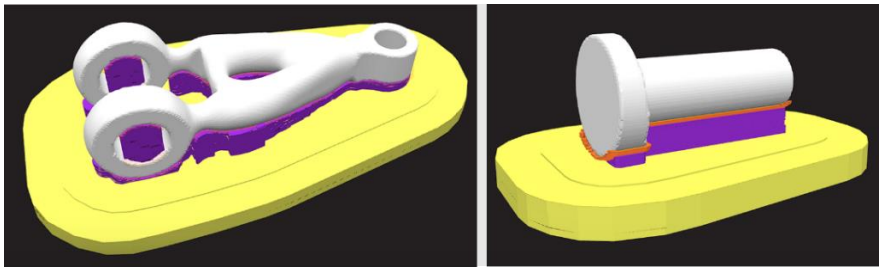

Figure 51 - Internal view of the lever and pin sliced in Eiger

Pressure will lock the pin in place using liquid nitrogen. After submerging the pin in the liquid nitrogen, it will contract, and then placing it in the hole will expand to its original geometry at room temperature and be tied in by pressure.

3.5. Optimization for Onyx reinforced with Carbon Fibers

This section will focus on the optimizations in Onyx reinforced with carbon fibers composite, including Onyx alone. As previously stated, the workflows can be reused, using the former optimization processes. However, adaptations are inevitable to fit the material properties and printing limitations.

For composite reinforced materials slicing in Eiger has many variables to consider. It is possible to select the filament materials for the exterior and the reinforcement, the number of wall and reinforcement layers, the laying pattern type of fiber fill, and where it is placed. Associated with the lack of properties in literature and the diverse variables that affect the part properties, it is challenging to identify the suitable properties to use in static analysis. Although it is possible to introduce the orthotropic properties in the Orthotropic Linear Elastic Property block, there is a lack of properties and consistency in the literature. Therefore, using the Isotropic Linear Elastic Property block, values from Avanzini, A. *et al.*[33], who found the properties of a quasi-isotropic sample, can be considered appropriate to estimate the behavior (as a simplification). The properties introduced in the block are Young's modulus and Poisson ratio, which according to the authors are 11.820 GPa and 0.33, respectively [33].

Finding the density was challenging since it depends on not only the previously stated variables but also the geometry and volume of the part, which conditions the fiber quantity and placement. The density is an imported input because nTopology calculates the mass based on the volume of the part. Without this factor, it is harder to get a reliable indication of the mass change between optimization steps.

One of the attempts to find the density consisted in slicing a solid 10x10x10 mm cube in Eiger and finding out how much it would weigh. It is also essential to understand that Markforged printers always lay Onyx wall layers to get a better surface finish and for the

parts to become watertight and place the fiber reinforcement in the interior between those Onyx walls. Varying the cube size proved that the number of fibers would vary and therefore, the mass and density, as demonstrated in Table 4. As size increased, the ratio between the onyx and fiber reinforcement volumes decreased, and density increased, varying from 0.44 to 1.34 g/cm^3. Therefore, this was not an effective way to obtain this value.

Table 4 – Density of different size cubes

cube size (cm)	mass (g)	Volume (cm^3)		density (g/ cm^3)	Vonyx/Vfiber
		Onyx	carbon fiber		
1x1x1	1.2	2.2	0.5	0.44	4.7
3x3x3	33.6	9.6	20.5	1.12	0.5
5x5x5	158.8	21.3	103.0	1.28	0.2
8x8x8	663.4	54.0	440.5	1.34	0.1

Another attempt to find this density was carried out by slicing a previously optimized wing as an approximation. In Figure 52 are represented two wings, the top one is Inconel's half-complete wing, and the bottom varies in thickness between 2 and 6 mm. For slicing it was defined two (2) exterior Onyx wall layers (0.80 mm) and carbon fibers for the reinforcement infill with isotropic fibers with four (4) different orientations (quasi-isotropic infill). These steps were important, not only to estimate density but also to understand where and how Eiger deposits fibers. In the wing optimized for Inconel, it is possible to observe in blue thee only eight (8) small layers of carbon fiber reinforcement (0.08 cm3) on the part, and the rest is Onyx layers. This is quite a small volume of fibers and not enough to represent the composite material, because the walls are thin, and there is no place to lay the reinforcement. Before concluding that the outer walls (shell) need to be thicker, it was necessary to understand the effect of the build orientation on the fiber deposition. As it is also possible to see in Figure 52, positioning the wing horizontally leads to significantly higher deposition of fibers, having 3.71 cm3. However, this orientation produces many interior supports that are impossible to remove.

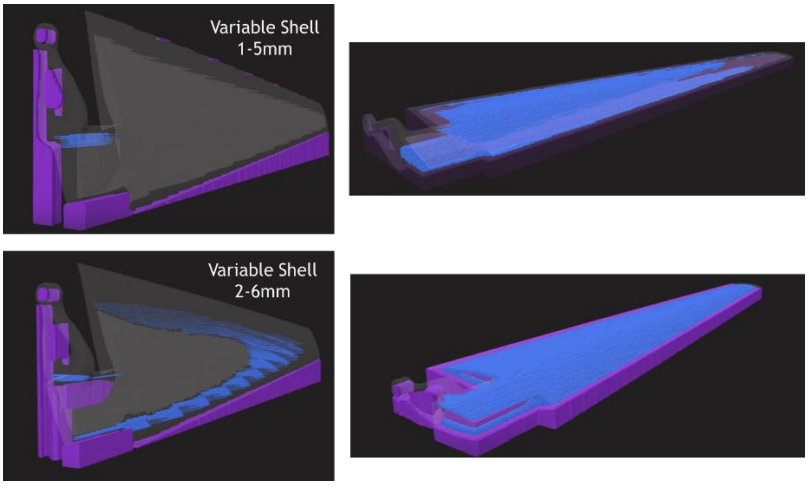

Figure 52 – Slicing the half of the Inconel complete wing with different variable shells using carbon reinforcement parameters, taken from Eiger

The lack of fibers is related to the fact that Eiger lays Onyx on the interior walls of the shell as well as the outside walls, leaving a small or inexistent gap for the reinforcement placement. Therefore, both shell thickness and part orientation are essential for design and optimization. Another density estimation was made with a similar part but thicker walls to accommodate better and account for the reinforcement fibers. Using the optimized design of the Inconel complete wing and changing the variable shell to values between 2 and 6 mm (bottom wing from Figure 52), obtained a new wing for this purpose. It was sliced in Eiger, having 1.10 cm^3 of fiber reinforcement with inclination. The horizontal build orientation placed 18.32 cm^3 of Onyx and 16.04 cm^3 of fiber reinforcement with 41.76 g in total, giving a density of 1.22g/cm^3. This value is fairly close to 1.25 g/cm^3, which is the estimation made by slicing the sample with the same geometry and conditions as the sample made by Avanzini, A. *et al.* [33].

The placement of the fibers in the parts influenced the subsequent optimization steps. The Inconel part results were key in identifying these factors since possible new optimizations will not deviate from these results. Knowing that the fiber deposition is constrained between the two walls and that a considerable area is required in each layer for fibers to be deposited, orientations other than horizontal from Figure 52 are inappropriate. On the other hand, the placement of supports inside the part is impossible to remove and will increase the weight. However, this increase is relatively small when compared to Inconel parts. It is also noteworthy that the lever, with those orientations, never has sections with the necessary areas to deposit carbon fibers, and therefore it must be analyzed as a different material.

Looking at these factors, it was decided on three (3) optimization options. They are: the creation of a variable shell and leaving the supports inside, conservation of a solid wing (no optimizations) with less restriction on fiber deposition, or optimization on Onyx alone freeing the part of the mentioned restrictions. Because the carbon fiber reinforcement is expensive (Onyx costs ~0.24 \$/cm^3 and Carbon fiber costs 3 \$/cm^3), keeping the wing solid and full of reinforcement material was discarded with a material cost of 560 USD.

3.5.1.1. Generative design for Onyx Reinforced with Carbon Fibers

This section explores the option of creating the variable shell, that leaves the interior supports generated by Eiger. nTopology allows the reuse and recycling of previous workflows, used for Inconel 625. Since the geometries and boundary conditions are the same, most of the preexisting workflow, both for static analysis and optimization, will be reutilized, tunning some parameters and adapting the optimization. The simulations for the composite material were made the same way as for Inconel, using the same geometries, forces, and constraints shown previously for Inconel. However, it was necessary to differ the material regions and properties in the same model, including Onyx and the carbon reinforcement.

The material in the wing varies between volumes of Onyx and carbon fibers, which can only be determined after exporting and slicing with the Eiger parameters. This is a limiting

factor and brings uncertainty to the results since the static analysis becomes a rough estimation, accumulated with the uncertainty from the composite anisotropy. However, the material block allows for material distinction between different regions in the same part. According to Eiger, the two (2) Onyx wall layers correspond to 0.8 mm. Therefore, for the static analysis, it was defined with a 0.8 mm Onyx shell and an interior with the properties of the quasi-isotropic sample from Avanzini, A. *et al.* [33]. Using the FE Region by Body block the volumes for the different materials were defined, using new bodies that suited those regions, and the result is represented in Figure 53. The properties for Onyx were 2.4 GPa for the Young Modulus, 0.35 for the Poisson Ratio, and 1.2 g/cm^3 for the density, and the carbon fiber reinforcement was 11.820 GPa for the Young Modulus, 0.33 for the Poisson Ratio and 1.2g/cm^3 for density.

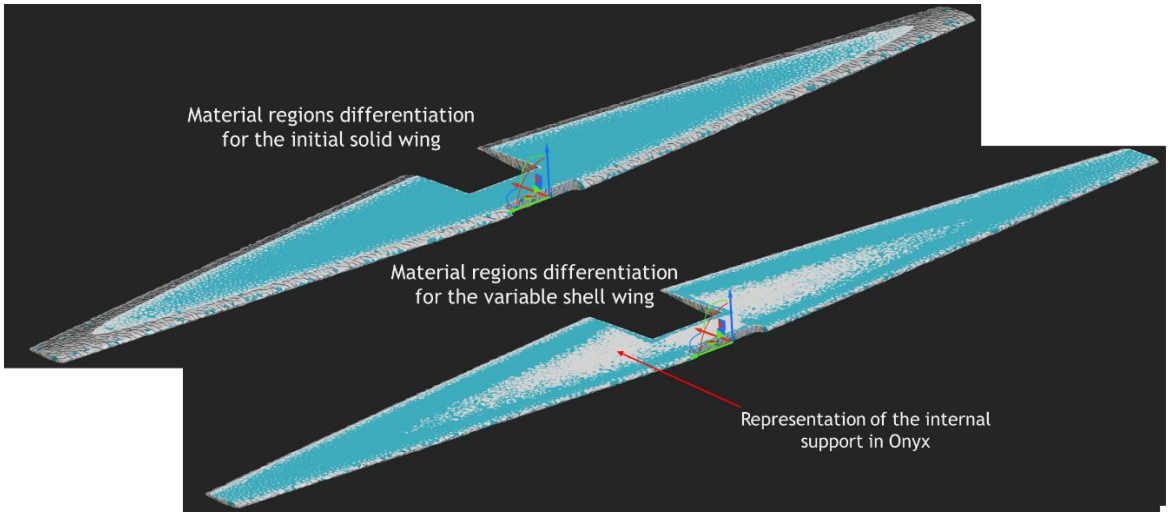

Figure 53 - Definition of the material regions in the complete wing, with Onyx in white and carbon fiber in blue, taken from nTopology

The static analysis result revealed a maximum displacement of 1.1 cm and maximum von Mises Stress of 34.31 MPa, which is lower than the yield limit for Onyx (40 MPa) and the ultimate tensile strength (used in this case since it has a linear behavior in the stress-strain curve) of the quasi-isotropic (194 MPa). Then, the scalar field was generated with the von Mises stress values and created a shell with variable thickness between 2 and 5 to provide space for fiber placement. Since this part will incorporate the internal supports, the static analysis was made taking this factor into account. Using the FE Region by Body block the outside layers and the interior region (supports) were considered Onyx, and the interior of the variable shell part was considered reinforcement material (quasi-isotropic properties). This static analysis determined a maximum stress of 33.94 MPa and the same 1.1 cm displacement. The lever optimization was similar to the previous development represented in Figure 39, and as noted before, its material is Onyx. The threshold value chosen was 0.3 and the static analysis showed maximum stress of 31.63 MPa. Another difference from the Inconel process is the search for the optimal building orientation since it is already defined. The final model is represented in Figure 54, as well as the result of the slicing process from Eiger.

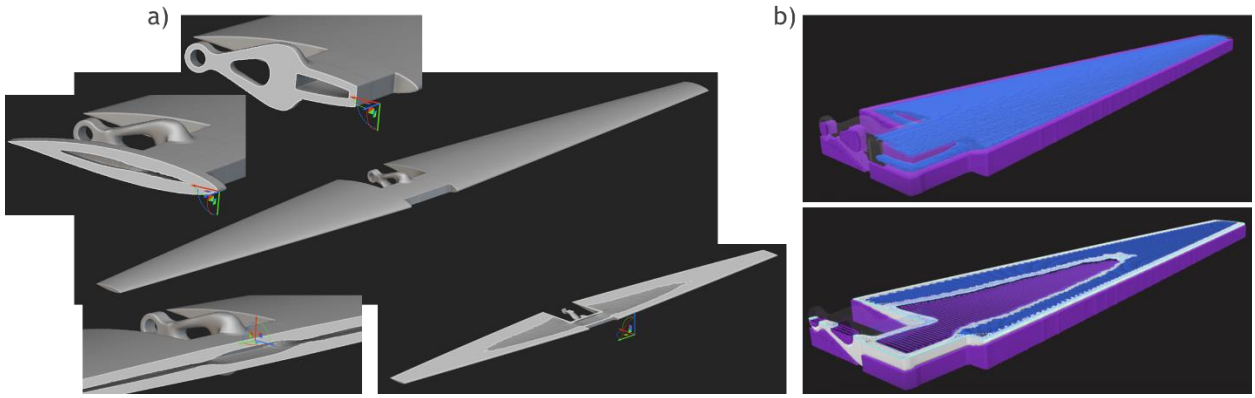

Figure 54 - Final result from the complete wing using carbon fiber reinforced Onyx, a) in nTopology and b) in Eiger

The mass estimation of the final wing is not very accurate, but it is approximated to 83.63 g in nTopology. Because the software doesn't take into account the mass of the supports generated, the weight prediction from Eiger is flawed. The mass calculated with no supports or brims was 88.26 g, but it will probably be a bit heavier due to interior supports.

Like the latter procedure Inconel's workflow was reused as the basis for individual wings' generative design. The changes in the material definition were the same, and after the static analysis, the maximum von Mises stresses found were 36.05 MPa and 33.74 MPa for the right and left wings, respectively. Both had a maximum displacement between 1.1 and 1.2 cm and weighted in Eiger about 44.2 g each. The same strategy to create the variable shell was executed, with a thickness variation between 2 and 5 mm. For the static analysis, when defining the materials for these pieces, the Onyx supports inside the part were once again taken into account, as demonstrated in Figure 55. The results proved that it would not fail because it has maximum stress of 36.69 MPa in the right wing and 37.64 MPa for the left wing, maintaining the same displacement. The mass estimated in nTopology was 41.66 g (right) and 41.78 g (left), while in Eiger 40.81 g (right) and 41.37 g (left) were obtained, not counting the mass of the supports.

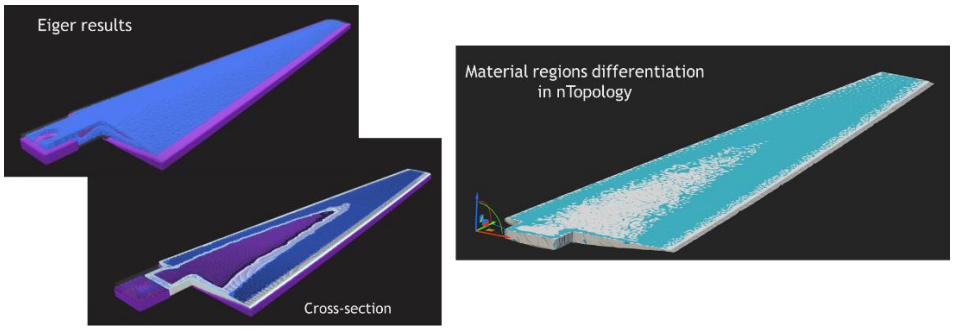

Figure 55 - Fiber placement in Eiger. Definition of the material regions in the right wing, with Onyx in white and carbon fiber in blue

The strategy used for lever optimization was the approach present in Figure 48. Keeping the same conditions for the topological optimization the chosen threshold value was 0.25.

After exporting the STL file and importing it into Eiger, it verified that the part presented regions with enough area for carbon fibers deposition, with the orientation shown in Figure 56. Thus, for the static analysis, it was necessary to differentiate the materials for the regions, and the analysis revealed that the maximum stress value is inside the lever with 18.33 MPa, not being enough to yield. This part has a material cost of 1.15 USD and is estimated to weigh 2.01 g.

The results for the static analysis in the initial wing, in the variable shell, and levers have a visual representation similar to the results from the Inconel parts. Static analysis for the complete wings can be consulted in Annex 4, and individual wings in Annex 5 and Annex 6.

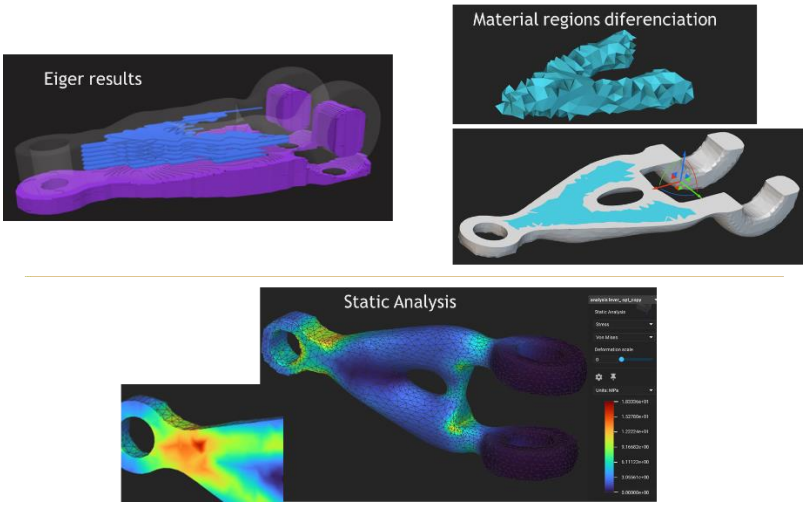

Figure 56 - Fiber placement in Eiger. Definition of the material regions in the lever with Onyx in white and carbon fiber in blue, and static analysis in nTopology

A complete set of optimized individual wings for Onyx reinforced with carbon fibers, as represented in Figure 57 has a material cost of 112.40 USD, and a print time of about 19 hours and 34 minutes.

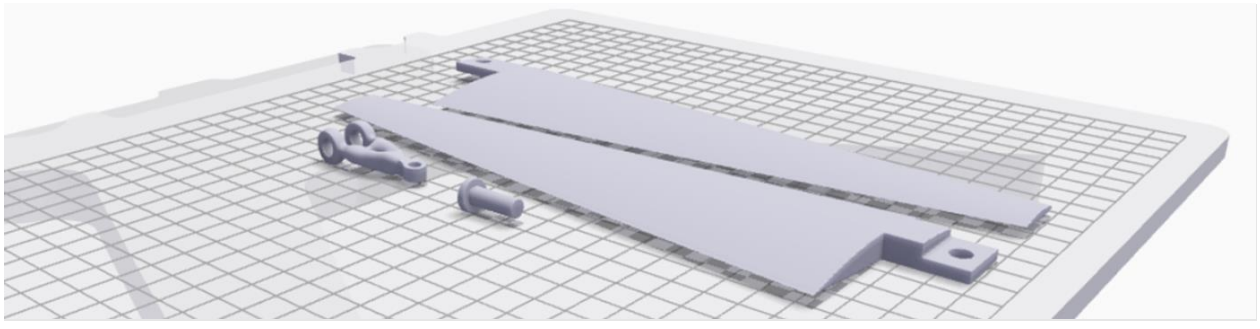

Figure 57 - Build for the set of optimized wings in Onyx reinforced with carbon fibers, from Eiger

3.5.1.2. Generative design for Onyx wings

This section will focus on the generative design optimizations for the complete and individual wings made in Onyx. Once again, the workflow reused was the one from Inconel,

and simulations were made the same way, using the same geometries, forces, and constraints shown previously. Initially, the material's properties were changed, which in this case is only Onyx, with the properties previously listed (2.4 GPa for the Young modulus, 0.35 for the Poisson ratio, and 1.2 g/cm^3 for the density).

The initial static analysis for the complete wing indicated that the maximum von Mises stress was 40.7 MPa, and since the tensile stress at a yield is 40 MPa, it is very close to the limit and is expected to yield. Therefore, Onyx cannot withstand the forces of a 25 Kg boat, and it was necessary to decrease the safety gap, considering a boat with 20 Kg. The initially attributed forces were already oversized considering a 25 Kg boat, even though 10 Kg is the expected mass. Additionally, there is a second oversize operation considering that changes in the angle of attack double the force. Decreasing to 20 Kg allows the Onyx to be considered, still giving a safety gap. Thus, the Lift force applied in all the boat foils is 400 N (accounting for the angle of attack), giving 100 N per complete wing, and 50N per individual wing. Since drag is 10% of the lift, it becomes 10 N for each complete wing and 5 N for the individual wing.

After these changes, the static analysis for the complete wing revealed that the maximum stress was 32.55 MPa with a maximum displacement of 4 cm. Then, the next step was to create a variable shell, and after experimenting with several values, it was applied thickness between 2 and 5 mm. It created a part with 74 g with a decrease in maximum von Mises stress to 30.91 MPa and displacement to 2.84 cm.

The development of the lever was the same as previously demonstrated for Inconel and Onyx reinforced with carbon fiber. The threshold of 0.22, resulting in a lever with a maximum von Mises stress of 27.44 MPa. After adding the lever to the complete wing, discovering the minimum support orientation, and adding the necessary interior support material, it was obtained the final wing with a mass of 76.63 g.

Afterward, it was carried out the optimizations of the individual wings. The static analysis determined a maximum von Mises Stress of 39.78 MPa and 36.61 MPa, for the right and left wing, respectively, as well as a maximum displacement of 2.8 cm and 2.9 cm. Once more, using the static analysis results, it was created the variable shell with a thickness between 2 and 5mm, added material to the joint volume, and subtracted the hole for the connection. These operations produced a right and left wing with a maximum stress of 34.84 MPa and 37.22 MPa, respectively, and a maximum displacement of 3.1 and 2.9 cm. Then, it was found the minimum support building orientations for both wings, represented in Figure 58, and added the interior support material, conferring a mass of 37.33 (right) and 37.01 g (left).

The topology optimization of the lever was carried out with the same approach as for Inconel and Onyx reinforced with carbon fiber. The threshold value chosen was 0.25, creating a lever with an expected mass of 2.05 g, with a maximum von Mises stress of 19.10 MPa.

Once again, the results for the static analysis in the initial wing, in the variable shell, and levers are visually similar to the results from Inconel previously demonstrated from Inconel and from the carbon fiber reinforced Onyx. Static analysis for the complete wings can be consulted in Annex 7, and individual wings in Annex 8 and Annex 9.

The meshes were exported and imported to Eiger to proceed with the slicing operations. In Eiger, the parts were sliced using a solid infill for the X7 printer. The prices were estimated, and the obtained masses were a bit lighter than the ones calculated in nTopology. A complete set of optimized individual wings for Onyx, as represented in Figure 58 has an estimated mass of 64.42 g, a material cost of 13.28 USD, and a print time of about 20 hours.

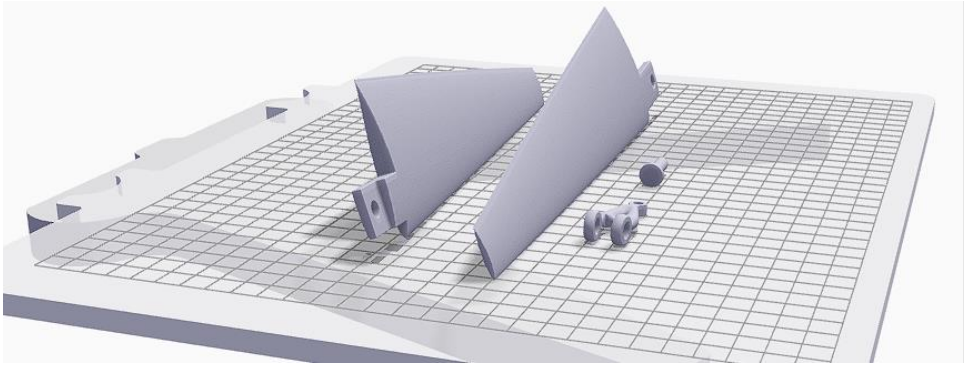

Figure 58 - Build for the set of optimized wings in Onyx, taken from Eiger

4. Results and discussion: material selection

Table 5 shows the results obtained in both software. The first three (3) columns of the results indicate the values obtained in nTopology and the remaining values in Eiger. Since no printers are currently available with the volume size for the Inconel complete wings, its values were not presented. Likewise, the results for the complete wing in the remaining materials were calculated for an FX20 printer, although it is now unavailable.

Among the present values, it is possible to identify some deviations between the masses obtained on the platforms that may be related to differences in densities. It is important to note that Inconel used a triangular infill in Eiger, hence the mass reduction obtained between the software. These differences are more noticeable between Onyx and carbon fiber reinforced Onyx since the density applied was the same for both, and the amount of reinforcement affects the density.

The material that allowed the highest mass reduction percentage was Inconel because it has a higher density and the highest Young's modulus that allows the reduction in thickness. Onyx wings reinforced with carbon fibers, on the other hand, obtained the lowest mass reduction due to the necessity of a considerable thickness for fiber deposition and due to the internal supports originating from the build orientation. It is worth noting that the masses for this case are merely indicative since the interior supports will remain

inside. The levers were the pieces where the largest reduction was obtained, around 61-65% because it is possible to change the outer boundaries becoming easier to remove material in the topology optimization.

Table 5 – Mass and cost results from the optimization for each material

						1 set of wings		4 sets of wings	
		initial mass (g)	final mass (g)	weight loss %	final mass Eiger (g)	Total mass (g)	total material cost	mass (g)	material cost
Inconel 625	complete wing	622.38	392.84	36.9%	-	-	-	-	-
	Right wing	291.61	190.62	34.6%	184.00	379.59	188.49 USD	1518.36	753.96 USD
	Left wing	292.48	192.19	34.3%	182.29				
	lever	37.69	12.99	65.5%	9.75				
	pin	4.80	-	-	3.55				
Onyx reinforced with Carbon Fibers	complete wing	88.91	83.63	5.9%	88.26	88.26	126.41 USD	353.04	505.64 USD
	Right wing	41.66	41.66	0.0%	40.81	84.83	112.40 USD	339.32	449.60 USD
	Left wing	41.78	41.78	0.0%	41.37				
	lever	5.27	2.05	61.1%	2.05				
	pin	0.69	-	-	0.60				
Onyx	complete wing	88.91	76.63	13.8%	78.05	78.05	16.61 USD	312.20	66.44 USD
	Right wing	41.66	37.01	11.2%	37.34	87.21	19.09 USD	348.84	76.36 USD
	Left wing	41.78	37.33	10.7%	46.88				
	lever	5.27	2.05	61.1%	2.15				
	pin	0.69	-	-	0.84				

The overall calculated masses indicate that, as expected, Inconel is the heaviest, with a total weight of 1.5 Kg with the four (4) foils on the boat. The carbon fiber reinforced one has an estimated mass of over 339 g since it incorporates the interior supports, and the Onyx alone will be around 349 g. Looking at the material costs it is evident that Inconel is the most expensive of this selection, followed by Onyx reinforced with carbon fibers, and Onyx alone is the lowest. The material cost for Onyx wings is about ten (10) times cheaper than Inconel, and it is possible to print the four (4) sets of Onyx wings for the whole boat and still be cheaper than one (1) set of carbon-reinforced Onyx. Nonetheless, Onyx wings don't withstand the same forces as the other two materials having a smaller safety gap and demonstrating high flexibility with almost 3 cm of displacement that changes the form of the part while performing. Moreover, its nylon matrix makes it a material prone to water absorption, which can originate problems [23].

Inconel would be the best option for a part where it was necessary to support a greater load, yet it is about four (4) times heavier than the other options. Onyx reinforced with carbon fiber is an intermediate option, which has an identical weight to the wings in Onyx, but it is about six (6) times more expensive. The carbon fibers allow the material to withstand higher forces and can lower expansion due to water absorption by Onyx.

5. Conclusions

As a response to the proposed challenge, the wings, and the rotation mechanism were created in Fusion 360, aiming to decrease the number of parts produced by AM. The work explored two (2) solutions for the wings construction, one having fewer components, and another due to the current volume build size limitation. Although it is currently not possible to print the complete wing, optimizations were made in the case that soon it will be possible. The optimization work explores three (3) materials for MEX: Inconel, carbon fiber reinforced Onyx, and Onyx. While optimizing the parts, some limitations regarding the part geometry and the Eiger slicer software were encountered.

In the wings, the external boundaries cannot be changed, and creating a shell of variable thickness proved to be an efficient way to reduce mass, even decreasing up to 37% in the complete Inconel wing. The introduction of lattices to support overhangs proved impossible due to limitations in Eiger in defining the overhang length since it inserts supports for nTopology lattices but does not insert them for Eiger's infill. In the case of Inconel, it was considered the change of orientation to avoid interior supports. In the case of carbon fiber reinforced Onyx, the flat orientation allowed the reinforcement deposition, and the interior supports were incorporated. This provides a rough surface finish that requires sanding and the application of a surface coating to improve the hydrodynamic.

In the lever, it was possible to change the outer boundaries and so topological optimization was used, achieving a 66% decrease in the Inconel lever for the two individual wings.

Regarding the selection of materials, Inconel proved to be the one that achieved the most significant weight reduction, yet it remains the heaviest, as well as the most expensive. Carbon fiber did not benefit as much from material reduction due to Eiger limitations when depositing the reinforcing fibers. This part keeps Onyx supports inside, thus it is expected a higher final mass than the calculated. Carbon fibers are an expensive material, and their introduction makes it an intermediate solution between Inconel and Onyx. Onyx proved to be the cheapest part by far, with the cost of the four (4) wings (76.36 USD) needed for the boat being less than one (1) carbon fiber reinforced Onyx wing (112.40 USD). However, this material cannot withstand the same forces, thus the lowered level of safety is very flexible, and the water may affect the geometry of the part due to expansion. Considering the final weight, cost, and the effect of the reinforcement, the variable shell wing with carbon fiber reinforced Onyx seems to be the most suitable material for MEX wing production.

nTopology software demonstrated to be a very useful and efficient tool for generative design and optimization of mass usage, as it allows control of each operation and gives great freedom in design. At the same time, this freedom and control turn the optimization procedures into a challenging and demanding process to be able to know and understand what to do.

5.1. Limitations and Future works

Some of the limitations encountered in the development of this work influenced its progress.

Markforged printers only print the files processed by Eiger, and it is not possible to escape certain aspects, such as the limitations of the overhang length, the type of support structures, and some characteristics of the fiber deposition.

One of the challenges was finding the properties for some materials since there is a lack of properties, especially in the carbon fiber reinforced Onyx. Besides, anisotropy was not analyzed. Moreover, all the static analyses in composite materials with finite elements are merely an estimation, and mechanical tests should be performed to confirm the material and design choice.

In nTopology, the freedom guaranteed by the software can be considered a strength and simultaneously a limitation since it is necessary to know and explore more solutions. It is relatively new software, and it updates several times a month, which can be beneficial if it corrects some errors but can be a limitation if they change any design strategy.

This work can be continued since there are more components to develop and optimize, including the lock mechanism between the strut and the torpedo. There are other printers available with different slicers that can explore other solutions and even with bigger chambers to print the complete wing or other parts with different orientations. Also, there needs to be more research to find the properties of the CFRP produced by AM, to obtain more reliable results.

Bibliography

1. Molland, A. and S. Turnock, *Chapter 3 - Physics of control surface operation* in *Marine Rudders and Control Surfaces: Principles, Data, Design and Applications*. 2017, Elsevier Ltd. p. 21-56.
2. Anderson, J.D., *Chapter 1 - Aerodynamics: Some Introductory Thoughts*, in *Fundamentals of Aerodynamic* 2017, McGraw-Hill Edication. p. 3-101.
3. Anderson, J.D., *Chapter 4 - Incompressible Flow over Airfoils*, in *Fundamentals of Aerodynamic* 2017, McGraw-Hill Edication. p. 321-419.
4. Administration, S.J.D.N.A.a.S., *NASA's first 50 years: historical perpesctives*. 2010: National Aeronautics and Space Administration.
5. Sacher, M., et al., *Flexible hydrofoil optimization for the 35th America's Cup with constrained EGO method*. Ocean Engineering, 2018. **157**: p. 62-72. DOI: https://doi.org/10.1016/j.oceaneng.2018.03.047.
6. America'sCup. *The technology*. 2022 10/4/2022]; Available from: https://www.americascup.com/the-technology.
7. Tipler, P.M., Gene, *Fluídos*, in *Física para cientistas e engenheiros*. 2009, LTC: Rio de Janeiro. p. 431-446.
8. Grabow, M., et al., *Influence of the manufacturing process on the interlaminar tensile strength of thick unidirectional continuous epoxy/carbon fibre composites*. Composites Part A: Applied Science and Manufacturing, 2022. **154**: p. 106754. DOI: https://doi.org/10.1016/j.compositesa.2021.106754.
9. Prüß, H. and T. Vietor, *Design for Fiber-Reinforced Additive Manufacturing*. Journal of Mechanical Design, 2015. **137**(11). DOI: https://doi.org/10.1115/1.4030993.
10. Raji, M., et al., *3 - Prediction of the cyclic durability of woven-hybrid composites*, in *Durability and Life Prediction in Biocomposites, Fibre-Reinforced Composites and Hybrid Composites*, M. Jawaid, M. Thariq, and N. Saba, Editors. 2019, Woodhead Publishing. p. 27-62. DOI: https://doi.org/10.1016/B978-0-08-102290-0.00003-9.
11. Leary, M., *Chapter 1 - Introduction to AM*, in *Design for Additive Manufacturing*, M. Leary, Editor. 2020, Elsevier. p. 1-6. DOI: https://doi.org/10.1016/B978-0-12-816721-2.00001-4.
12. Kumar, S.A. and R.V.S. Prasad, *Chapter 2 - Basic principles of additive manufacturing: different additive manufacturing technologies*, in *Additive Manufacturing*, M. Manjaiah, et al., Editors. 2021, Woodhead Publishing. p. 17-35. DOI: https://doi.org/10.1016/B978-0-12-822056-6.00012-6.
13. Krishna, R., M. Manjaiah, and C.B. Mohan, *Chapter 3 - Developments in additive manufacturing*, in *Additive Manufacturing*, M. Manjaiah, et al., Editors. 2021, Woodhead Publishing. p. 37-62. DOI: https://doi.org/10.1016/B978-0-12-822056-6.00002-3.
14. Varotsis, A.B. *What is Design for Additive Manufacturing?* 2022 30/5/2022]; Available from: https://ntopology.com/blog/what-is-design-for-additive-manufacturing/.
15. Zhang, X. and F. Liou, *Chapter 1 - Introduction to additive manufacturing*, in *Additive Manufacturing*, J. Pou, A. Riveiro, and J.P. Davim, Editors. 2021, Elsevier. p. 1-31. DOI: https://doi.org/10.1016/B978-0-12-818411-0.00009-4.
16. HUBS. *Additive technologies compared: Metal 3D printing*. 21/6/2022]; Available from: https://www.hubs.com/guides/metal-3d-printing/.

17. All3DP. *The Types of 3D Printing Technology in 2022*. 2021 21/6/2022]; Available from: https://all3dp.com/1/types-of-3d-printers-3d-printing-technology/.
18. Relvas, C., *Classificação dos Porcessos*, in *O mundo da Impressão 3D e do Fabrico Aditico*, engebook, Editor. 2018. p. 53 - 65.
19. Shanmugam, V., et al., *The mechanical testing and performance analysis of polymer-fibre composites prepared through the additive manufacturing*. Polymer Testing, 2021. **93**: p. 106925. DOI: https://doi.org/10.1016/j.polymertesting.2020.106925.
20. Blok, L.G., et al., *An investigation into 3D printing of fibre reinforced thermoplastic composites*. Additive Manufacturing, 2018. **22**: p. 176-186. DOI: https://doi.org/10.1016/j.addma.2018.04.039.
21. Diegel, O., A. Nordin, and D. Motte, *Additive Manufacturing Technologies*, in *A Practical Guide to Design for Additive Manufacturing*, O. Diegel, A. Nordin, and D. Motte, Editors. 2019, Springer Singapore: Singapore. p. 19-39. DOI: 10.1007/978-981-13-8281-9_2.
22. van de Werken, N., et al., *Additively manufactured carbon fiber-reinforced composites: State of the art and perspective*. Additive Manufacturing, 2020. **31**: p. 100962. DOI: https://doi.org/10.1016/j.addma.2019.100962.
23. Díaz-Rodríguez, J.G., A.D. Pertúz-Comas, and O.A. González-Estrada, *Mechanical properties for long fibre reinforced fused deposition manufactured composites*. Composites Part B: Engineering, 2021. **211**: p. 108657. DOI: https://doi.org/10.1016/j.compositesb.2021.108657.
24. Nurhudan, A.I., et al., *Additive manufacturing of metallic based on extrusion process: A review*. Journal of Manufacturing Processes, 2021. **66**: p. 228-237. DOI: https://doi.org/10.1016/j.jmapro.2021.04.018.
25. MarkForged. *Metal X System: An accessible end-to-end metal 3D printing solution for functional metal parts, next-day*. 2022 2/6/2022]; Available from: https://markforged.com/3d-printers/metal-x.
26. Yang, F., et al., *Effect of solution treatment temperature upon the microstructure and mechanical properties of hot rolled Inconel 625 alloy*. Journal of Materials Science, 2020. **55**: p. 1-14. DOI: 10.1007/s10853-020-04375-2.
27. MarkForged, *Inconel 625: Material Datasheet*. 2019: 480 Pleasant St, Watertown, MA.
28. Dikshit, V., et al., *Chapter 17 - Recent progress in 3D printing of fiber-reinforced composite and nanocomposites*, in *Fiber-Reinforced Nanocomposites: Fundamentals and Applications*, B. Han, et al., Editors. 2020, Elsevier. p. 371-394. DOI: https://doi.org/10.1016/B978-0-12-819904-6.00017-7.
29. Papa, I., et al., *Impact behaviour and non destructive evaluation of 3D printed reinforced composites*. Composite Structures, 2022. **281**: p. 115112. DOI: https://doi.org/10.1016/j.compstruct.2021.115112.
30. MarkForged, *Material Datasheet - Composites*. 2022: Watertown, Massachusetts.
31. Fernandes, R.R., A.Y. Tamijani, and M. Al-Haik, *Mechanical characterization of additively manufactured fiber-reinforced composites*. Aerospace Science and Technology, 2021. **113**: p. 106653. DOI: https://doi.org/10.1016/j.ast.2021.106653.
32. MarkForged, *Design Guide for 3D Printing with Composites*. 2020.
33. Avanzini, A., D. Battini, and L. Giorleo, *Finite element modelling of 3D printed continuous carbon fiber composites: Embedded elements technique and experimental validation*. Composite Structures, 2022. **292**: p. 115631. DOI: https://doi.org/10.1016/j.compstruct.2022.115631.

34. Jois, K.C. and D. Höwer, *12 - Modeling and analysis of laminated composites: classical and contemporary approaches*, in *Advances in Modeling and Simulation in Textile Engineering*, N.T. Akankwasa and D. Veit, Editors. 2021, Woodhead Publishing. p. 301-349. DOI: https://doi.org/10.1016/B978-0-12-822977-4.00007-8.
35. Tam, D.K.Y., et al., *10 - High-performance ballistic protection using polymer nanocomposites*, in *Advances in Military Textiles and Personal Equipment*, E. Sparks, Editor. 2012, Woodhead Publishing. p. 213-237. DOI: https://doi.org/10.1533/9780857095572.2.213.
36. Zhao, S., et al., *Functionally graded graphene reinforced composite structures: A review*. Engineering Structures, 2020. **210**: p. 110339. DOI: https://doi.org/10.1016/j.engstruct.2020.110339.
37. nTopology. *The Engineer Guide: Generative Design*. 2022 [cited 2022 23/5]; Available from: https://ntopology.com/generative-design-guide/.
38. Varotsis, A.B. *Generative Design Tools with Full Control*. 2020 28/05/2022]; Available from: https://ntopology.com/blog/generative-design-tools-that-put-you-in-control/.
39. Brush, K. *finite element analysis (FEA)*. 14/6/2022]; Available from: https://www.techtarget.com/searchsoftwarequality/definition/finite-element-analysis-FEA.
40. SimScale. *What Is FEA | Finite Element Analysis?* 2021 14/6/2022]; Available from: https://www.simscale.com/docs/simwiki/fea-finite-element-analysis/what-is-fea-finite-element-analysis/.
41. Autodesk. *Unify design, engineering, electronics, and manufacturing with Fusion 360*. 2022 1/7/2022]; Available from: autodesk.com/products/fusion-360/overview?term=1-YEAR&tab=subscription.
42. Okada, Y., *nTop Live: What is Implicit Modeling in nTopology*. 2021, nTopology.
43. MarkForged. *Eiger Deployments*. 2022; Available from: https://support.markforged.com/portal/s/article/Eiger-Deployments.
44. Speer, T. *Low Reynolds Number Hydrofoils*. 1999; Available from: http://www.tspeer.com/Hydrofoils/h105/h105.htm
45. MarkForged. *X7: The turnkey industrial carbon fiber 3D printer for many types of functional parts*. 2022 2/6/2022]; Available from: https://markforged.com/3d-printers/x7.
46. MarkForged. *FX20: An ULTEM Filament capable large format 3D printer for big, strong, high temp parts — usable from factory floor to flight*. 2022 2/6/2022]; Available from: https://markforged.com/3d-printers/fx20.
47. SimScale. *What is von Mises Stress?* 2021 5/6/2022]; Available from: https://www.simscale.com/docs/simwiki/fea-finite-element-analysis/what-is-von-mises-stress/.
48. Mata, M., M. Pinto, and J. Costa, *Topological Optimization of a Metal Extruded Doorhandle using nTopology*. U.Porto Journal of Engineering, 2022. **Pre-print**.
49. MarkForged, *Design Guide for 3D Printing with Metals*. 2022.

Annex 1

Static analysis of Inconel complete wing after variable shell thickness operation

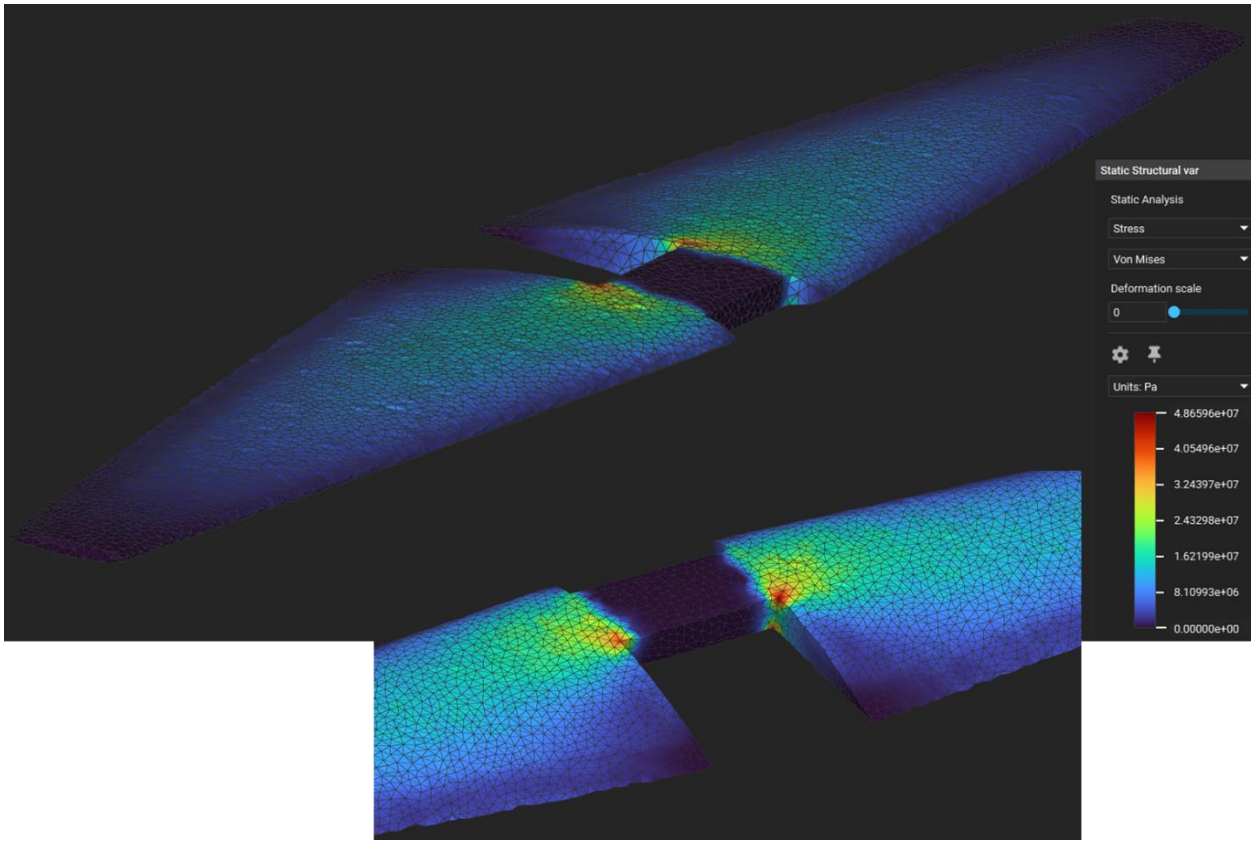

Annex 2

Initial static analysis of Inconel's right and left wing

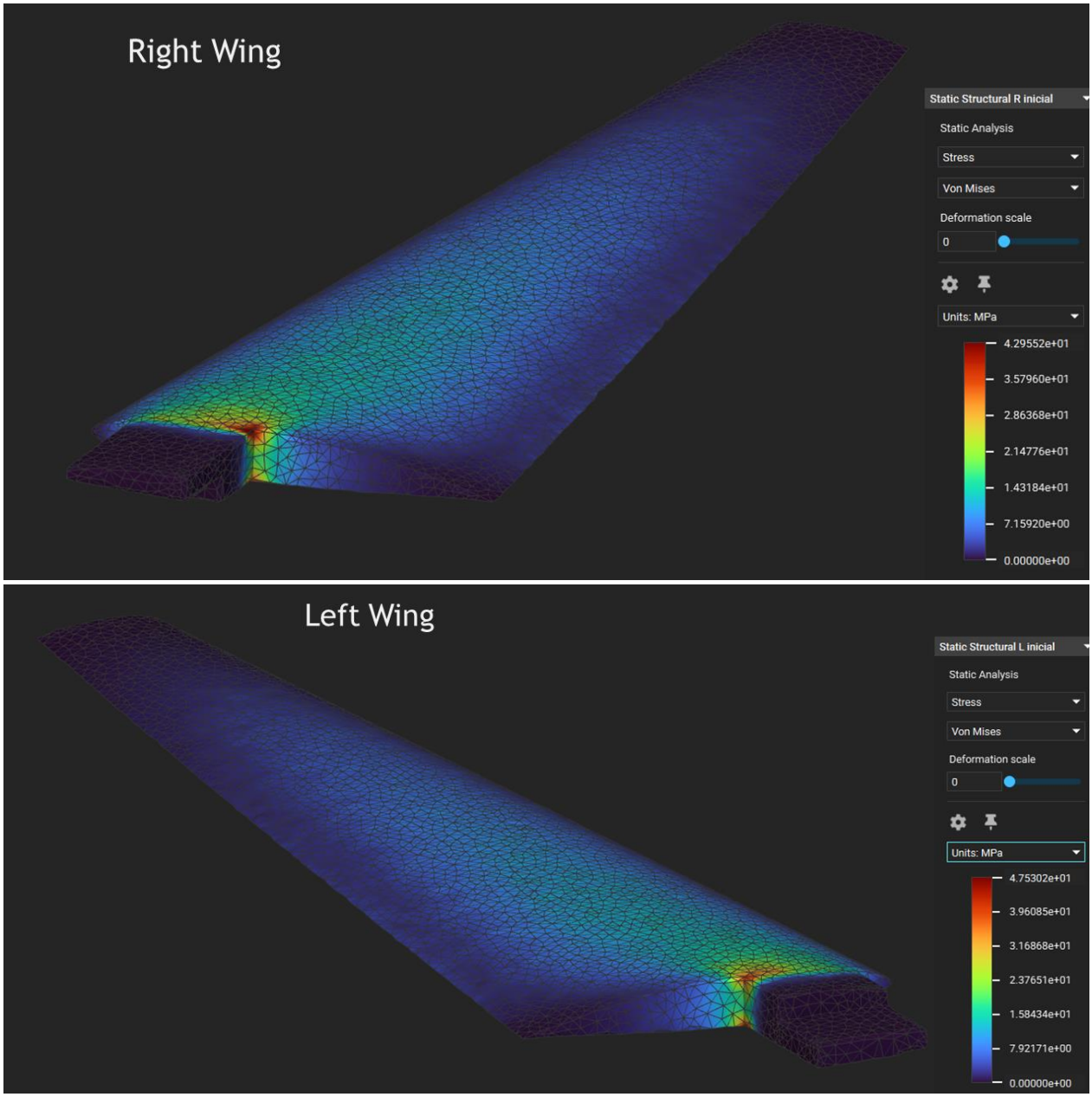

Annex 3

Static analysis of Inconel right and left wing after variable shell thickness operation

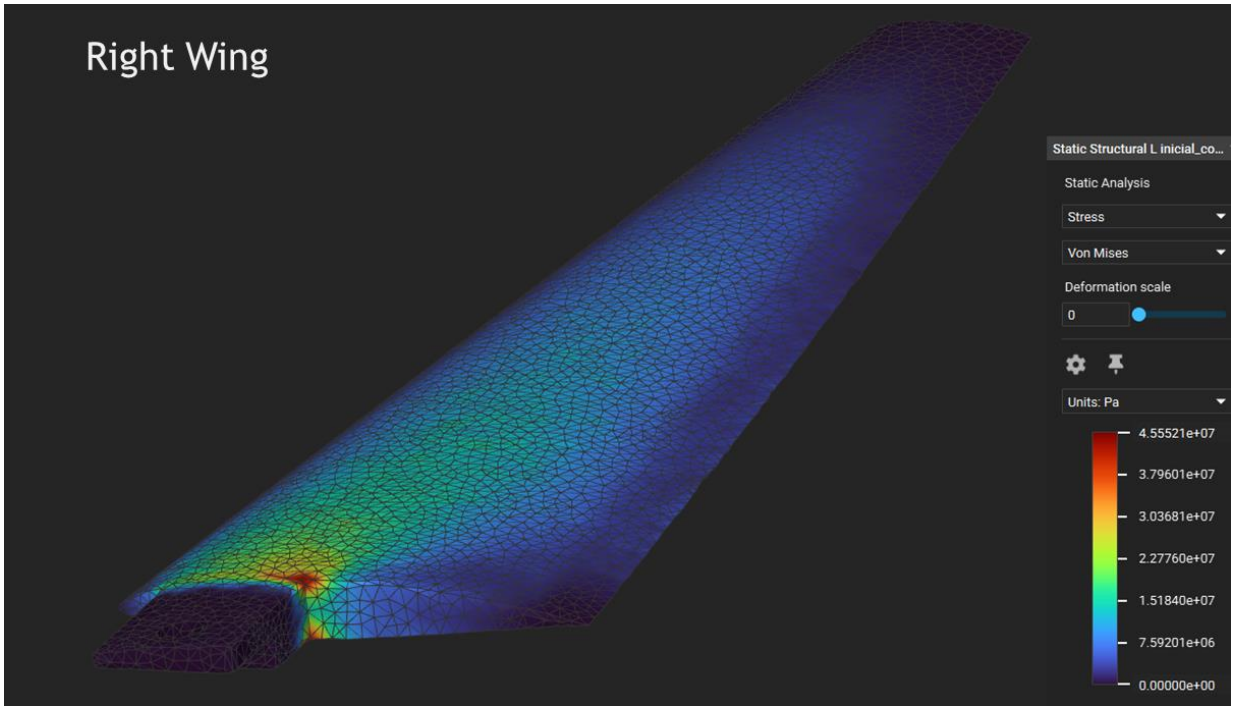

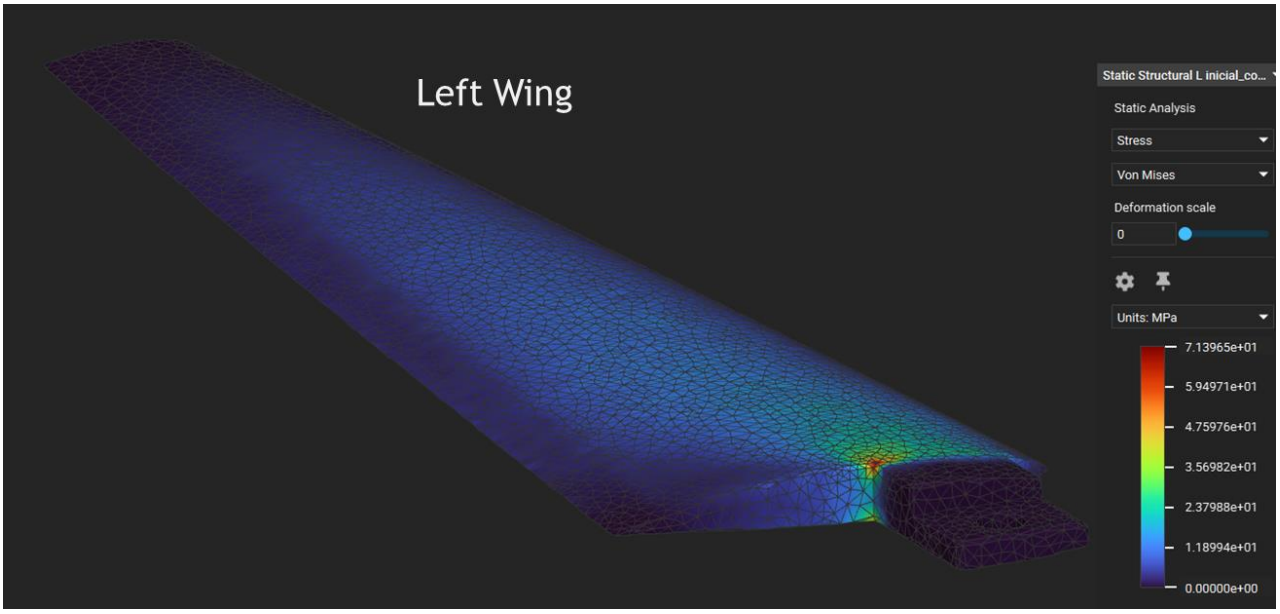

Annex 4

Static analyses of Carbon Fiber Reinforced Onyx complete wing before and after variable shell thickness operation, and initial Onyx lever

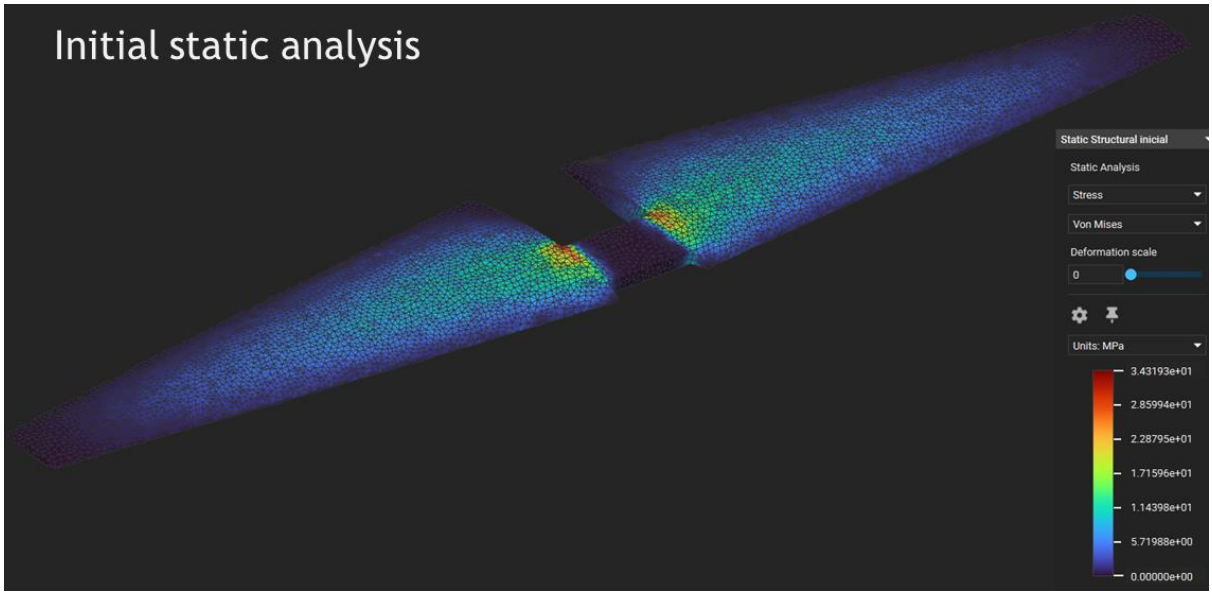

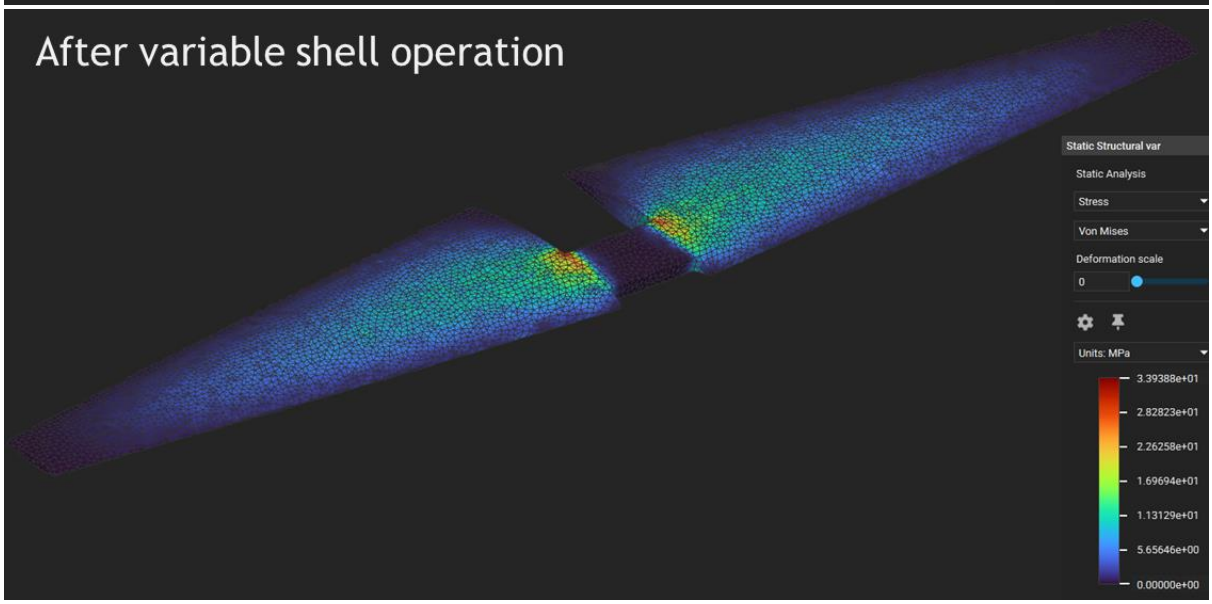

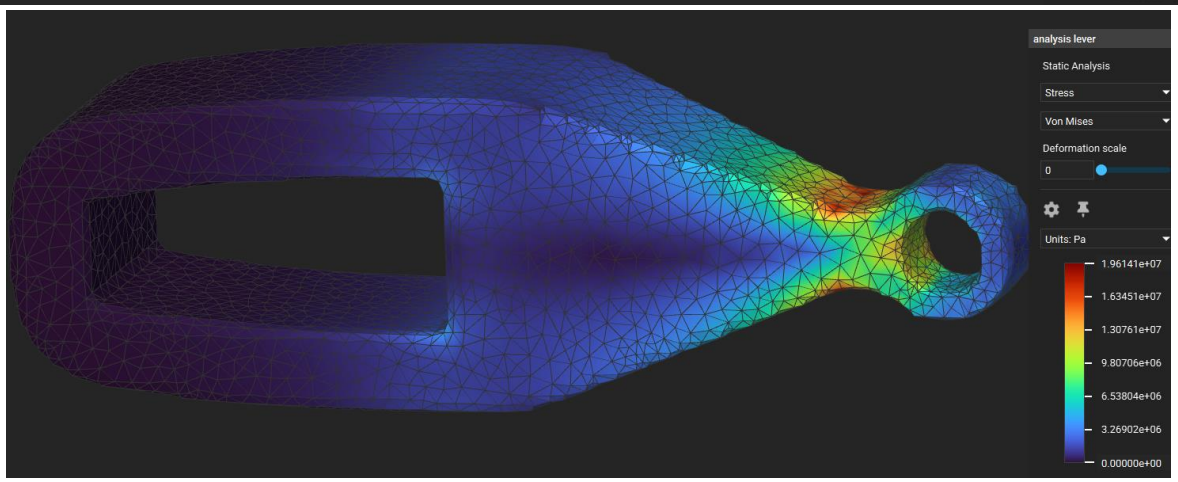

Annex 5

Initial static analysis of Carbon Fiber Reinforced Onyx individual wings

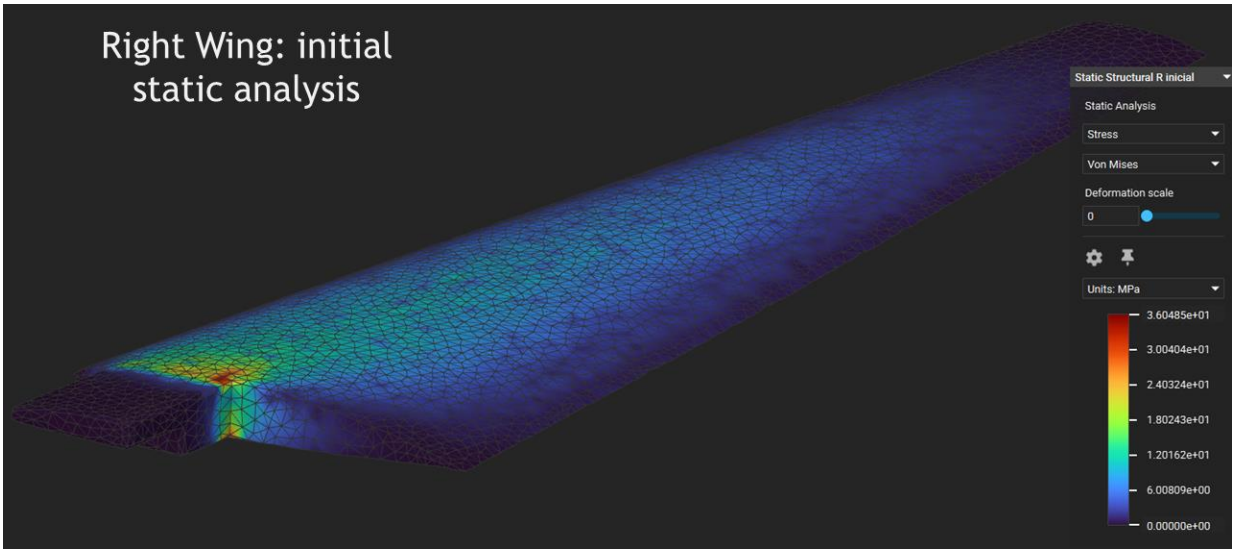

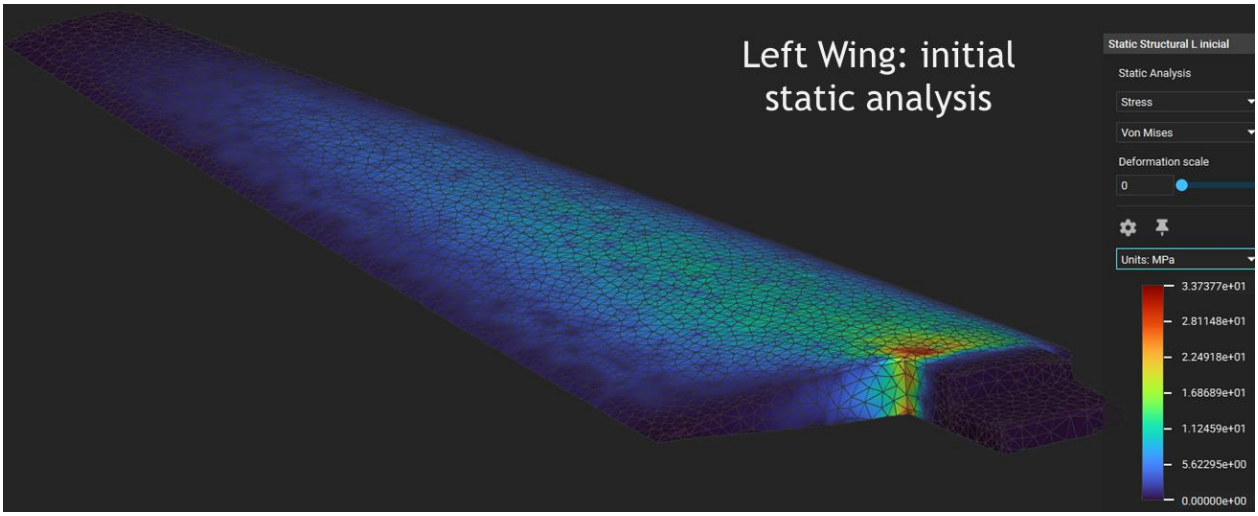

Annex 6

Static analysis of Carbon Fiber Reinforced Onyx individual wings after variable shell thickness operation

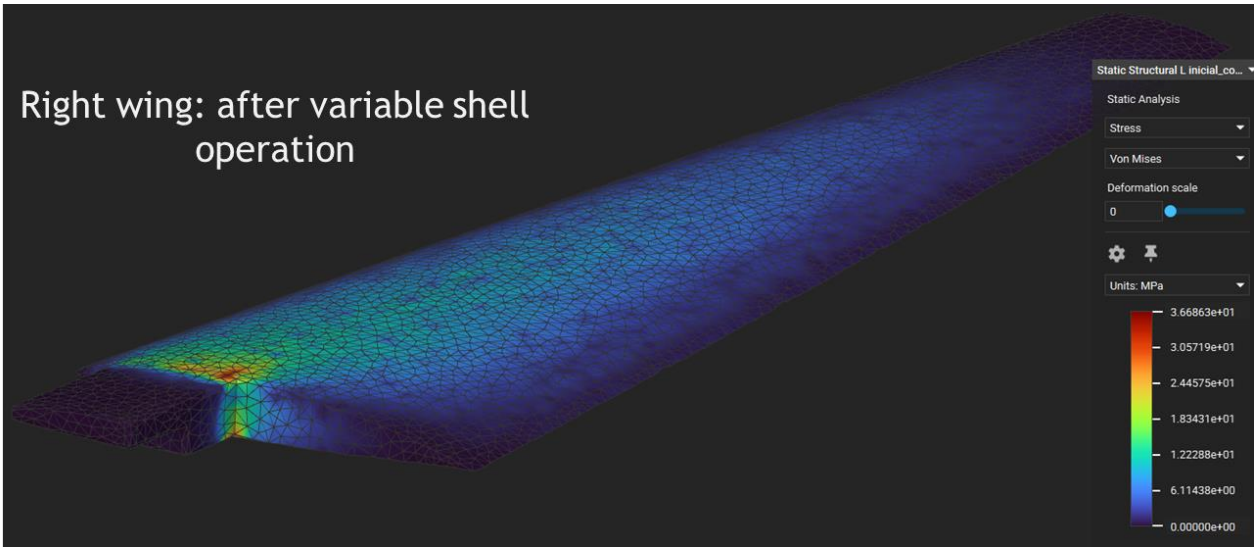

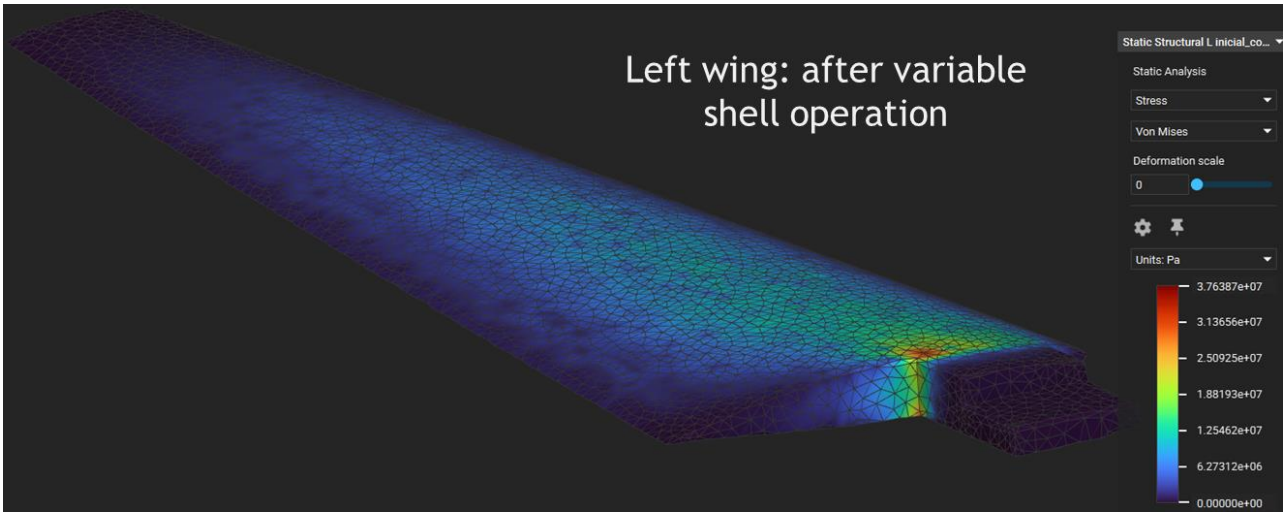

Annex 7

Static analyses of Onyx's complete wing before and after variable shell thickness operation.

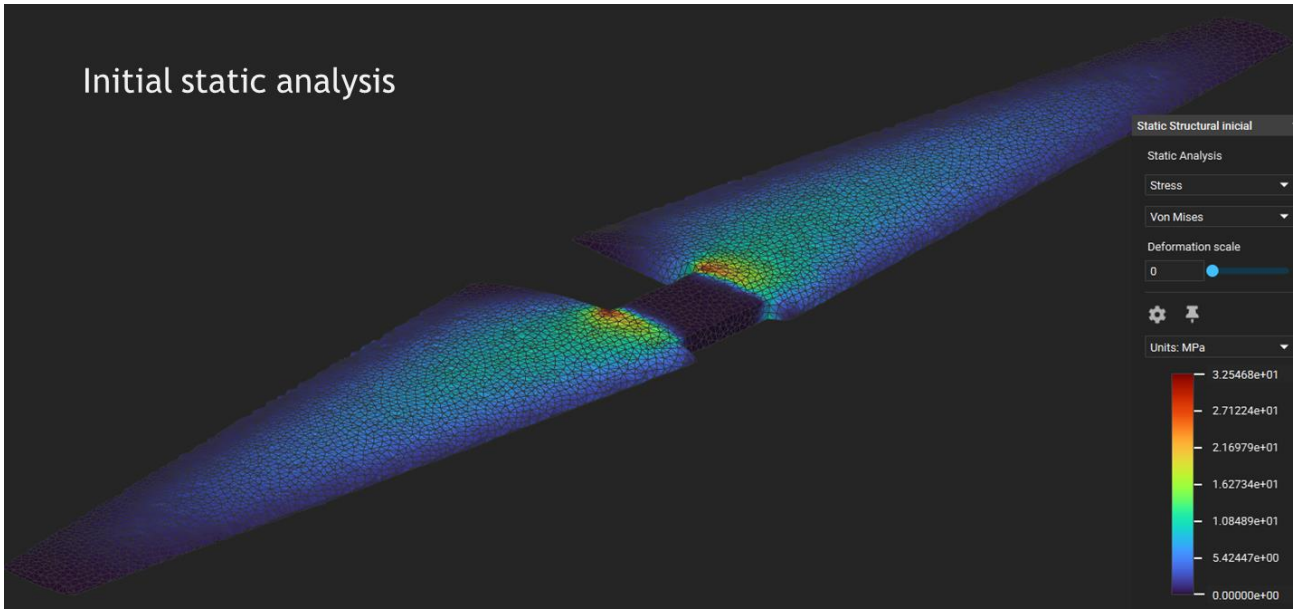

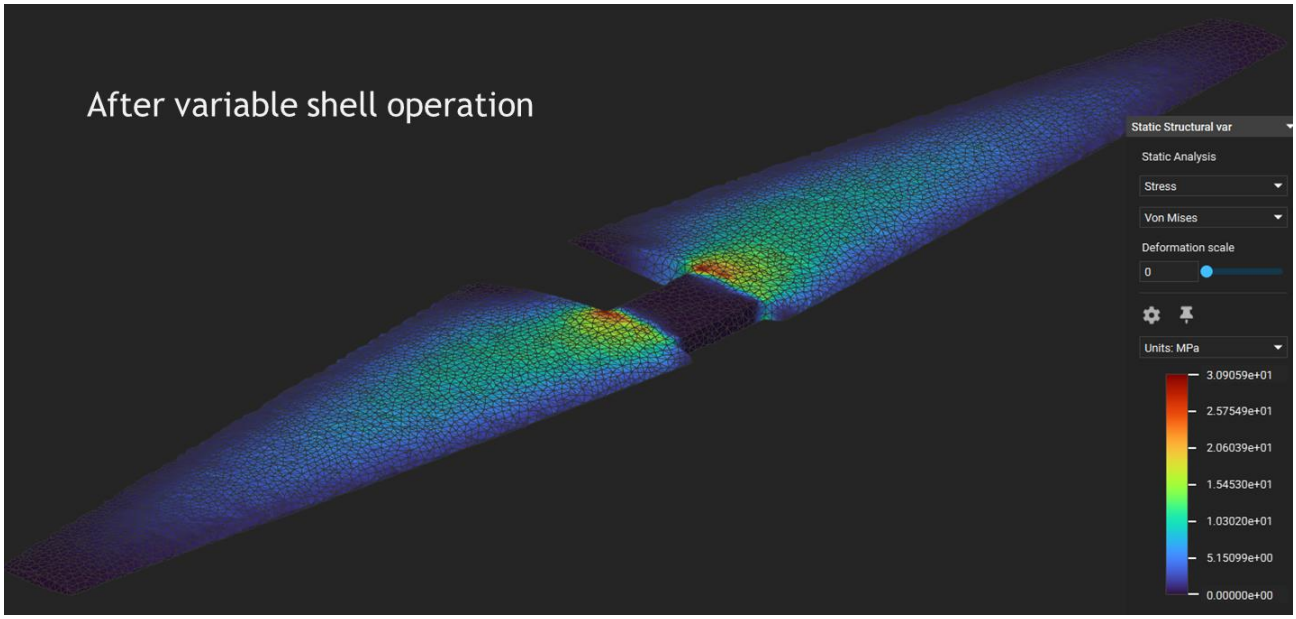

Annex 8

Initial static analysis of Onyx individual wings

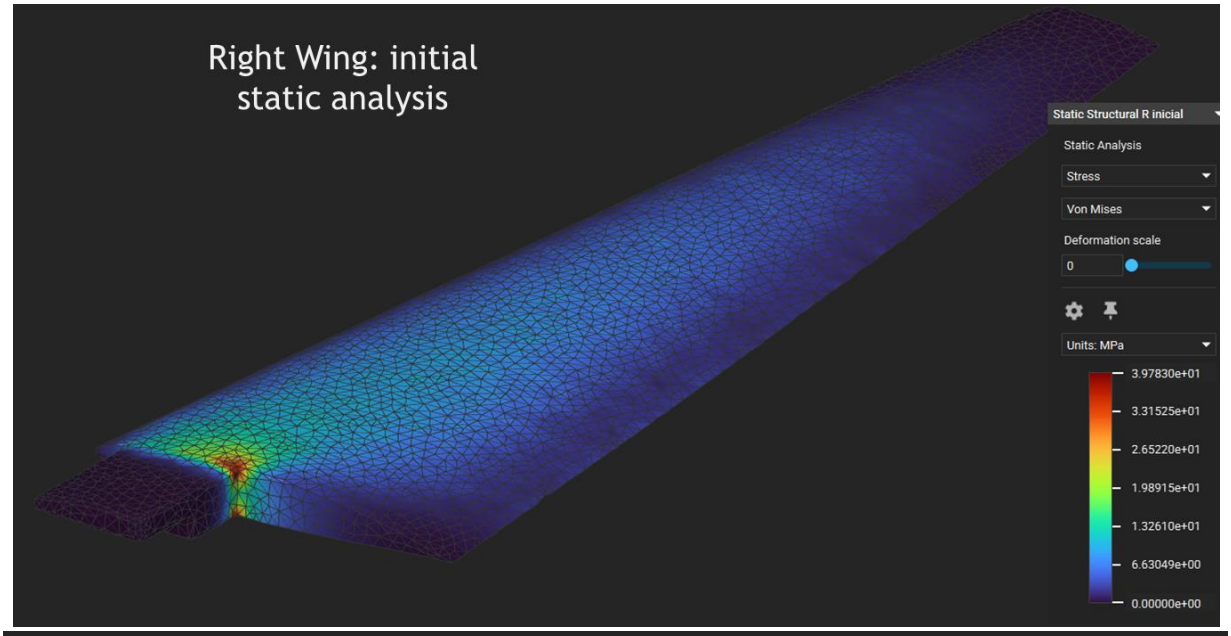

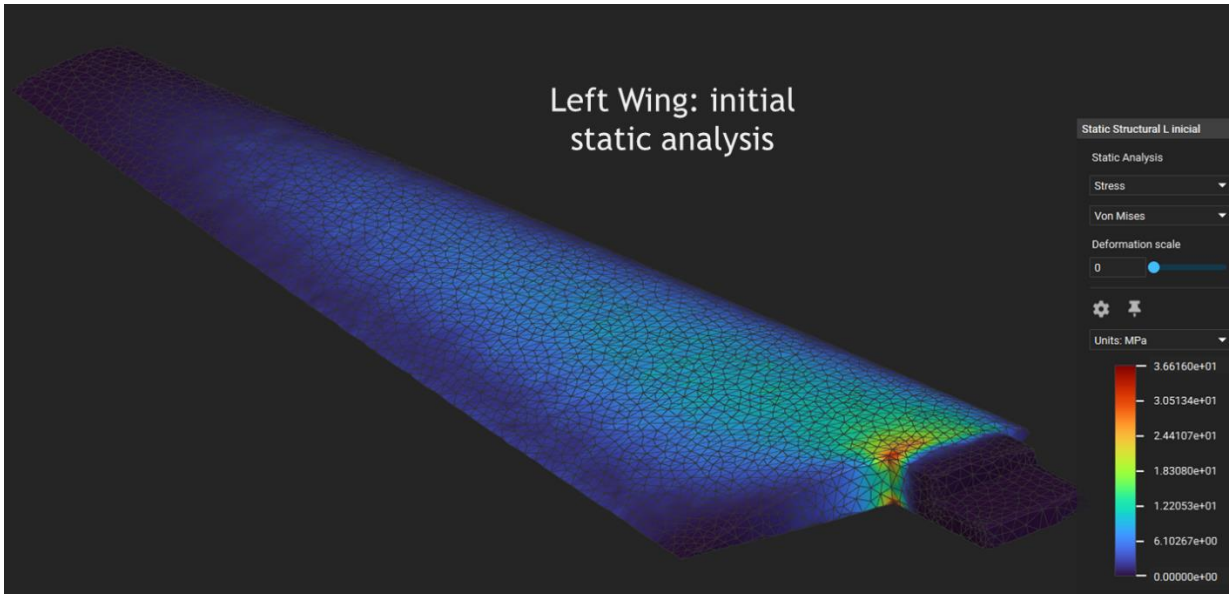

Annex 9

Static analysis of Onyx individual wings after variable shell thickness operation